3.2 Combustion Inorganic Transformation

COMBUSTION INORGANIC TRANSFORMATIONS

Annual Technical Progress Report
for the Period January 1, 1991 - June 30, 1992

by

Chris J. Zygarlicke, Research Supervisor
Karen A. Katrinak, Research Associate
Thomas A. Erickson, Research Supervisor
Bruce S. Folkedahl, Research Associate
Kevin C. Galbreath, Research Associate
Donald P. McCollor, Research Associate
Murali Ramanathan, Research Associate

Energy and Environmental Research Center
Combustion and Environmental Systems Research Institute
University of North Dakota
Box 8213, University Station
Grand Forks, ND 58202

Technical Monitor: Philip M. Goldberg

for

U.S. Department of Energy
Office of Fossil Energy
Pittsburgh Energy Technology Center
626 Cochran Mill Road
P.O. Box 10940, MS 922-H
Pittsburgh, PA 15236

July 1992

Work Performed Under Cooperative Agreement No. DE-FC21-86MC10637

TABLE OF CONTENTS

(continued)

TABLE OF CONTENTS (continued)

(continued)

TABLE OF CONTENTS (continued)

LIST OF FIGURES

(continued)

LIST OF FIGURES (continued)

(continued)

LIST OF FIGURES (continued)

(continued)

LIST OF FIGURES (continued)

LIST OF TABLES

(continued)

LIST OF TABLES (continued)

COMBUSTION INORGANIC TRANSFORMATIONS

1.0 EXECUTIVE SUMMARY

1.1 Task 1: Prediction of Fly Ash Particle Size and Composition

Two models have been developed to predict fly ash particle size and composition from initial coal composition: 1) a stochastic model, "ATRAN1," which combines coal inorganics in a random manner and outputs a predicted fly ash particle size and composition; and 2) an expert system model, "ASHPERT," which gives a first-order estimate of fly ash size and composition, relying heavily on a large empirical database. Both models input data obtained through computer-controlled scanning electron microscopy (CCSEM), chemical fractionation, bulk elemental composition, and proximate analyses.

The stochastic model ATRAN1 has been modified and automated. It is used to predict the partitioning of inorganics during combustion and incorporates a mass balancing algorithm to extend its use to lower-rank coals. Three coals were used for testing and modification of the existing model: Eagle Butte, Kentucky #9, and a blend of Eagle Butte (70%) and Kentucky #9 (30%). The predicted Eagle Butte fly ash contained a larger amount of nucleated submicron particles due to the large amount of organically associated constituents present in the coal. Experimental fly ash produced using particle residence times and temperatures associated with fouling and slagging conditions in a boiler was generated from the coals in order to compare experimental and predicted fly ash composition and size. Slagging conditions include shorter particle residence times and higher gas temperatures at the point of collection than fouling conditions. The CCSEM mineral phase composition of the experimental blend fly ash compared fairly well with that of the predicted compositions. Particle-size distributions (PSD) of the experimental and predicted fly ash also compared fairly well.

The ASHPERT database was increased to include 45 coals and ashes. The fly ash included in the ASHPERT database no longer needs to be exclusively drop-tube furnace (DTF)-generated, but can also originate from pilot- or full-scale combustion sources. Also included for each coal in ASHPERT is proximate/ultimate and chemical fractionation data (if a low-rank coal). X-ray fluorescence (XRF) elemental composition data are also included for both the coal and the fly ash. The mineral particle-type classification program MINER has also been incorporated into ASHPERT. This addition considerably enhances the applicability of ASHPERT in other areas of combustion modeling.

1.2 Task 2: Laboratory-Scale Combustion Testing

A synthetic coal containing pyrite and kaolinite was produced and combusted in the Energy and Environmental Research Center (EERC) DTF. Fly ash was collected and analyzed using CCSEM to examine interactions between mineral species. The results for previous sodium-silica-sulfur and calcium-silica-sulfur are presented along with the pyrite-kaolinite system data. The results obtained are as follows:

- The Na(org.)-Si-S system exhibits interaction between species at 900°C to produce sodium sulfate-silicate phases; above 900°C, silica

dominates due to the loss of sodium and sulfur by devolatilization and decomposition. The PSD of the fly ash decreased with increasing temperature as the result of either char fragmentation or the loss of low melting point sodium silicate or sulfate species which tend to "glue" or cause coalescence of the ash particles.

- The Ca(org.)-Si-S and Ca(min.)-Si-S systems exhibit interactions, primarily between calcium and silica, throughout the 900° to 1500°C temperature range. Unlike the Na(org.)-Si-S system, the calcium-containing system exhibited increased levels of Ca silicates with increasing temperatures. This is primarily due to the lower volatility of calcium as compared to sodium, allowing for more calcium to be retained on the char particle during combustion. Some anhydrite was formed, but was probably the result of SO_2 reacting with the surface of the calcium or quartz grains in the cooling zone of the ash quench probe. Particle agglomeration was seen at the highest temperature studied for the Ca(org.)-Si-S and Ca(min.)-Si-S systems.

- Interaction between ash components occurs over a broader temperature range for calcium-containing ash than for organic sodium-containing ashes. However, softening and rounding of the particles occur at lower temperatures for the sodium-containing ash.

- An enhanced rate of carbon conversion was observed for the Ca(org.)-Si-S over that of the Ca(min.)-Si-S at 900°C. This is in agreement with previous studies showing the catalytic effect of organically-bound calcium during combustion.

- The Ca(org.)-Si-S and Ca(min.)-Si-S systems give generally similar compositional diagrams over the temperature range examined, except for the scarcity of calcium-sulfur species in the Ca(org.)-Si-S system.

- The Fe(min.)-Al-Si system loses nearly all the sulfur from the pyrite at 900°C, leaving kaolinite and iron oxide. The system shows only a small degree of interaction between the kaolinite and iron until 1500°C, when an increased amount of iron aluminosilicate components form.

Combustion testing in the EERC DTF was completed for an Eagle Butte (70%)/Kentucky #9 (30%) coal blend. Approximately 1000 pounds of blended coal was prepared. Coal analyses revealed that the blending operation was quite successful since the physical and chemical parameters measured for the blend are each equivalent to weighted averages of the components in the parent coals. The blend was combusted in the DTF at a gas temperature of 1500°C. Short residence time chars and a carbon-free fly ash were produced in the DTF. Fly ash that was generated from the Eagle Butte/Kentucky #9 blend was collected on a bulk filter and also aerodynamically size-segregated in a six-stage multicyclone. The fly ash revealed very little interaction between the mineral components of the two different coals. Viscosity distributions of liquid phases in the fly ash under slagging conditions for the blend were intermediate between that of a weighted average of the parent fly ashes and the Kentucky #9. The base deposit of the blend grown under slagging conditions was effectively the same as that of the Kentucky #9. Viscosity distributions of the main portion of the deposits grown under fouling

conditions were similar for the blend and the parent coals. Iron-rich particles derived from the pyrite in the Kentucky #9 coal experienced only limited interaction with aluminosilicates, most of which had sources in the Kentucky #9.

1.3 Task 3: Development of Analytical Methods

A round-robin CCSEM analysis has been initiated involving the following seven laboratories: EERC, Ames Laboratory at Iowa State University, Sandia National Laboratory, the University of Kentucky, the R.J. Lee Group, the Netherlands Energy Research Center, and CSIRO of Australia. In order to design the round-robin, information was gathered from each of the participating domestic laboratories regarding their CCSEM systems. The EERC then prepared a detailed protocol describing scanning electron microscopy (SEM) system configuration for analysis of standard coals and sent the protocol together with sample sets to the participating laboratories. Three Argonne National Laboratory premium coals are being considered for round-robin use including Illinois #6, Pittsburgh #8, and Wyodak. The results of the round-robin testing will be used to initiate standardization of the CCSEM technique.

A correction for improving the accuracy of CCSEM elemental compositions was devised. This procedure involves the extraction of k-ratios during acquisition of raw CCSEM data, followed by correction of these k-ratios for atomic number (Z), absorption (A), and fluorescence (F) effects. This is called a ZAF correction and results in more accurate quantitative chemistries of individual fly ash particles or coal minerals. Three bituminous coals and five ashes were analyzed using the CCSEM-ZAF technique. To determine the accuracy of the CCSEM-ZAF technique, coal and ash compositions determined through CCSEM were compared to bulk compositions as measured using XRF. Results indicate the CCSEM-ZAF data require corrections for Ca, Mg, and Si, because these elements occur in significant concentrations in the submicron-size fraction. In the future, appropriate corrections will be made using results obtained through mass balance calculations and through analysis of individual submicron particles. These two techniques are described separately below.

Particle-by-particle scanning electron microscope (PBPSEM) analysis has been refined into a fully automated technique. It uses advanced image analysis together with the standard CCSEM procedure to yield the size and composition of coal minerals on an individual particle basis. PBPSEM greatly enhances ash formation and deposition models by providing much more comprehensive coal input data. The PBPSEM program uses completely automated digital image acquisition, processing, and image segmentation. This is a major advance over the semiautomated program described earlier (1). In PBPSEM, the major operating parameter affecting the sizing and location of particles is the determination of the difference between coal and minerals in the grey-level histogram. The method currently used for determining this difference works well for homogeneous systems. The present emphasis is on developing a technique to evaluate the reproducibility of grey-level histograms in heterogeneous coal systems and also on developing ways of improving the distinction between the different components in the system. Testing of the PBPSEM method continues, with the goal of expanding its applicability.

A method has been devised to balance the mass of organically and mineralogically associated inorganics in coal so that their sum equals the total ash content of the coal. An algorithm to determine the distribution of organically associated inorganics was created using CCSEM, chemical fractionation, and XRF data. The inorganics are divided into soluble minerals, insoluble minerals, organically associated inorganics, and insoluble submicron minerals. The technique was modified to better estimate the amount of submicron silica. The mass balancing technique was tested on the Kentucky #9, Eagle Butte, and Kentucky #9/Eagle Butte blend coals. Kentucky #9 contained little organically associated material, whereas the Eagle Butte coal had large amounts of organically associated calcium and magnesium. The quantity of organically bound material in the Kentucky #9/Eagle Butte blend was intermediate between that of the two parent coals.

A new technique, termed scanning electron microscopy with image analysis (SEM-IA), was developed for analysis of individual submicron ash particles. SEM-IA provides data similar to that of the CCSEM technique for 1- to 100-μm-diameter particles. A freeze-dried dispersion method was developed as an alternative sample preparation technique. Using this method, ash particles are suspended in propanol and dispersed onto pieces of vitreous carbon measuring approximately 1 cm^2. Freeze-drying maintains an adequate separation between particles, as required for SEM-IA. During analysis, size measurements of the individual particles are not made in real time as they are in CCSEM, but only after a large number of duplicate images of a sample field of view have been acquired and averaged to remove noise. This additional image processing step is necessary to obtain accurate size measurements for the smallest particles. The image-averaging ability of the SEM-IA technique provides size and composition distribution data for particles with diameters an order of a magnitude smaller than those that can be analyzed by CCSEM, or approximately 0.1-μm minimum diameter.

2.0 GOALS AND OBJECTIVES

The aim of this project was to achieve an overall understanding of the physical and chemical changes that occur in the inorganic matter of coal during combustion by developing a means to predict the state (vapor, liquid, or solid), composition, and size of the inorganic material at any point in a combustion system, given the coal composition and combustion conditions. The work was divided into three tasks.

Task 1 involved developing expert systems to predict fly ash composition and size from initial coal characteristics using two approaches. The first is a stochastic model, "ATRAN1," that simulates the coalescence, fragmentation, and decomposition of initial coal minerals during their transformation to fly ash particles. The second model, "ASHPERT," produces a first-order estimate of fly ash size and composition that can easily be integrated with other expert systems. Data for use in ASHPERT were generated in the Pittsburgh Energy Technology Center (PETC) mineral matter programs at the EERC for 45 test coals and ashes. Inorganic components were measured for the coals and ashes. CCSEM and chemical fractionation were used to determine the association, size, composition, and juxtaposition of the inorganic components. All of these data are used by ASHPERT to predict the size and composition of ash particles based on coal composition and combustion conditions.

Task 2 involves laboratory-scale testing of the physical and chemical changes of inorganic phases during combustion. Chars and ashes were examined to determine their bulk composition, phase distribution, and morphology. Data were obtained using SEM and electron microprobe analysis (EMA), XRF, and x-ray diffraction (XRD). The goal was to track the transformation of inorganic constituents of representative coals at various degrees of coal particle burnout until fly ash was produced. The DTF system was used to produce chars at various degrees of burnout and, ultimately, a carbon-free fly ash. Model mineral/coal mixtures were also produced and combusted to examine some of the transformations in detail. The database generated in this task was used to formulate the predictive models described under Task 1.

Task 3 involves development of CCSEM methods for determining the size, composition, and juxtaposition of mineral grains in pulverized coals. An additional aspect of this task is the extension of CCSEM methods to submicron minerals and fly ash particles. Proper determination of the inorganic components in coal is an essential requirement in understanding and ultimately predicting the transformations of inorganic components during coal combustion. To obtain a more complete understanding of the coal compositions, chemical fractionation was used to measure the abundance of organically associated inorganic constituents in the lower-rank subbituminous and bituminous coals.

During the past three years, the project has focused on developing consistent and quantitative techniques for analyzing the inorganic components of coals, chars, and fly ash. This emphasis is essential because the fate of inorganic matter during combustion cannot be predicted accurately without the availability of consistent and reliable data. In conjunction with the above three tasks is an ongoing effort to evaluate all data for precision and accuracy. A further goal of the quality control effort is to obtain fully quantitative, standardized data. Quality-control measures were applied to coal and ash characterization data as well as to char and fly ash formation tests in the DTF.

2.1 Task 1: Prediction of Fly Ash Particle Size and Composition

The objectives of the fly ash particle size and composition prediction task were as follows:

1. Develop an algorithm which will allow for the addition of organically bound inorganics to the stochastic model ATRAN1.

2. Characterize coal inorganics in Eagle Butte, Kentucky #9 and Eagle Butte/Kentucky #9 blend coals using CCSEM and chemical fractionation. These data were used to operate the mechanistic stochastic model for fly ash particle size and composition prediction.

3. Generate experimental fly ash under slagging and fouling conditions for comparison with stochastic predictions.

4. Enhance the ASHPERT database to include CCSEM data for 45 coals and corresponding fly ash samples. Include additional information such as XRF and proximate/ultimate data.

2.2 Task 2: Laboratory-Scale Combustion Testing

The objectives of the laboratory-scale combustion testing were as follows:

1. Production, characterization and combustion testing of synthetic coal/char model mixtures for the purpose of studying inorganic transformations in systems limited in inorganic constituents. The systems studied included:

   a. Sodium-silica-sulfur (simulation of organically bound Na).
   b. Calcium-silica-sulfur (simulation of organically bound Ca).
   c. Calcium-silica-sulfur (mineral-bound Ca as calcite).
   d. Iron-aluminosilicate (using pyrite and kaolinite).

2. Combust well-characterized Eagle Butte and Kentucky #9 parent coals and a 70% Eagle Butte/30% Kentucky #9 blend in order to determine the transformations of inorganic components.

2.3 Task 3: Development of Analytical Methods

The objectives of the analytical methods development task during this year were as follows:

1. Begin an interlaboratory round-robin CCSEM analysis of prepared coal samples.

2. Evaluate the accuracy of the ZAF correction method for CCSEM data.

3. Develop a PBPSEM, a new CCSEM method which uses image analysis to characterize coal minerals on a particle-by-particle basis.

4. Determine the amount of mineral versus organically bound inorganic matter in three coals using a mass balancing procedure.

5. Extend automated SEM analysis methods to submicron particles, and evaluate by comparison with standard CCSEM results.

3.0 TASK 1: Prediction of Fly Ash Particle Size and Composition

3.1 Introduction

The key to developing a model to predict the composition and size of fly ash is a well-established database of coal mineral and corresponding fly ash data for coals of varied ranks. In order to understand the physical and chemical transformations that occur during combustion, it is particularly important to have sufficient quantitative data on the inorganic content of coal and fly ash. Mineral and ash characterization results were used to establish a foundation for model development and verification. Data were obtained using SEM and electron microprobe techniques along with standard inorganic analysis.

3.2 Equipment and Procedures

Most of the characterization of coal minerals and the corresponding ash was performed using CCSEM. The technique is discussed below in the section on Task 3, Development of Analytical Methods. CCSEM yields size and composition information for discrete minerals and ash particles. Chemical fractionation was used to measure the finely dispersed minerals and organically bound inorganics that are beyond the detection limits of the SEM (2). Another technique used for analyzing just the fly ash is scanning electron microscopy point count (SEMPC), which yields ZAF-corrected chemistries, but does not include size data. The method and accessory data-processing software were developed at the EERC. SEMPC involves microprobe analysis of about 250 random points in a polished cross-sectioned sample and is used to determine the relative abundance of phases in ashes and deposits (3). Data for each point are transferred to a computer file for later processing, including calculation of molar and weight ratios of elements. Using these ratios, points with compositions of known phases (common to ashes and coal minerals) are identified and counted. The software also determines the proportion of unknowns, those for which there are no known phases corresponding to the chemical composition. For this study, it was assumed that the unknown phases were amorphous. The average chemistry of all points is calculated for each sample in order to obtain a bulk composition.

3.3 Predictive Model for Fly Ash Size and Composition

3.3.1 Introduction

Two models have been developed at the EERC for use in predicting fly ash particle size and composition from CCSEM analyses of coal. Both models are phenomenological, requiring detailed coal input data and empirically derived knowledge of inorganic transformation phenomena occurring during combustion. The first model, "ATRAN1," is stochastic and simply combines initial coal inorganics in a random manner in order to predict the resultant fly ash particle size and composition. The acronym is derived by shortening the phrase "ash transformation" and adding the number "1" to indicate future refinements and modifications of the code. ATRAN1 is considered stochastic because it randomly combines data from coal mineral analyses to produce predictions of fly ash compositions. The model does not operate in a completely random manner in that associations among coal minerals (i.e., locked vs. liberated) influence the predictions. The second model, "ASHPERT," is an expert system yielding a first-order estimate of fly ash size and composition. Both models are designed to emulate pulverized coal combustion and, hence, use data derived from coals ground to 70%-80% -200 mesh.

3.3.2 Experimental

Both ATRAN1 and ASHPERT use CCSEM data as their primary input regarding the identity, chemistry, size, quantity, and mineral-to-coal association (locked or liberated) of the minerals. Data are required on an individual-particle basis in order to model transformations and interactions between individual minerals locked within and liberated from coal particles. CCSEM data provide all of the above parameters for minerals greater than 1 μm in average diameter, whereas chemical fractionation results are used for information on organically bound inorganics or minerals less than 1 μm in size.

Fly ash was generated in a vertical laminar-flow furnace (DTF) for comparison with the predicted fly ash. The DTF is a laboratory-scale furnace system that simulates conditions in commercial combustors without the high cost associated with pilot-scale combustion testing. The combustion tests for the work reported here were performed using slagging and fouling conditions which include gas temperatures of 1500°C, particle residence times of 1-3 seconds, an oxygen atmosphere of about 21%, and a filter trap to collect bulk ash. Fouling conditions involve longer particle residence times (~3 seconds) and cooler temperatures in the zone just prior to the fly ash collection probe while slagging conditions involve residence times of 1 to 2 seconds and much higher temperatures in the collection zone. The resultant ash was analyzed for chemistry and particle size using CCSEM, similar to the analysis of coal minerals. More details of the DTF assembly are given below in the section on laboratory-scale combustion testing (Task 2).

3.3.3 Stochastic Model Development and Results

ATRAN1 has been modified and improved. The program now incorporates a mass balancing algorithm to extend its use to lower-rank coals. Three coals were chosen for testing the program: Eagle Butte subbituminous, Kentucky #9 bituminous, and a blend of Kentucky #9 (30%) and Eagle Butte (70%). These three coals were characterized using CCSEM, and the results were used to run ATRAN1. Figure 1 through 6 show comparisons of the experimental and predicted results for fly ash mineral phase compositions and PSDs for each of the test coals. ATRAN1 predicted fly ash compositions fairly well (Figures 1, 3, and 5), although there are still problems with modeling the interactions of calcium and iron with silicates and aluminum. The predicted PSDs were reasonably accurate for each of the Eagle Butte and Kentucky #9 parent fly ashes (Figures 2 and 4), but were unsatisfactory for the blend ash (Figure 6). The problems with prediction of PSD probably stem from the inadequacy of current methods for quantifying submicron particulates, especially for cases involving Ca-rich subbituminous coal. Eventual refinement and acceptance of the SEM-IA technique for individual submicron particles, as described separately below, may allow actual phases of individual grains to be determined for use in future versions of ATRAN1.

3.3.4 Particle Size and Composition Distribution Expert System

The ASHPERT expert system for fly ash particle size and composition distribution (PSCD) modeling has been completed. A significant accomplishment is the restructuring and expansion of the ASHPERT database. At the time of writing this report, the database contains the proximate/ultimate, XRF chemical fractionation, and CCSEM analyses data for 45 samples. Another significant accomplishment is the incorporation of the rule-based particle mineral-type classification expert system "MINER" into ASHPERT. This has considerably enhanced the applicability of ASHPERT in other areas of combustion systems modeling and also has permitted numerous algorithmic simplifications. Lastly, "hooks" for modules to perform statistical analyses of the database have been added to ASHPERT. This facilitates the recognition of patterns and trends in the data and expedites the formulation and modifications of ASHPERT's rules. A direct result of these additions and modifications is a measurable increase in ASHPERT's expertise which is now able to approximate PSCDs with an average error of 10% relative to their experimentally measured values.

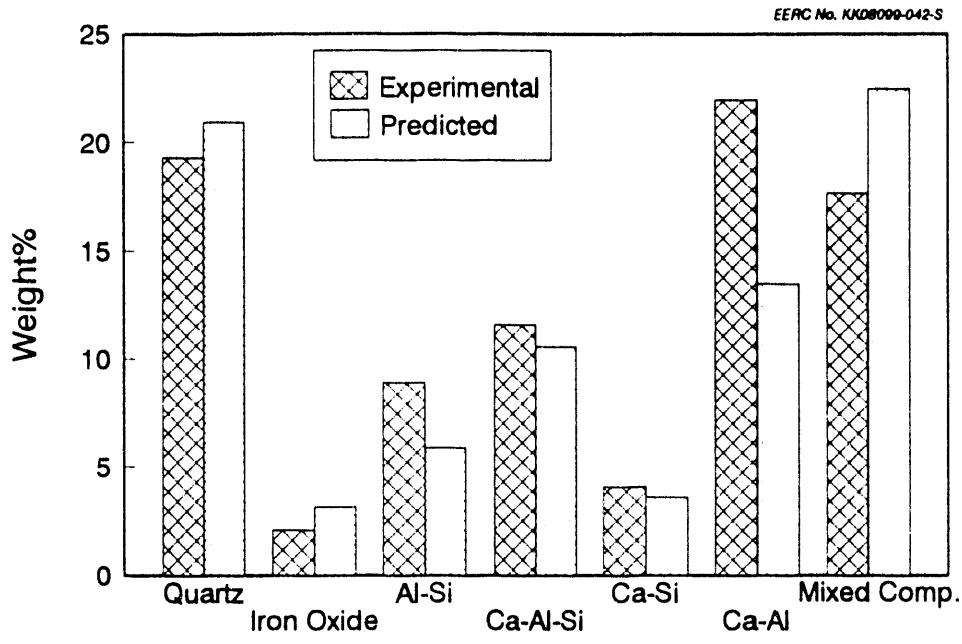

Figure 1. Experimental and predicted compositions for Eagle Butte fly ash.

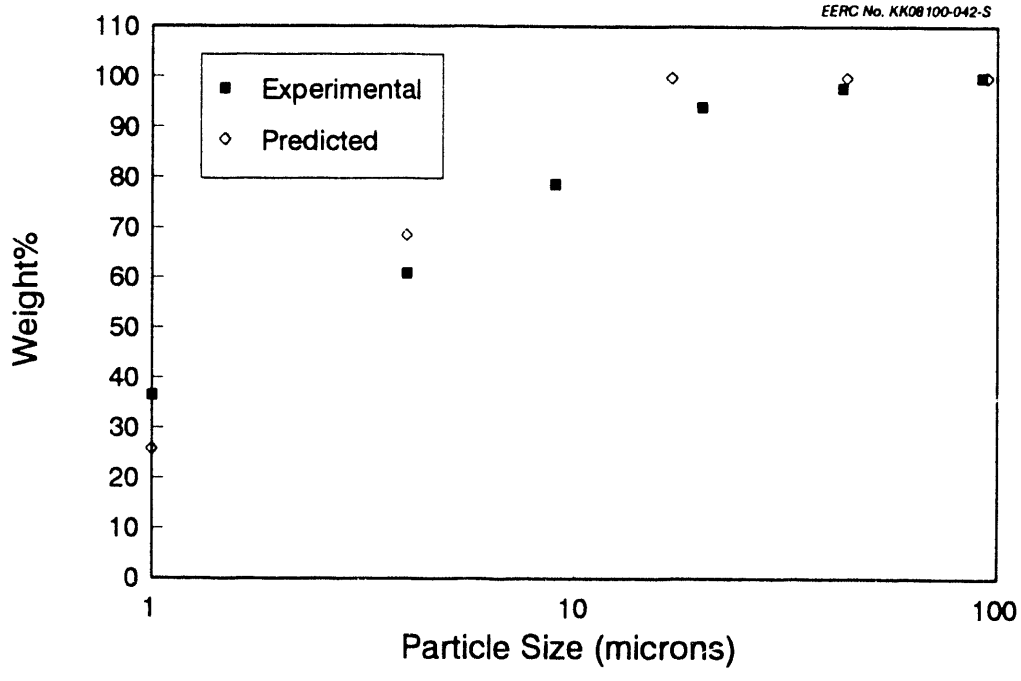

Figure 2. Experimental and predicted particle-size distributions for Eagle Butte fly ash.

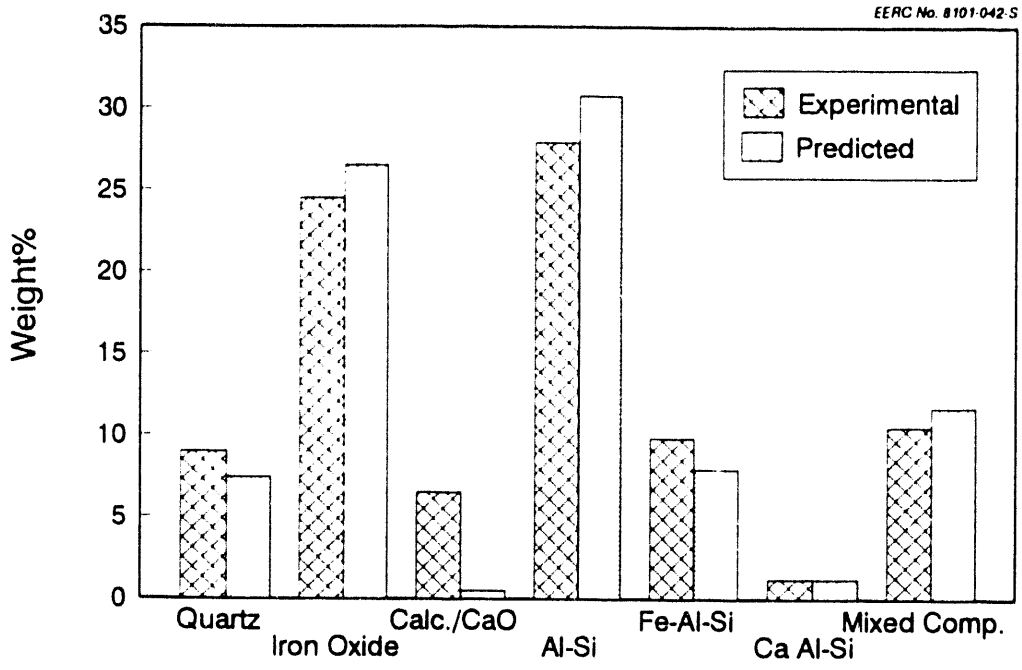

Figure 3. Experimental and predicted compositions for Kentucky #9 fly ash.

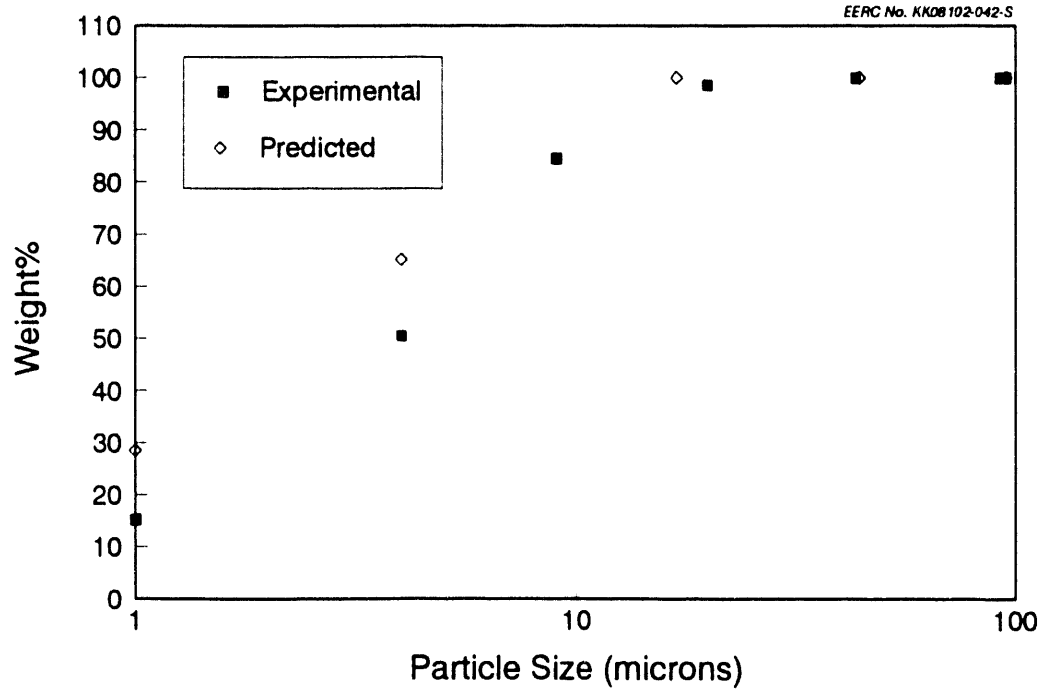

Figure 4. Experimental and predicted particle-size distributions for Kentucky #9 fly ash.

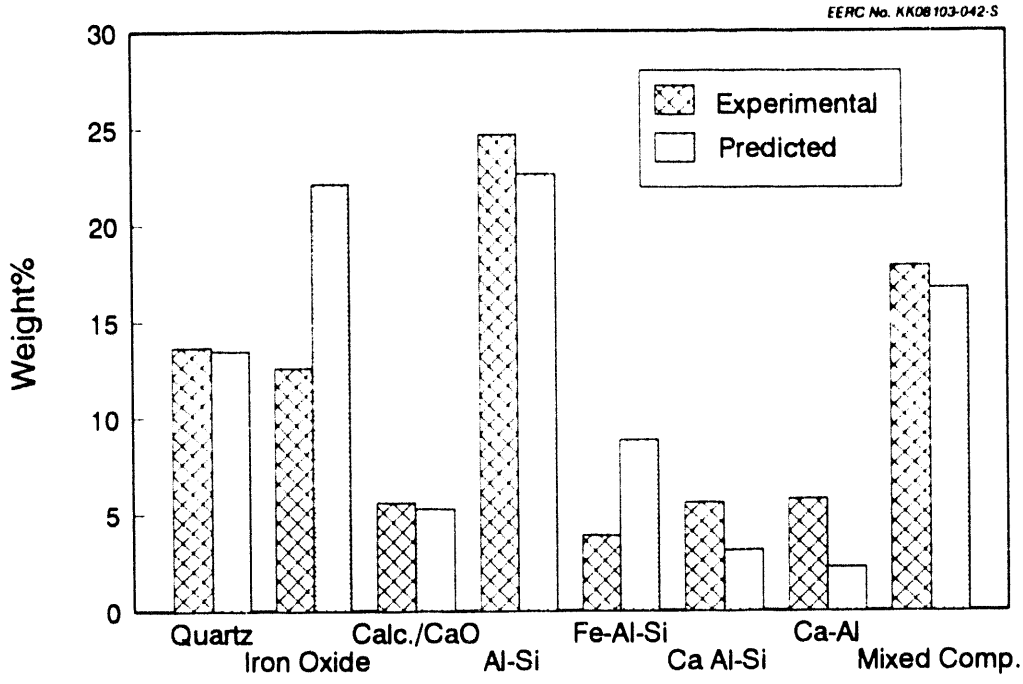

Figure 5. Experimental and predicted compositions for Eagle Butte/Kentucky #9 blend fly ash.

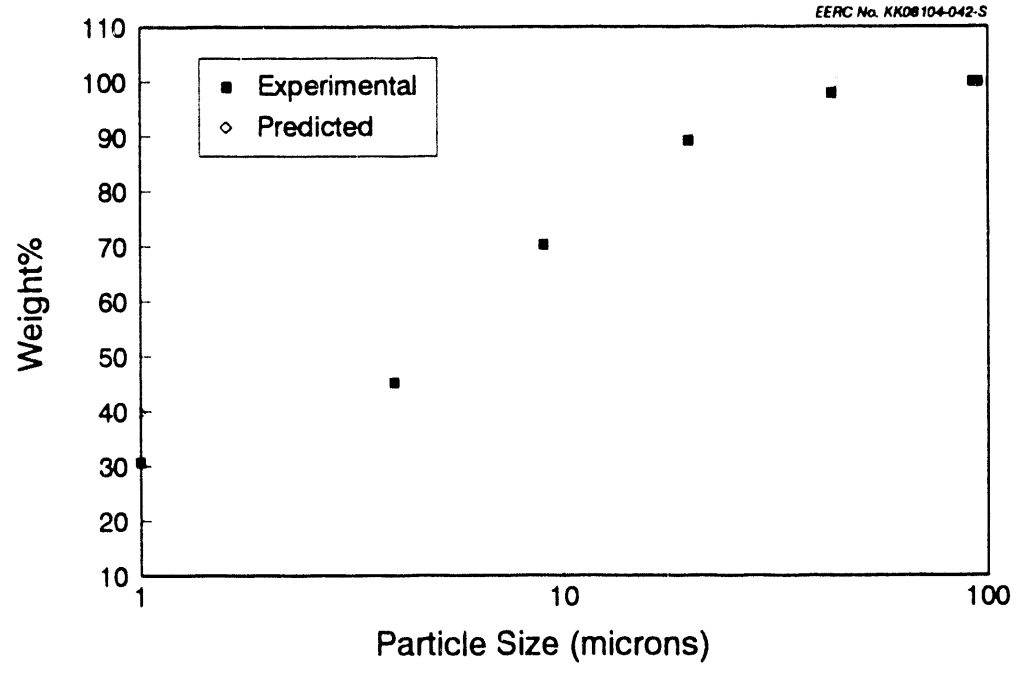

Figure 6. Experimental and predicted particle-size distributions for Kentucky #9 blend fly ash.

The organization of this section is as follows. In Section 3.3.4.1 we discuss the PSCD modeling problem and the need for an empirical tool such as ASHPERT. A detailed description of the ASHPERT database is undertaken in Section 3.3.4.2. The ASHPERT knowledge base, its implementation, and the results obtained are described in Section 3.3.4.3. Section 3.3.4.4 contains remarks on future directions and extensions to ASHPERT.

3.3.4.1 Introduction

Particle size is fundamentally important in the combustion of pulverized coal and coal-water slurry. Ignition, stability, combustion efficiency, and pollutant formation are all strongly influenced by the fuel PSD. In addition, the compositions of individual particles play a major role in determining the chemical, thermal, and structural characteristics of ash deposits that accumulate on boiler walls and heat-transfer surfaces during combustion.

The evolutions of the PSCD functions are determined by a complex sequence of both cooperative and competing physical and chemical processes. Construction of a model to describe PSCD evolution is further complicated by the fact that PSCDs are, in general, dependent on the location within the boiler, and this location dependence is itself dependent on previous deposition histories. Thus, to solve the problem in any generality, a large set of coupled, ordinary and partial differential equations needs to be addressed. This set minimally includes the following:

- Navier-Stokes and continuity equations
- Species (kinetic) rate equations
- Species mass balance equations
- Heat equation with, in general, nonlinear, nonisotropic conductivity tensor, and nonlinear source terms
- Constitutive or other intra- and interparticle stress energy (tensor) relations

These equations, together with the complicated boundary conditions on boiler walls and heat-transfer surfaces, make the task of a general solution a formidable one.

The PSD models currently reported in the literature make certain simplifying assumptions regarding evolutionary mechanisms and may be categorized into two broad classes, viz., deterministic and stochastic. In deterministic models, the underlying principle is simply mass balance: a distribution $\phi(t)$ at time t is allowed to evolve to a distribution $\phi'(t')$ at time t' subject to the constraints that all process involved in transforming to preserve the net mass of the particles. All deterministic PSD models, therefore, can be succinctly described by an evolution equation of the form (4-7):

$$\frac{\delta \phi}{\delta t} = F(\phi)$$

The specific functional form of $F(\phi)$ above depends on the details of the processes (agglomeration, fragmentation, continuous or discrete mass loss, etc.) considered in the model.

In the case of stochastic approaches to PSD evolutions, the underlying idea is simply a redistribution of the initial distribution, but subject to some extremization principle or, failing that, subject to a set of empirically determined "local redistribution rules" (8-10). The stochastic models are thus computational or numerical in nature and are typified by Monte-Carlo or percolation lattice type calculations. In general, stochastic models, especially when ensemble-averaged, produce better results than their deterministic counterparts.

A major drawback of either the stochastic or the deterministic class of models is the difficulty in incorporating the (element or species) composition distributions and redistributions within their framework. Although it is conceptually very natural to speak of the species distributions giving rise to the particle's molar volume and, hence, its "size," computationally it is easier to deal with just a single distribution. However, composition distributions are indispensable in other combustion systems modeling areas such as fly ash deposition, NO_x, precipitator, and emissions control models.

Another drawback in regard to these deterministic and stochastic models is the difficulty of incorporating temperature as a parametric variable. The problem here is not so much as including temperature as a formal parameter of the model, but in the determination of the temperature dependence of the model-specific parameters (fragmentation rates, power law exponents, lattice bond breakage rates, etc). Lacking such data, the applicability of these models to PSD evolutions in situations involving sharp thermal gradients is limited. Although this limitation is indirectly redressed through randomizing the lattice bond breakage rates in the percolation lattice model (9), the assignment of probability measures to the lattice bond breakage events as a function of a (time-dependent) temperature distribution, which is physically appealing, does not appear to be straightforward.

The development of an expert system for approximating PSCD evolutions was undertaken primarily due to the widespread availability and growing acceptance of CCSEM analyses. CCSEM, which combines SEM, automated image analysis, and energy-dispersive x-ray spectroscopy, enables the analysis of a statistically significant number of particles and provides realistic representations of PSCDs both in the parent coal and its subsequent fly ash.

From a more pragmatic perspective, the compelling reason for an expert system is that it can serve as an interim tool for a "quick and dirty" means of providing realistic PSCDs to other areas of modeling while the refinement of the more rigorous and conventional approaches is in progress. In fact, conventional approaches too can benefit from the expertise of the system by defining additional goals and eliciting specific responses or even, in some circumstances, obtaining limits on model-specific parameters.

3.3.4.2 ASHPERT Database

The ASHPERT database is a relational database (11). The fundamental or basic tuple is a "sample" which is used as the generic term for a specimen of coal. (Note that the term sample is used in its statistical sense.) The attributes of each sample include a (unique) name, biography, location, rank, ownership category, proximate/ultimate, XRF, chemical fractionation, and CCSEM analyses. A sample need not have all its attributes included, i.e., values for some or all the attributes of a sample may be missing which facilitates

incremental updates of the database. The name field of the attribute of a sample, however, must be included since it serves as the primary (identification) key. A fairly sophisticated and general purpose database manager--which is itself a rule-based quasi-expert system--handles the routine chores of searching, sorting, indexing, report generation, and so on.

While many of the attributes of a sample are self-explanatory, a few comments are in order. The "name" attribute as mentioned earlier, is a mandatory field and should preferably be unique. The "biography" field permits biographical or other notes about the sample to become part of its record. Since some of the samples in the database have contractual or copyright restrictions regarding their data, the "ownership category" attribute of a sample serves to limit access to the sample data. Currently, only two ownership categories are supported, viz., PUBLIC and PRIVATE. A PUBLIC ownership category--the default--means that the sample does not have any access restrictions. A PRIVATE ownership category implies that the sample can be accessed only by the project manager or principal investigator of the project under which the sample was submitted for analysis. The project manager or principal investigator may authorize others access to PRIVATEly owned samples. The proximate attribute is another tuple with attributes moisture, volatile matter, fixed carbon, and ash. (This is the standard ASTM definition of a proximate analysis.) Likewise, the ultimate and XRF attributes correspond to the standard ASTM definition of ultimate and ash analyses. The default units for the attributes of the proximate, ultimate and XRF analyses fields is "weight percent," while the default analysis environment for the proximate and ultimate fields is "as-received." (These defaults can be changed.)

The CCSEM attribute is a more complex one. It is also a tuple with the attributes type, source, magnification, and file name. The "type" attribute which can be either COAL or ASH serves to distinguish the CCSEM analyses for the parent coal from its fly ash. The "source" field whose domain is DTF (drop-tube furnace), PPF (pilot-plant furnace), FSF (full-scale furnace), AFU (ash-fouling unit) or MINE (coal mine) can be used to identify the source of the coal or fly ash. Two "magnification" values are currently supported, viz., 50x and 240x, corresponding to the magnifications used in a CCSEM analysis. (A third magnification, 1000x, has recently been added to the CCSEM procedure and is soon expected to be supported.) The results of a CCSEM analysis are usually written to a file: the "file name" attribute thus is a placeholder for this information.

CCSEM analysis files contain the chemical and physical or geometric parameters for the particles in the analyzed sample (Coal/Ash). The format of these files are all identical: these are pure ASCII files, each line of which is the analysis data of a single particle. The files include columns for particle number, x-ray counts, normalized spectral intensities for the twelve elements analyzed, particle coordinates, particle diameter, area, perimeter, and shape factor. A detailed explanation of SEM analysis can be found in Goldstein and others (12) while that of CCSEM can be found in Dinger (13).

The entire ASHPERT database comprises data for 45 samples spread over 180 files and requires about 15MB of storage. As mentioned above, many of the samples are PRIVATEly owned, and thus the full database itself is expected to be distributed only to a restricted number of people. However, a version of ASHPERT will be available to the general public which will have a smaller

number of coals in the database. It is also expected that the database will increase in the near future; data for another 10 samples is almost complete. The compilation, entry, validation, and debugging of the database took about 14 months, with the majority of the time being spent in compilation and data entry. Approximately six months were spent in designing and developing the database manager and its associated set of software tools.

The 45 samples currently in the database represent widely variant ones in terms of geographic origin, bulk chemistry, rank, and combustion characteristics, as shown in Table 1.

A comparison of PSCDs is also corroborative of the dispersed nature of this set of samples. However, some surprising trends are also to be observed. Figures 7 and 8 are the PSDs and MFDs (mineral frequency distributions) respectively, for a randomly selected set of six samples from the database. In order to respect the PRIVATE nature of some of the samples, the samples in the database have been serialized; the numbers appearing in Figures 7 and 8 are these serial numbers. A very striking trend immediately obvious from Figure 7 is the similarity in the "shape" of the PSD curve for the various coals and the corresponding fly ashes. All of these curves are similar to normal distribution curves with a "skewed" peak. This trend is not surprising because PSDs are expected to be "log-normal" distributions (14). A more unusual trend is the close tracking of the coal PSD curve by the fly ash PSD curve.

However, this "tracking" between the coal and fly ash PSD curves is not all too spectacular, as Figures 9 and 10 show. Figure 9, a scatter plot of the coal versus ash mean particle radii for the samples in the database, clearly exhibits the deviations between the coal and ash particle sizes. The solid regression line in this figure has an R^2 of only 0.07 and is a power law function of the form $y = ax^b$. Figure 10 is a scatter plot of the coal versus ash PSD curve standard deviations. Here, the points appear to be more tightly clustered, yet there are more outliers as well. The regression line is again a power law function with an R^2 of also about 0.07.

Figure 8 shows that no observable trend appears in the mineral distributions between the various coals. The numbers on the x-axis of the histograms are the mineral types. For example, mineral type 1 is quartz, mineral type 2 is alumina, etc. Likewise, there is no observable trend in the mineral distributions between the various fly ashes. However, the fly ash MFD appears to track the parent coal MFD fairly well, except for some of the major mineral types such as 1 (quartz), 9 (kaolinite), 11 (K-Al silicate), 13 (Ca-Al silicate), 20 (pyrite), and 33 (amorphous). Since the amorphous "mineral type" is a default mineral type, variations in the other mineral types will usually involve variations in the amorphous category.

Only a few coal-fly ash pair MFD curves have been displayed in Figure 8; thus one important trend that appears on viewing the MFDs for all the samples in the database is not easily observable. This trend relates to the continuity of the fly ash MFD on the parent coal's MFD: for instance, in Figure 8, the MFDs for coals 26 and 37 are fairly similar to each other; on comparing the MFD for ashes 26 and 37, it is seen that these are also similar and, what is more, the extent of the differences between the MFD for ashes 26 and 37 appears to be proportional to the extent of the differences between the MFD for these coals. The coal-fly ash pair MFD curves of the full database do

TABLE 1

ASHPERT Coal and Fly Ash Database

Coal Name	Rank	Location	Source of Fly Ash	% Ash
70% Eagle Bt/30% KY #9	Subbtuminous/Bituminous	WY/KY	DTF	7.3
75% Eagle Bt/25% KY #9	Subbtuminous/Bituminous	WY/KY	DTF	7.7
70% WY/30% OK Blend	Subbtuminous/Bituminous	WY/OK	Pilot	8.9
70% WY/30% OK Cleaned	Subbtuminous/Bituminous	WY/OK	Pilot	6.5
90% WY/10% OK Blend	Subbtuminous/Bituminous	WY/OK	Pilot	7.1
Beulah	Lignite	North Dakota	DTF	10.4
Bituminous	Bituminous	West Virginia	DTF	NA
Bituminous-High Load	Bituminous	Utah Han. Bas.	Full Scale	6.2
Bituminous-Low Load	Bituminous	Utah Han. Bas.	Full Scale	6.2
Dietz	Subbituminous	Montana PRB	DTF	4.6
Eagle Butte	Subbituminous	Wyoming PRB	DTF	5.6
Eagle Butte	Subbituminous	Wyoming PRB	Penn State Pilot	5.4
Eagle Butte	Subbituminous	Wyoming PRB	Full Scale	5.2
Illinois #6	Bituminous	Illinois	DTF	16.6
Illinois #6 MFP	Bituminous	Illinois	Pilot	4.2
Illinois #6 Parent	Bituminous	Illinois	Pilot	9
Illinois #6 SOAP	Bituminous	Illinois	Pilot	4.3
Island Creek	Bituminous	Kentucky	Pilot	6.8
Island Creek	Bituminous	Kentucky	Pilot-XS Air	6.7
Jader	Bituminous	Pennsylvania	Pilot-XS Air	8.7
Jader	Bituminous	Pennsylvania	Pilot	8.7
Kentucky #9	Bituminous	Kentucky	DTF	14.2
KY #9 Gravimelt 7a	Bituminous	Kentucky	DTF	0.5
Bituminous/Coke Blend	Lignite	Saskatchewan	Pilot	7.0
Bituminous	Bituminous	Mexico	Pilot	38.5
Subbituminous	Subbituminous/Bituminous	Wyoming	Pilot	3.6
Pitts #8 Gravimelt 9c	Bituminous	Pennsylvania	DTF	0.3
Pittsburgh #8 MFP	Bituminous	Pennsylvania	Pilot	3.3
Pittsburgh #8 Parent	Bituminous	Pennsylvania	Pilot	9.5
Pittsburgh #8 SOAP	Bituminous	Pennsylvania	Pilot	4.4
Robinson	Subbituminous	Montana	Penn State Pilot	8.6
Bituminous	Bituminous	Mexico	Pilot	30.1
San Miguel	Lignite	Texas	DTF	46.4
Subbituminous	Subbituminous/Bituminous	Philippines	Pilot	19.8
Subbituminous	Subbituminous	Wyoming PRB	Full Scale	4.89
Subbituminous	Subbituminous	Wyoming PRB	Full Scale	5.65
Subbituminous	Subbituminous	Wyoming PRB	Full Scale	4.94
Subbituminous	Subbituminous	Wyoming PRB	Full Scale	5.15
Subbit./Bit. Blend	Subbituminous/Bituminous	Wyoming PRB	Pilot	NA
Upper Freeport	Bituminous	Indiana	DTF	24.2
Upper Freeport MFP	Bituminous	Indiana	Pilot	5.4
Upper Freeport Parent	Bituminous	Indiana	Pilot	10.7
Upper Freeport SOAP	Bituminous	Indiana	Pilot	5.2
Utah Blind Canyon	Subbituminous	Utah Han. Bas.	DTF	6.1
Wyoming 100% (Wyodak)	Subbituminous	Wyoming	Pilot	8.0

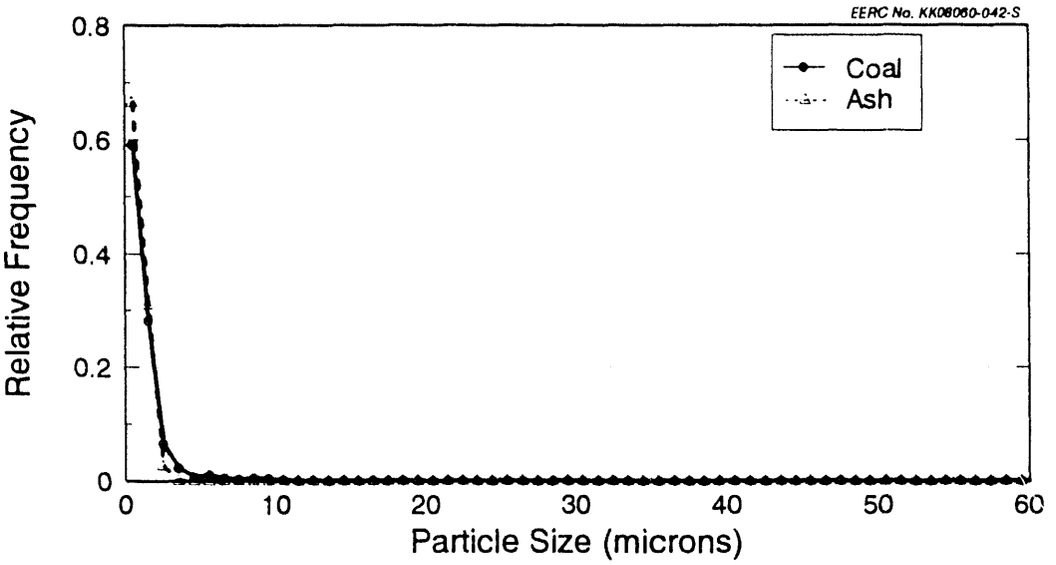

Figure 7a. Particle-size distribution for Sample #5 from the ASHPERT database.

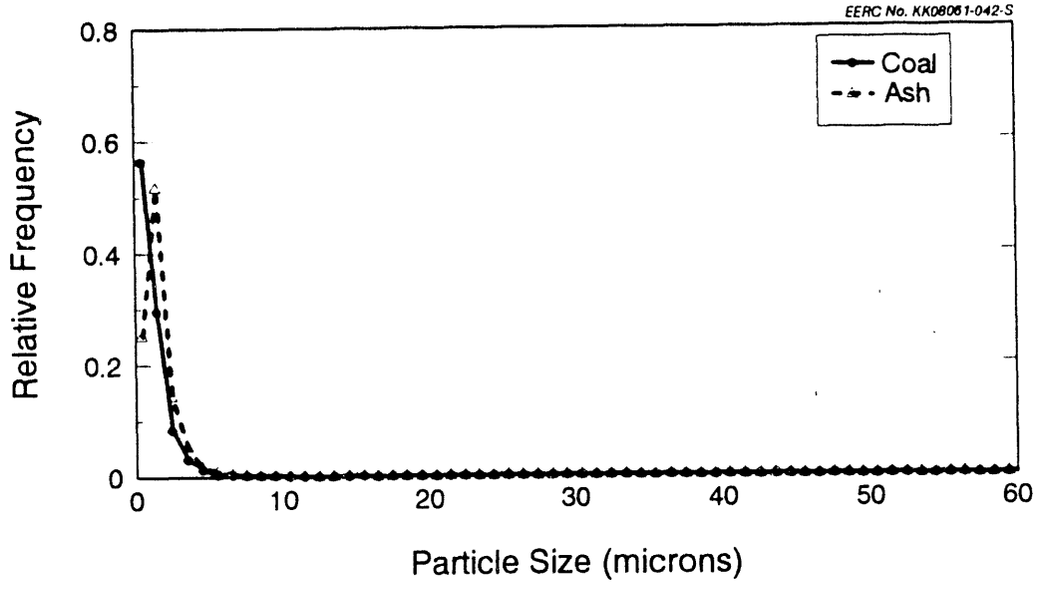

Figure 7b. Particle-size distribution for Sample #11 from the ASHPERT database.

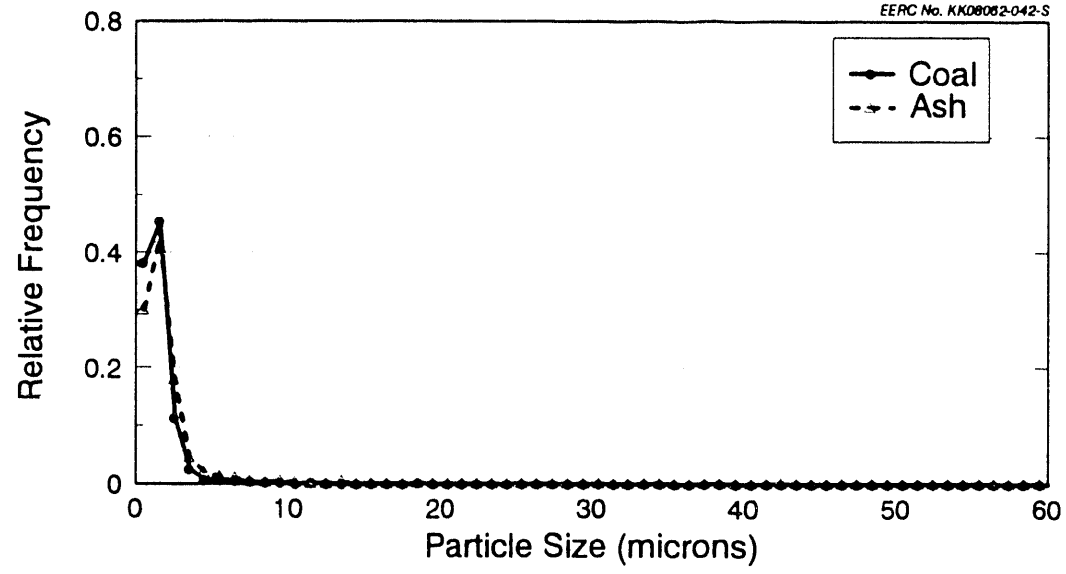

Figure 7c. Particle-size distribution for Sample #14 from the ASHPERT database.

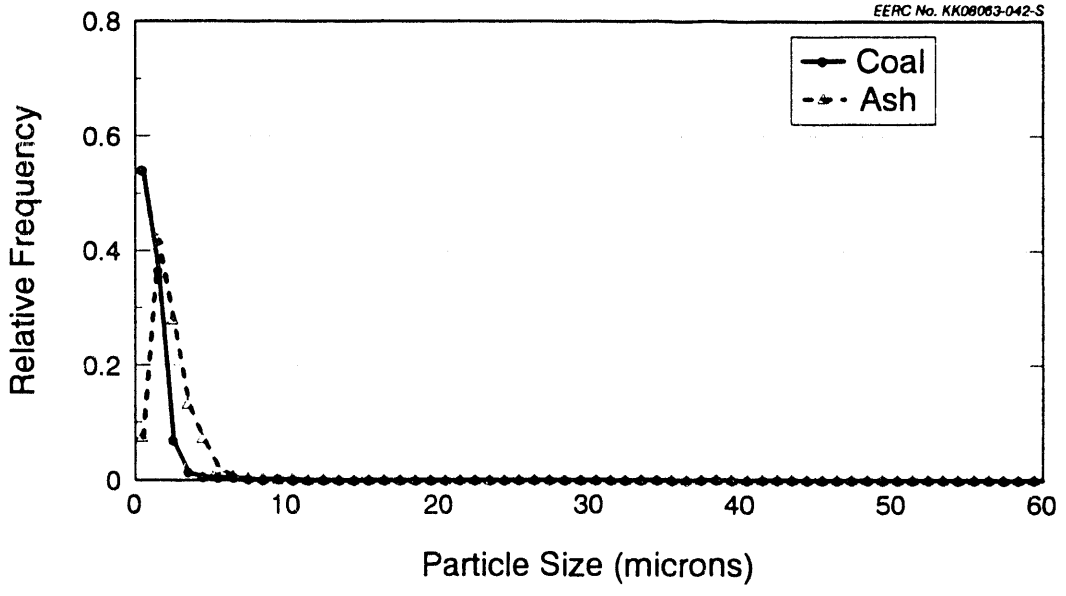

Figure 7d. Particle-size distribution for Sample #26 from the ASHPERT database.

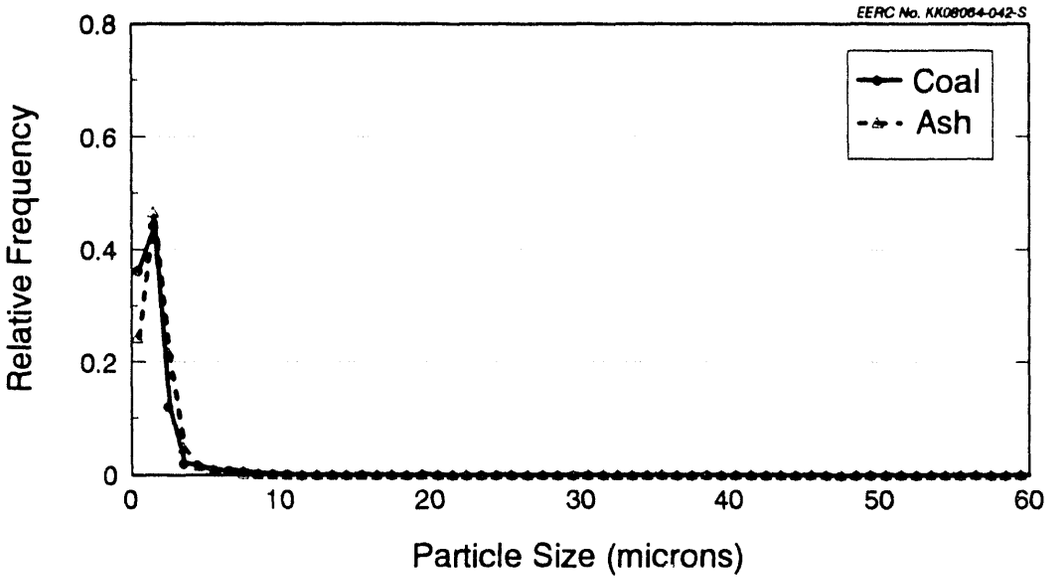

Figure 7e. Particle-size distribution for Sample #37 from the ASHPERT database.

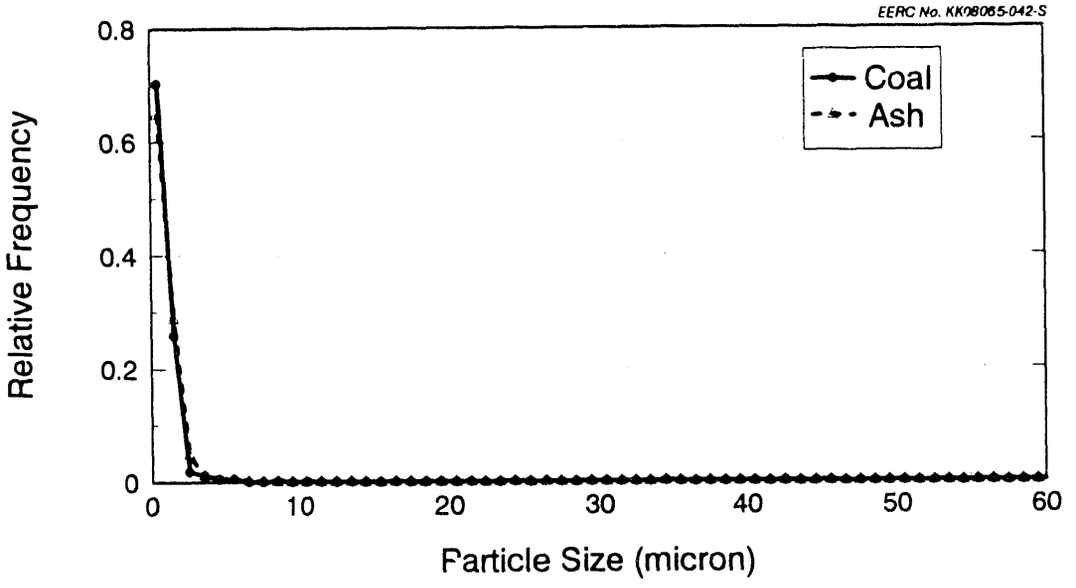

Figure 7f. Particle-size distribution for Sample #42 from the ASHPERT database.

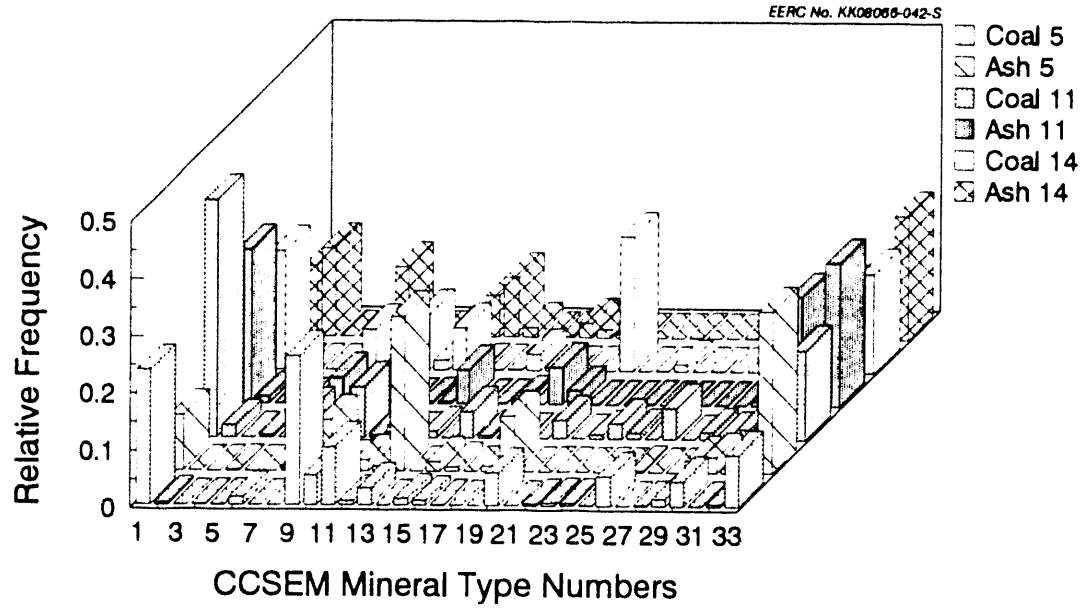

(a) ASHPERT Samples #5, 11, and 14

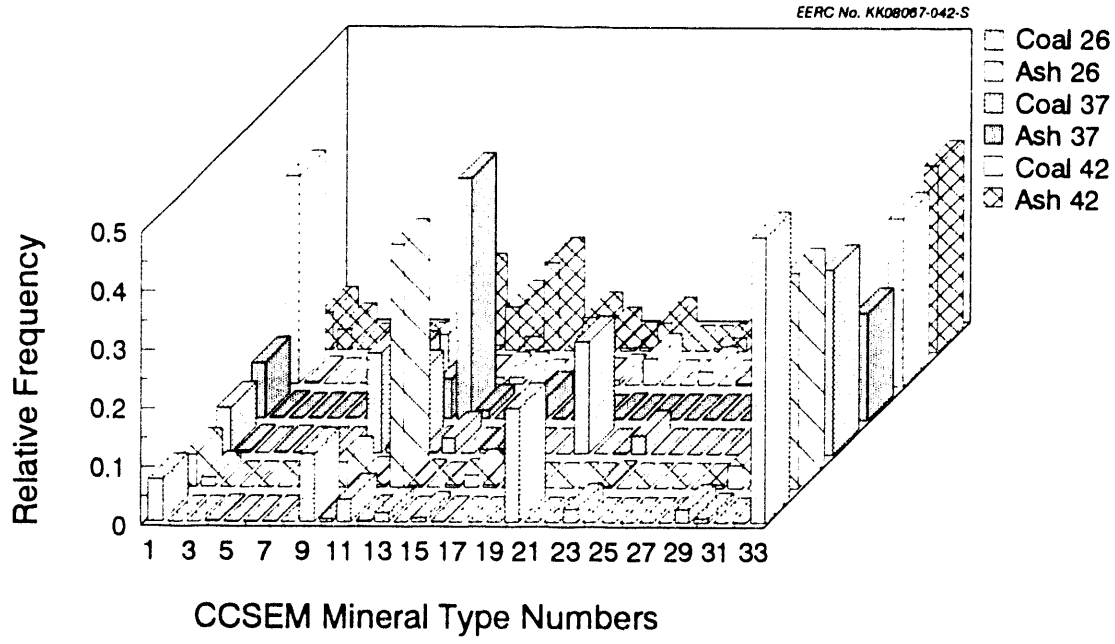

(b) ASHPERT Samples #26, 37, and 42

Figure 8. Mineral frequency distribution for six samples from the ASHPERT database.

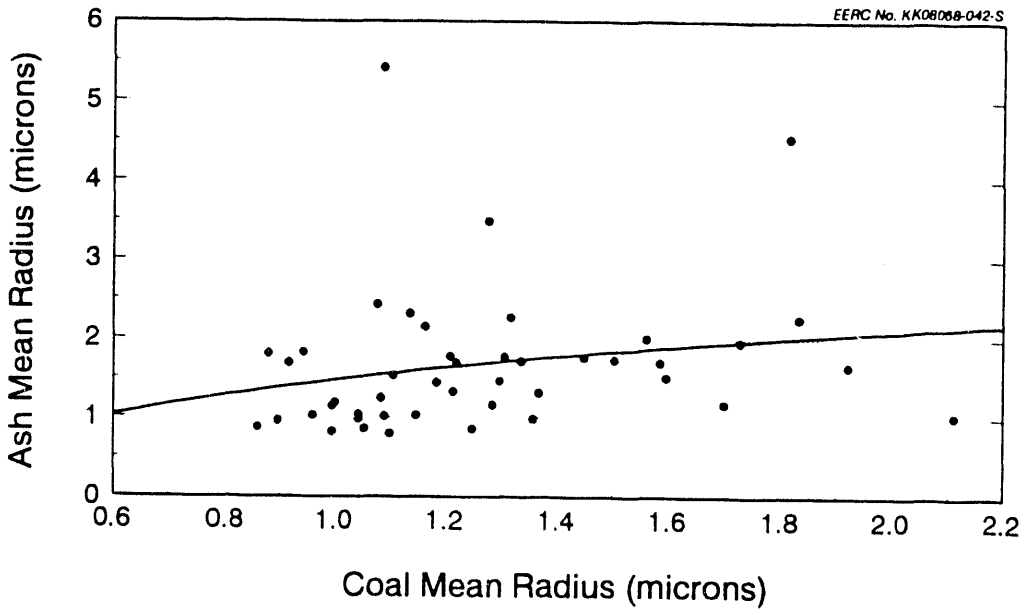

Figure 9. Mean particle radii for coals and corresponding fly ashes.

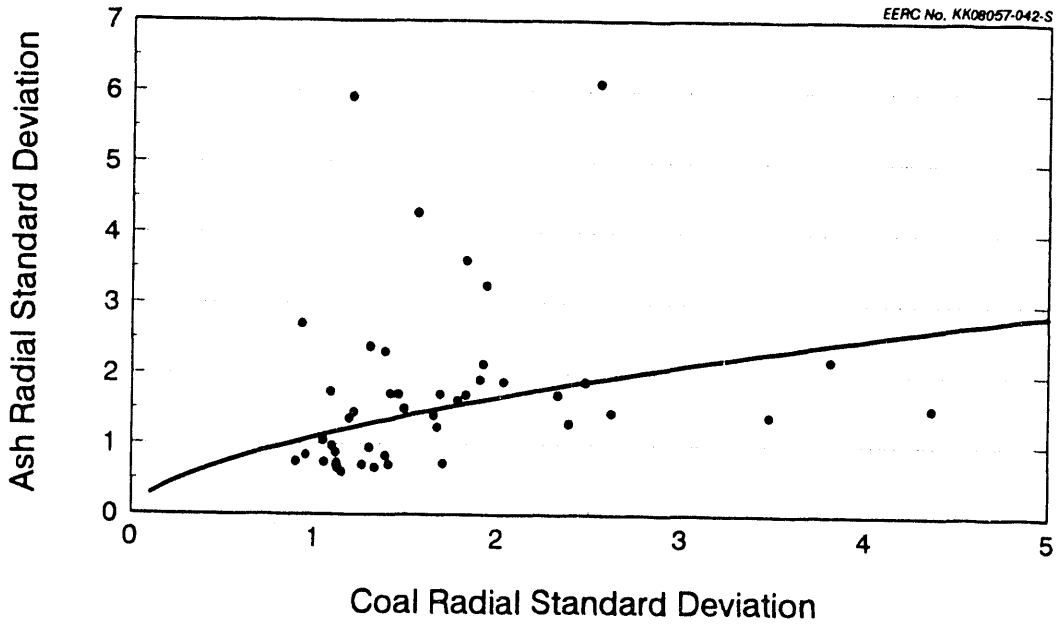

Figure 10. Standard deviations of the particle-size diameter curves for coals and ashes.

exhibit this trend, although there are instances where violations to this trend or "rule" are also observed. Since the continuity of the fly ash PSCD on the coal PSCD is one of the basic rules of ASHPERT (see next section), a more sophisticated analysis of the database to justify this rule will be one of the first tasks to be undertaken in related future work.

3.3.4.3 Implementation of ASHPERT

ASHPERT has been implemented as a loosely knit collection of support programs centered around a supervisory or control program (which is ASHPERT per se). The support programs include the relational database manager module(s), a library of database information specific to the ASHPERT database, postprocessing and data management procedures for proximate, ultimate, XRF, chemical fractionation, and CCSEM analysis data, a set of the more common statistical analysis routines, a dynamic library of inferential rules or methods, and a general purpose inference engine (which can "reason" both by backward and forward chaining). (It must also be noted that since ASHPERT's rules or methods may be complete programs in themselves, ASHPERT may also invoke operating system routines, and other application programs like compilers, linkers, etc.). A broad design philosophy such as this was deemed necessary if ASHPERT was to serve as a useful research tool and be able to evolve in step with its expanding knowledge base and expertise. The experience gained so far from working with ASHPERT has more than amply justified such a design philosophy. For instance, it took less than a week to modify, debug, and link the database routines to manage the restructured and expanded database. A drawback of such an approach, however, is that the program is not user friendly at all: a considerable amount of technical expertise and familiarity with the ASHPERT family of programs is expected of the user.

The dynamic knowledge base or inferential library facility of ASHPERT is especially useful in understanding, correlating, and extracting patterns in the data. Goals can be set on the fly, depending perhaps on the results of previous goals. Parameters can be altered dynamically and extensive simulations and "what-if" scenarios executed. For example, the MFD of a coal can be transformed to a hypothetical fly ash MFD depending on user-specified rules on how the transformation is to be performed. Such "rules," as mentioned earlier, may be entire procedures or programs (in C++): ASHPERT will simply compile, link, and execute these programs. As another example, one may ask for all possible ways of transforming a coal MFD to its fly ash MFD. A useful result of such simulations, which are very time-consuming, is an understanding of the relative importance of the various modes--coalescence, fragmentation, surface recession, etc.--of transformation. Additionally, the results of such "data reduction" and exploratory goals can be appended to its knowledge base, adding to the expertise of the system.

One of the design goals of ASHPERT was, of course, an "expert" for predicting fly ash PSCDs from the parent coal's PSCD. This particular goal is thus an intrinsic or inbuilt goal in ASHPERT and can be invoked or "sought" whenever desired. Since the basic or primary assumption in PSCD evolutionary models is that identical coals, combusted under identical conditions, will behave identically, the key issue in formulating a set of rules for this goal is "when can a coal be considered not identical to another ?" Rephrasing this question as "when is a coal a 'neighbor' or "is in the neighborhood" of another coal ?" it becomes clear that what is needed as "rules" is a

specification of a topology on the set C of all coals. Such a topology must reflect the intrinsic granularity or particulate nature of coals as well as their redistributions upon being transformed into fly ash. To this end, quite a few topologies have been implemented and tested. The PSD, EDF, and PSCD topologies described and tested in Ramanathan (15) were somewhat disappointing, with the predicted values in error by as much as 22.5%. A retest of these topologies with the expanded database did reduce the error, but only down to about 18%. An intense and fairly exhaustive statistical analysis of the database revealed surprisingly strong correlations between the coal MARS and fly ash MARS, where MARS (Mineral And (mean) Radius Space) is defined to be the subset:

$$\text{MARS} = \left\{ (m_1, \ldots, m_p, \mu, \sigma) \;\middle|\; \begin{array}{l} m_1 \geq 0, \ldots, m_p \geq 0, \; m_1 + m_2 + \ldots + m_p = 1 \\ \mu = \text{Mean (PSD)}, \; \sigma = \text{Std. Dev. (PSD)} \end{array} \right.$$

The MARS subset is thus seen to be the Cartesian product of the MFD vector with the PSD vector, with the latter being characterized by its mean radius and standard deviation. The simplest transformation model relating the coal MARS with the fly ash MARS subsets is, of course, the linear (or, more precisely the affine) transformation model. That is, we hypothesize that there exists a linear (affine) (and, hence, continuous) operator

$$T: \text{MARS(Coals)} \longrightarrow \text{MARS(Ash)}$$

mapping coals to their corresponding fly ashes. In order to determine the operator T, an overdetermined system of linear equations with multiple right hand sides needs to be solved. An l_2 - norm minimizing solution has been obtained. Figures 11 and 12 show the experimental versus predicted scatter plots for the fly ash PSD mean radius and standard deviation, respectively. There is very little scatter in the plots: the experimental and predicted values agree very well, with an average error of about 5%. Parts (a-d) of Figure 12 show the experimental versus predicted fly ash mineral (relative) frequencies for the mineral types 1 (quartz), 9 (kaolinite), 20 (pyrite), and 33 (amorphous), respectively. Once again, very little scatter appears, and the largest average error is only about 8%. This MARS topology, together with the linear transformation model, is clearly seen to be the best of all the topologies and transformation models tested so far.

3.3.4.4 Prediction of Composition and Size for Unknown Coal

The predictive capabilities of ASHPERT were tested using the subbituminous Dietz coal from the Powder River Basin in Montana. Its composition, as determined using standard bulk and CCSEM analysis, is shown in Table 2. Ash was produced in the EERC DTF. Composition and size distributions of the drop-tube ash, as measured using CCSEM, was compared with the same data produced by ASHPERT. Figure 13 illustrates the experimental and predicted CCSEM phase compositions for the Dietz ash, on a frequency basis. The 33 phases identified using CCSEM (and also predicted with ASHPERT) are presented along the horizontal axis. There is a strong correlation between the measured and predicted phases in the Dietz fly ash. Major correlated phases include quartz (type 1), kaolinite (type 9), Ca-Al silicate (type 13), Ca aluminate (type 19), and the unknown/mixed category (type 33). Figure 14 shows the experimental and predicted size distribution frequencies. The size

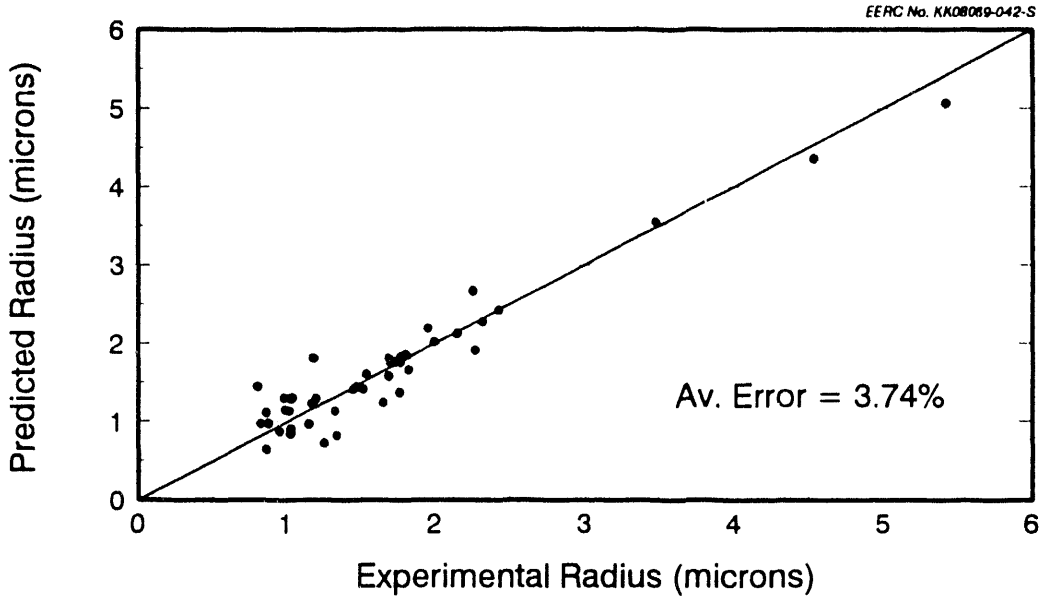

(a) Mean radii

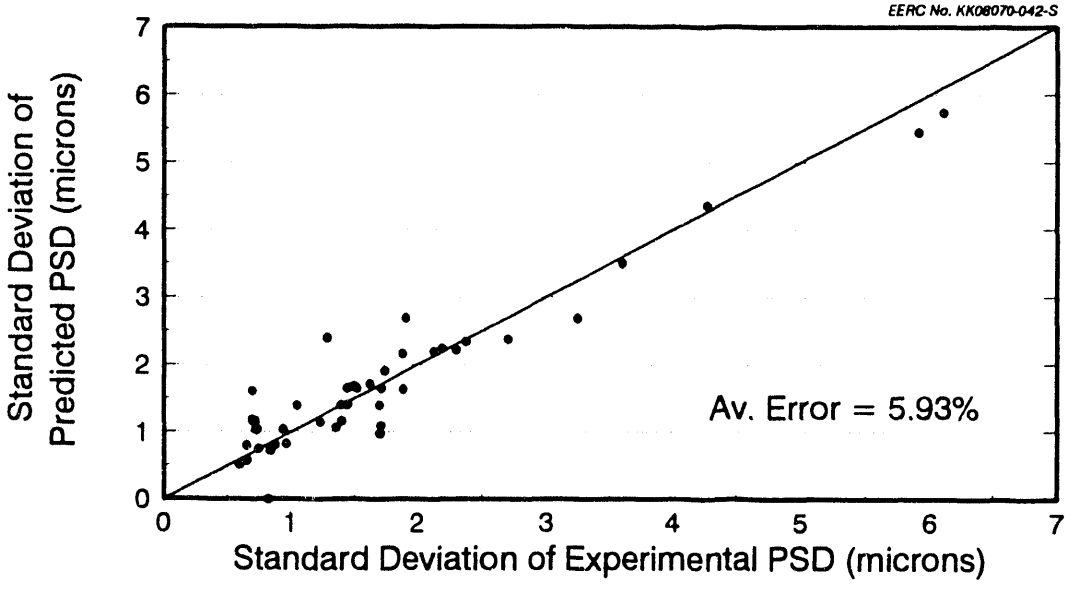

(b) Standard deviations

Figure 11. Experimental and predicted fly ash particle-size distributions.

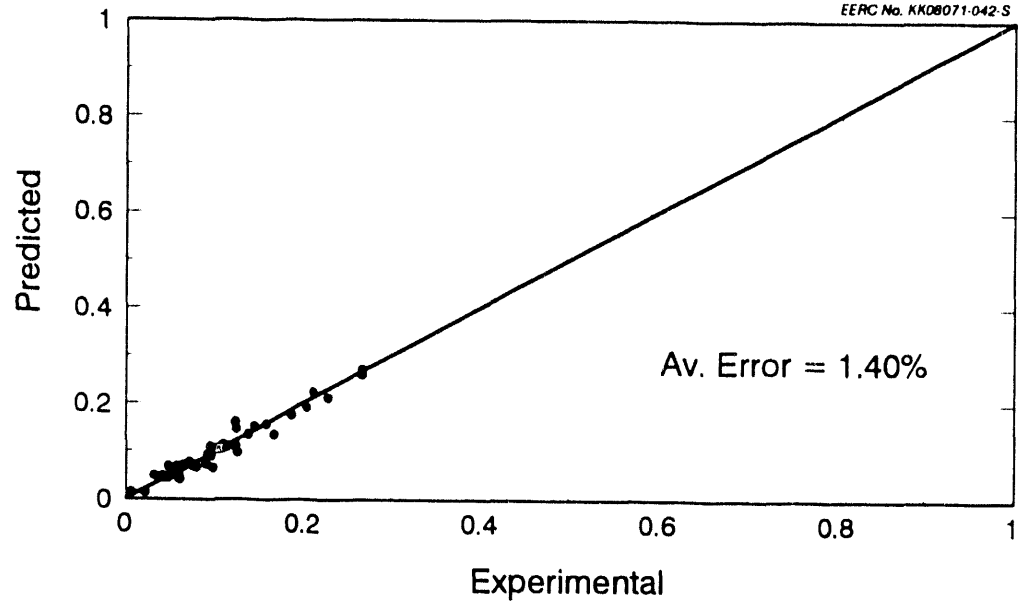

Figure 12a. Experimental and predicted particle-size distribution for quartz.

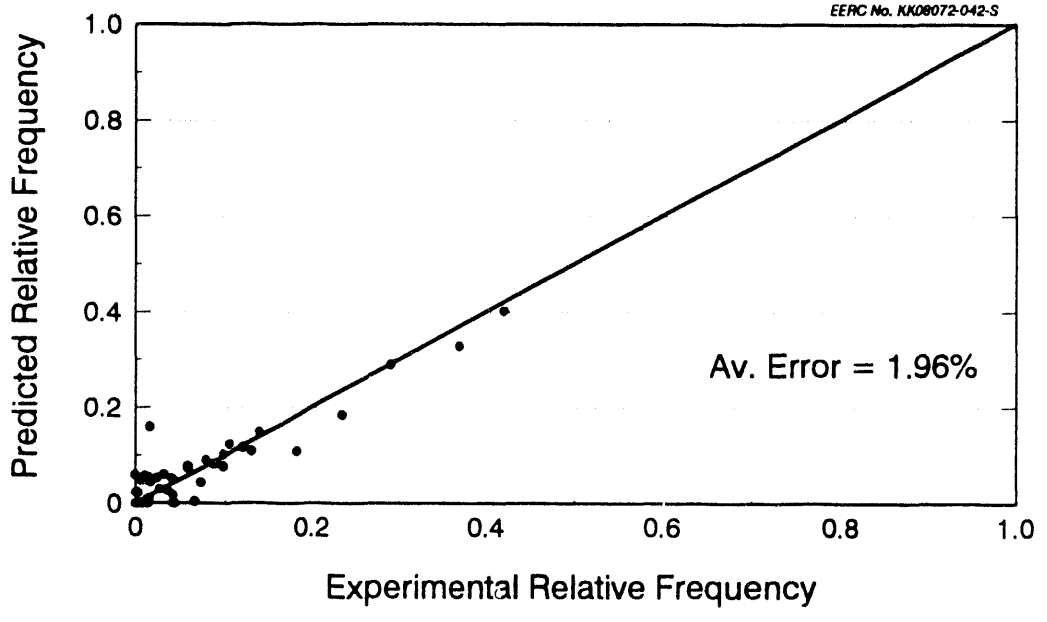

Figure 12b. Experimental and predicted particle-size distribution for kaolinite.

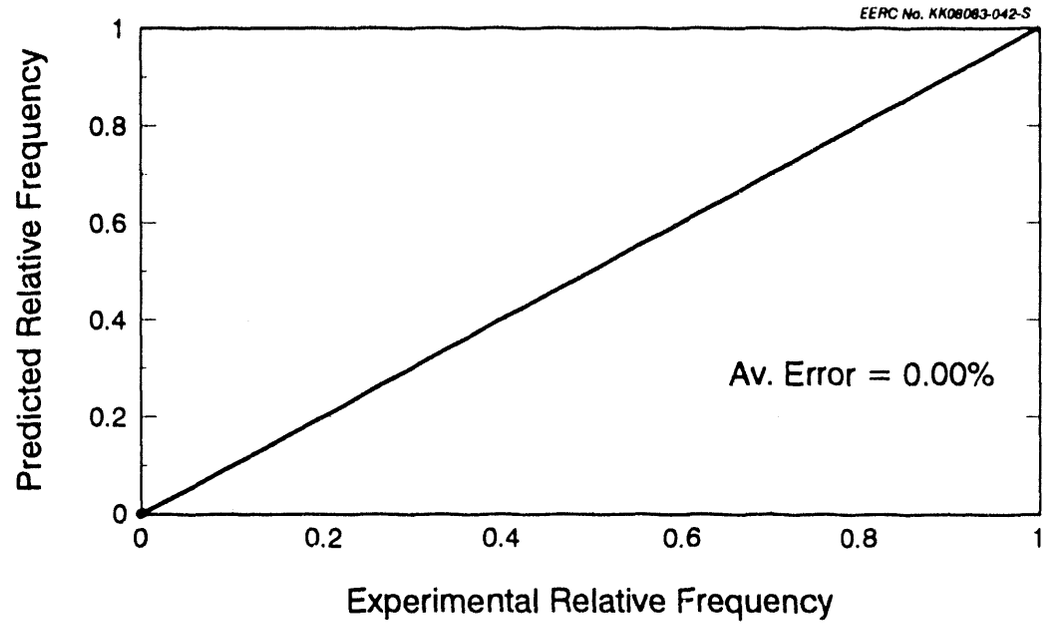

Figure 12c. Experimental and predicted particle-size distribution for pyrite.

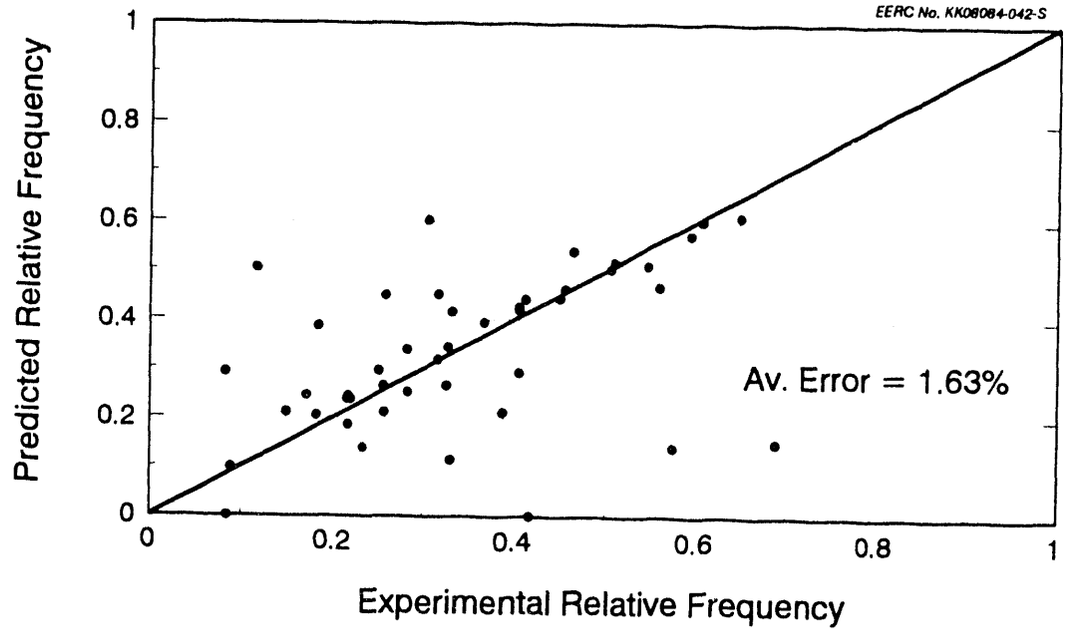

Figure 12d. Experimental and predicted particle-size distributions for "amorphous" type.

TABLE 2

Composition of Dietz Subbituminous Coal

Parameter	Wt%
Proximate	
Moisture	23.66
Volatiles	31.95
Carbon	40.31
Ash	4.08
Ultimate	
Hydrogen	3.78
Carbon	54.91
Nitrogen	0.68
Sulfur	0.38
Oxygen	12.47
Ash	4.08
Oxides	
SiO_2	36.0
Al_2O_3	20.8
Fe_2O_3	4.9
TiO_2	2.2
P_2O_5	0.7
CaO	13.3
MgO	4.5
Na_2O	2.2
K_2O	0.3
SO_3	14.9
Minerals	
Quartz	30.8
Kaolinite	35.4
Montmorillonite	5.9
Aluminosilicate	2.1
Pyrite	11.7
Unknown	5.6
Total Minerals	3.2

distributions do not correlate as well as the phase composition data. The size distribution predicted by ASHPERT is skewed toward large particle sizes, suggesting the Dietz coal contains fine particulates (including organically associated material) which was not sufficiently described in the ASHPERT database. This problem will be mitigated by expansion and improvement of the database.

3.3.4.5 Conclusions

The ASHPERT expert system with a database of 45 coals and ashes has been tested using four different topologies and two different transformation models. The MARS topology with the linear transformation model appears to be the best rule combination, with an average error of 8%. The diversity of the ASHPERT database enables the program to be used in modeling a wide range of combustion systems.

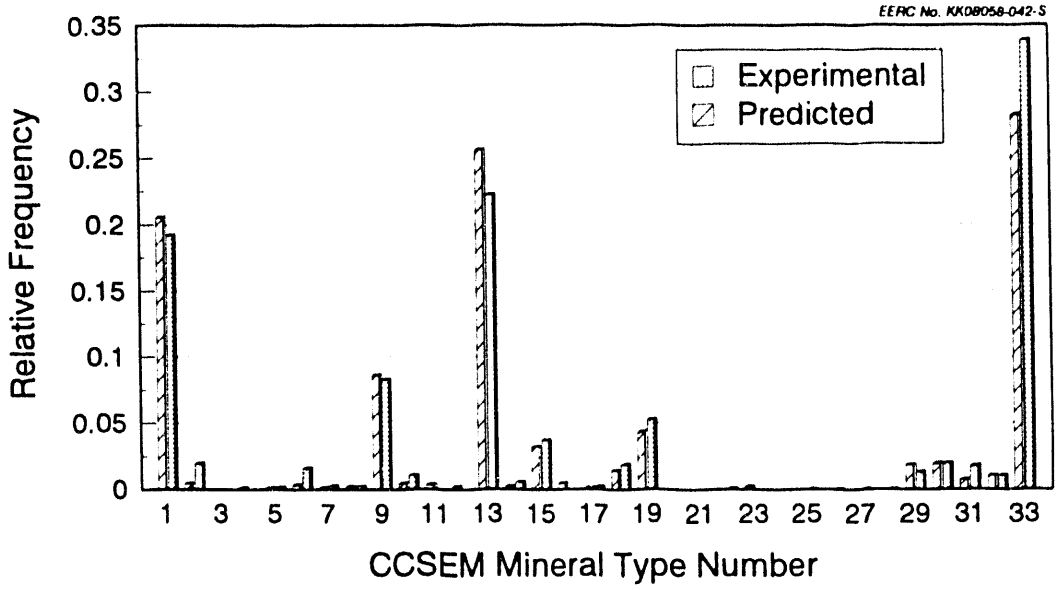

Figure 13. Experimental and predicted CCSEM phase composition for Dietz coal ash, on a frequency basis.

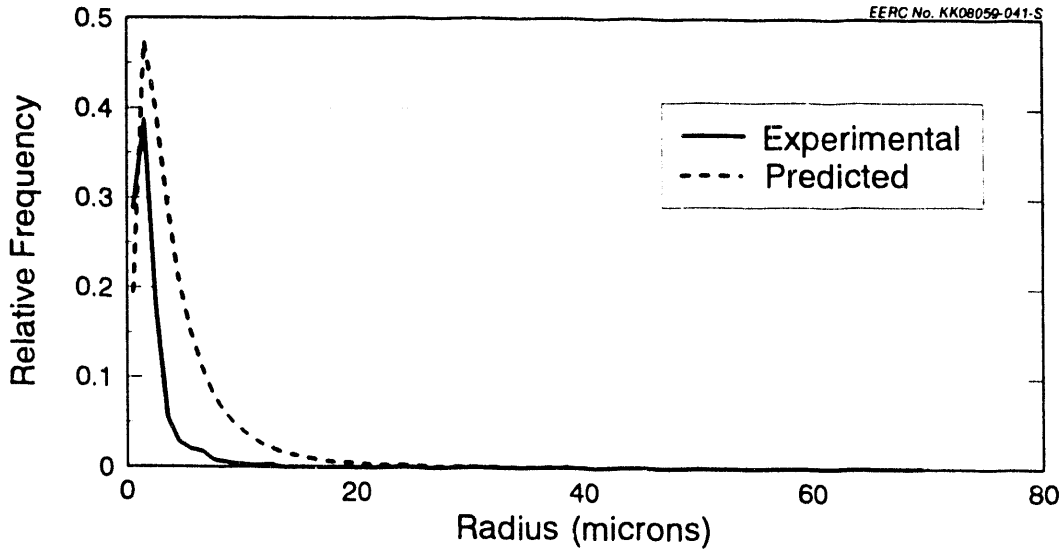

Figure 14. Experimental and predicted particle-size distribution for Dietz coal ash, on a frequency basis.

4.0 TASK 2: LABORATORY-SCALE COMBUSTION TESTING

4.1 Introduction

Coals contain a variety of inorganic species including significant quantities of both organically associated cations and discrete minerals. Problems associated with inorganic constituents in coal combustion systems include ash deposition, formation of fine particulates, and corrosion and erosion of boiler parts. Of specific interest are the interactions between those inorganic constituents that result in the formation of low melting point phases during combustion and gas cooling. These phases are often the cause of ash deposition problems on boiler heat-transfer surfaces. The formation of low melting point phases results from complex physical and chemical transformations of inorganic components of coals during combustion. The transformations of the inorganic constituents depend upon their association in the coal and upon combustion conditions. Volatilization and condensation of sodium is being investigated using DTF experiments in order to gain insight into the formation of liquid phases in and on the surfaces of entrained ash particles. The primary goal of this task is to determine the factors affecting the size and composition of fly ash particles.

4.2 Equipment and Procedures

4.2.1 Drop-Tube Furnace System

The DTF is a laboratory-scale, entrained flow, tube furnace used to combust coal and produce ash under closely controlled conditions. Combustion parameters such as initial hot zone temperature, residence time, and gas cooling rate can be closely controlled and monitored.

The furnace system, shown in F 5, is housed in a three-floor laboratory specifically designed fc and efficient operation of the system. The furnaces are mounted o ce bars extending through all three levels and can be moved to accommodate specific applications. The adjoining control room provides a clean, climate-controlled environment for the electronic equipment associated with the drop-tube system.

The furnace assembly consists of a series of vertical tube furnaces illustrated in Figure 16. These furnaces possess a total of four independently controlled, electrically heated zones. Each of these furnaces can be used separately or in conjunction with the others. This allows for maximum flexibility and precise control over combustion conditions.

Coal and primary and secondary air are introduced into the furnace system by means of a preheat injector. This system injects primary air and coal into the furnace at ambient temperature from a water-cooled probe assembly at the center of the tube. Secondary air is typically heated to 1000°C and introduced into the furnace through a mullite flow straightener. Thus the material to be combusted is introduced into the top of the furnace, along with preheated secondary air, and travels down the length of the furnace in a laminar flow regime. Various sampling probes or collection devices can be used with the DTF to collect ash samples. Downstream of the sampling probe and collection filter, the combustion gas is cooled and passes through a filter before entering a diaphragm pump. The pump is designed so that no air can leak into the sampling gas. The gas leaving the positive pressure side of

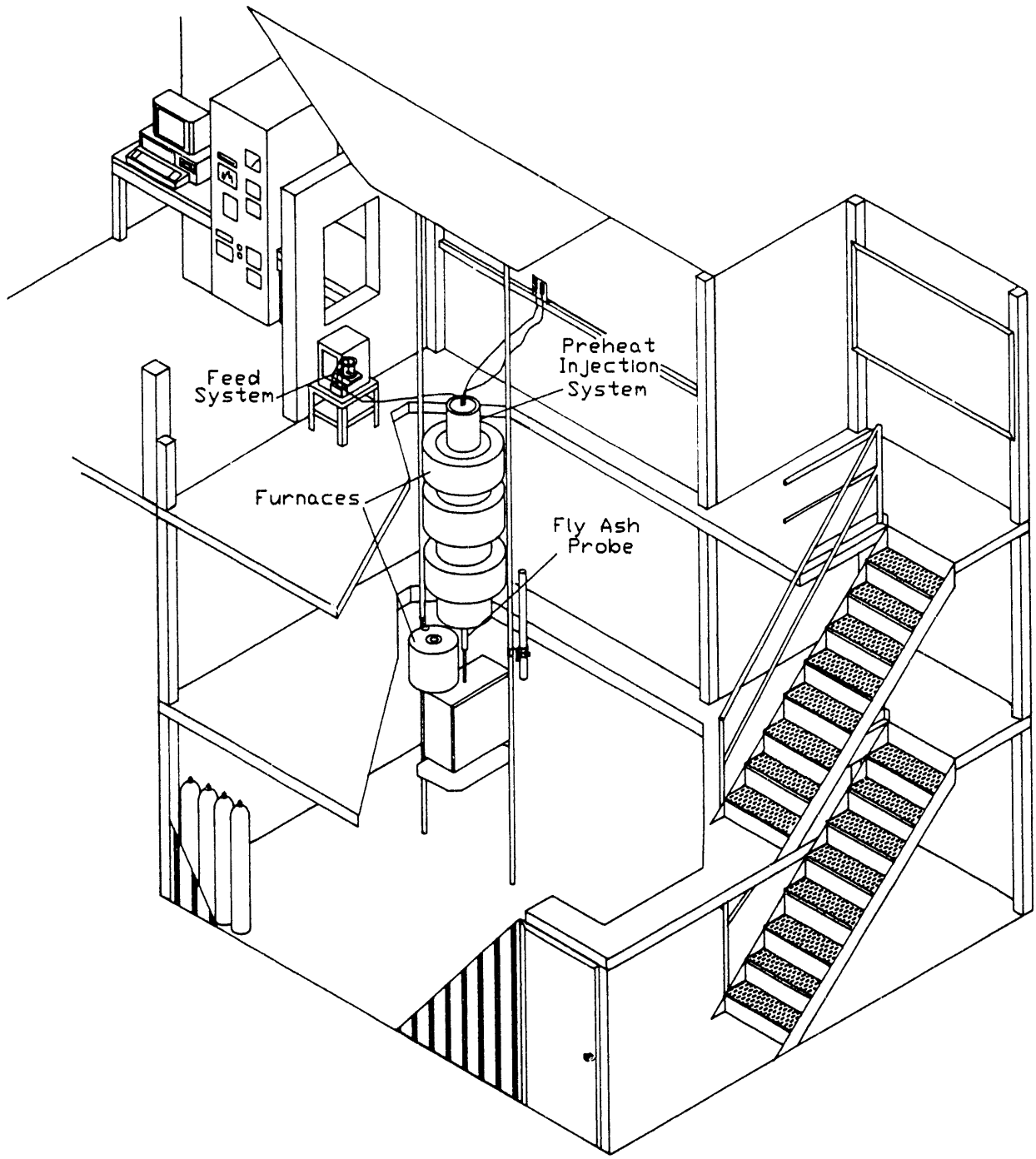

Figure 15. Drop-tube furnace facility.

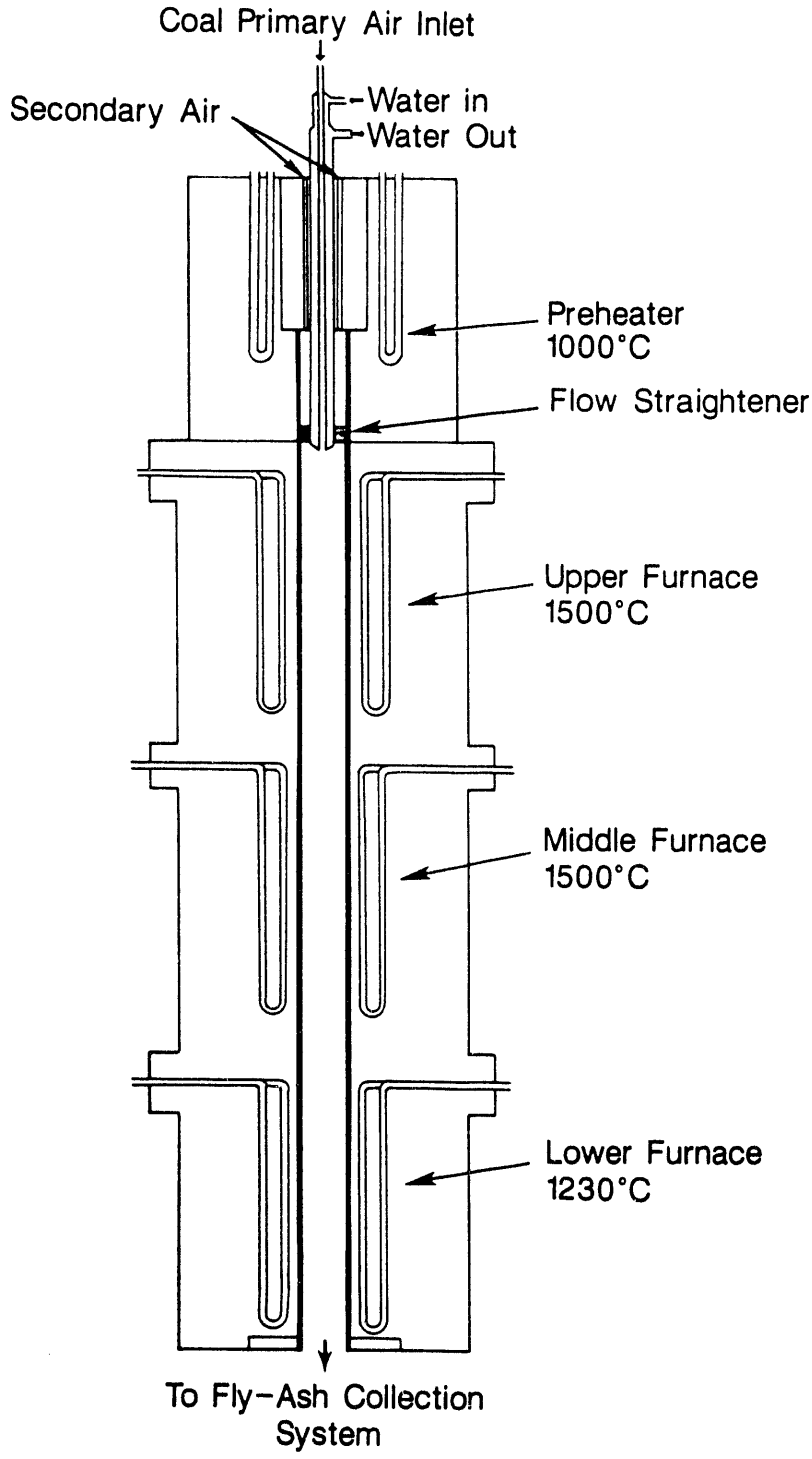

Figure 16. Cross-sectional diagram of the drop-tube furnace.

the pump is passed through a flowmeter, which measures the volume of gas being pulled through the probe. After the flowmeter, part of the gas is directed through carbon monoxide, carbon dioxide, and oxygen analyzers. The concentrations of these gases can be read directly from the digital displays on the analyzers. The analog output signals from the analyzers are routed both to a chart recorder and to an A to D board on a personal computer (PC). The gas concentrations and the coal feed rates obtained from the coal feed system are logged by the PC for data interpretation. The configuration of this system is shown in Figure 17.

The coal feed system is designed to feed particles of various sizes in the pulverized coal range at rates of 0.05 to 0.5 g per minute and at primary carrier gas rates of approximately one liter per minute. The basic apparatus, shown in Figure 18, consists of a pressurized cylinder into which a container filled with coal is placed. A rotating brush and stirrer attached to a variable-speed motor feeds the coal from the container into a funnel where it is transported through the feed tubing into the furnace injector by the carrier gas. The coal feeder is mounted on a Mettler PM 2000 top-loading balance that is accurate to 0.01 gram. It is equipped with a RS232C interface which allows real-time coal feed rates to be read and stored on a PC.

A short residence time probe is used to collect ash samples at any residence length. The probe consists of four concentric, water-cooled, steel tubes. The outer shell is used to introduce the quench gas at the top of the probe. The combustion products pass through the innermost shell, and the remaining shells carry the cooling water. The probe is covered with an alumina insulating cylinder with an outer diameter of two inches (Figure 19).

The probe is inserted into the bottom of the furnace at a set distance calculated from the desired residence time. The quench gas and the vacuum are turned on. The coal is fed through the preheat injector, the combustion products are quenched upon entering the probe, and the residue char or ash is collected on a filter attached to the probe's innermost shell.

A fly ash quenching probe, shown in Figure 20, can be attached to the bottom of the DTF to cool the fly ash before collection. The system is reliable and versatile. Several collection devices can be added to the probe to collect fly ash.

The Environmental Protection Agency Southern Research Institute six-stage cyclone (EPAFSC) is used routinely to collect fly ash (Figure 21). The EPAFSC is designed to make six equally spaced particle-size cuts (d_{50}) on a logarithmic scale within the range of 0.1- to 10-millimeters diameter. The advantage of this system is that it can be used to collect the relatively large amounts of sample needed for chemical and morphological analysis.

In addition to the EPAFSC, the University of Washington Mark 5 source test cascade impactor (STCI) is used during selected combustion tests. The STCI was developed as a means of measuring the size distribution of particles in stacks and ducts at air pollution emission sources. The Mark 5 impactor produces size cuts of fly ash particles by inertial separation. These data are used for comparison with the EPAFSC data to provide more detailed information concerning the effects of combustion conditions on the size distribution of the fly ashes.

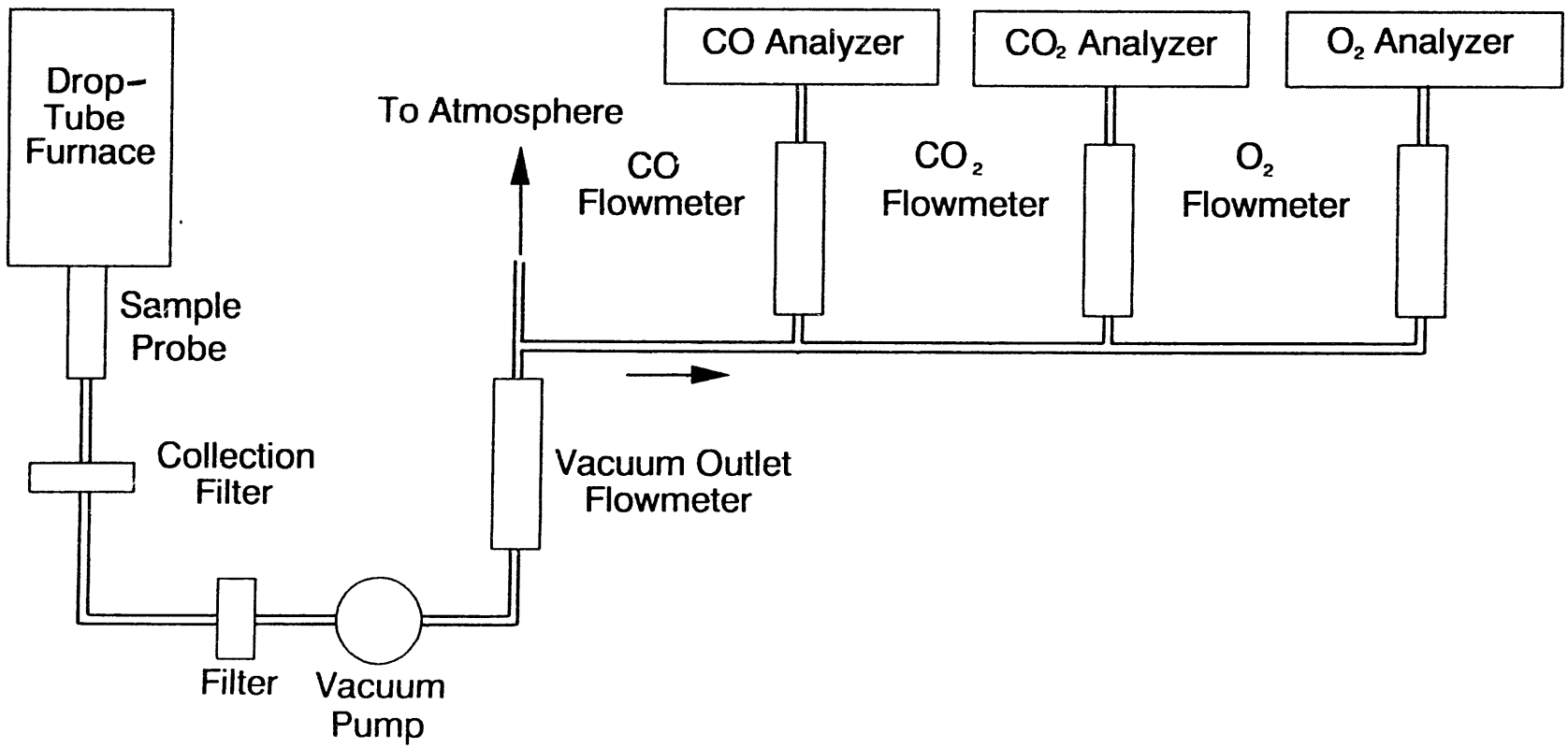

Figure 17. Configuration for sampling.

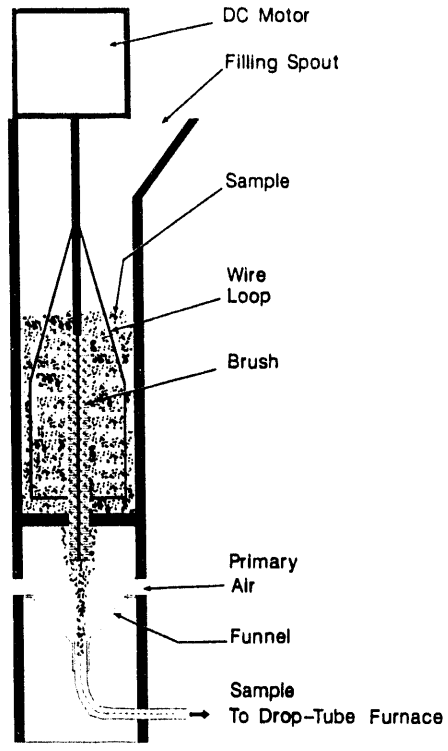

Figure 18. Drop-tube furnace coal feeder.

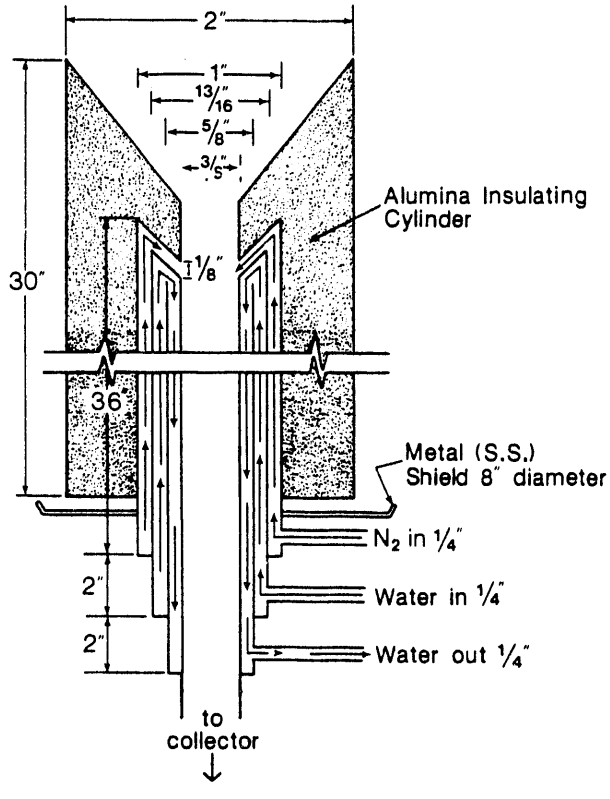

Figure 19. Short residence time probe.

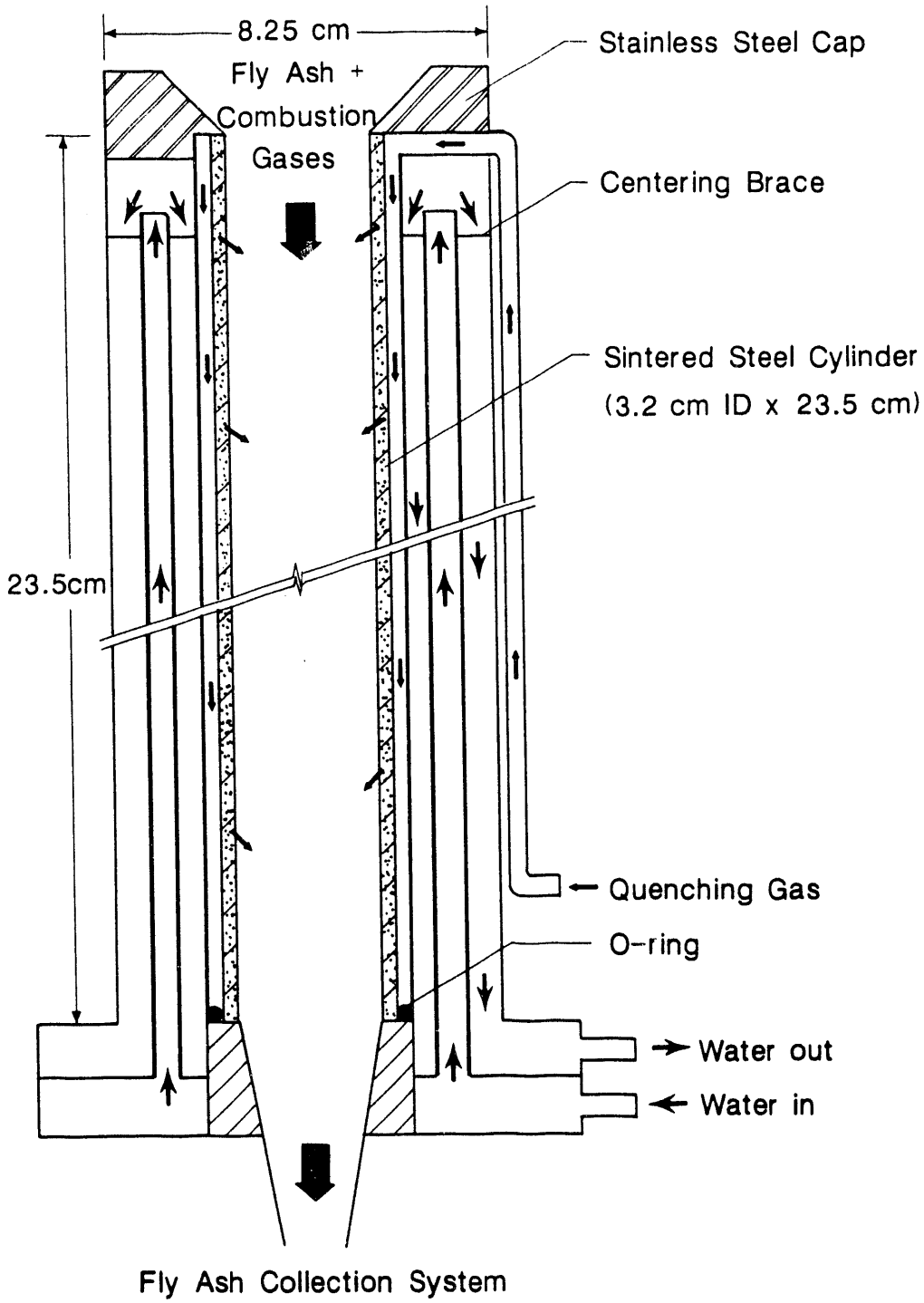

Figure 20. Fly ash quenching probe.

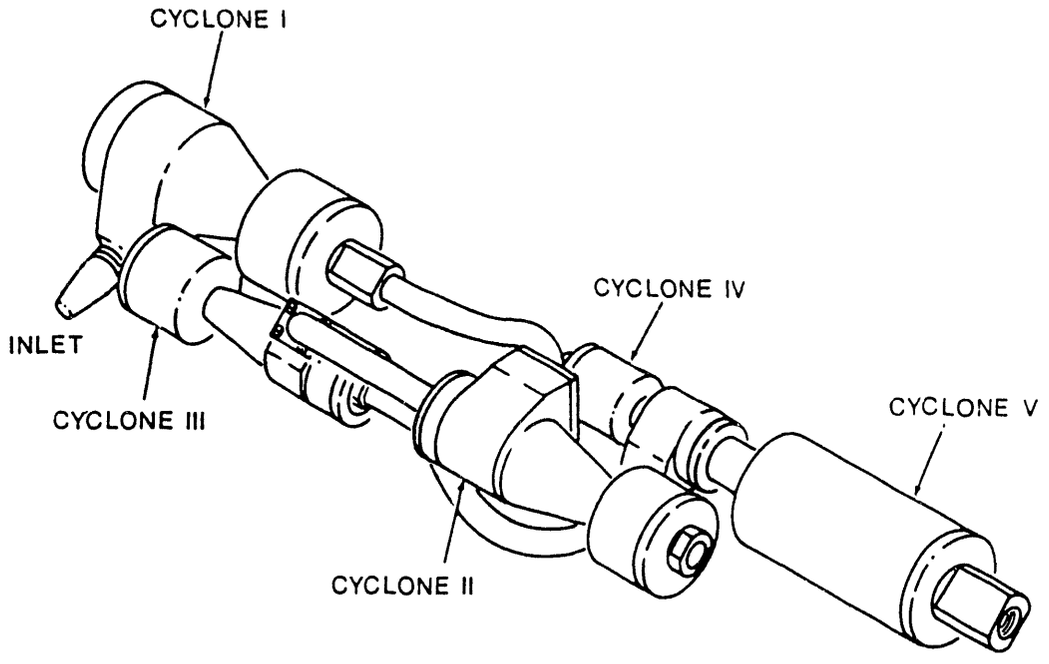

Figure 21. Six-stage multicyclone.

4.2.2 Determination of Carbon Conversion

The thermogravimetric analysis (TGA) determination of carbon conversion by the ash tracer method is performed on a small (approximately 50 mg) sample of the collected char giving information similar to that of a proximate analysis. The sample is heated in an argon atmosphere from ambient temperature up to 900°C. Weight loss from the sample between ambient and 110°C and from 110° to 900°C are reported as "moisture" and "volatile matter," respectively. Air is then introduced to combust the sample, and the resultirg weight loss reported as "combustibles." The weight of the remaining residue is reported as "ash."

The use of bulk ash as a tracer to determine carbon loss is based on the assumption that there is no significant volatilization or loss of ash during TGA. From a similar TGA or proximate analysis of the parent coal, the percentage of ash in the parent coal has also been determined. It is assumed that the amount of ash has not changed; hence the increase in percentage of ash in the collected char is a measure of the carbon consumed during combustion and calculated by:

$$\% \text{ carbon converted} = 100 \left[1 - \frac{OA}{RA} \frac{RV+RC}{OV+OC} \right] \qquad \text{[Eq. 1]}$$

where OA = % ash in the original coal
RA = % ash in the residue collected
OV = % volatile matter in the original coal
RV = % volatile matter in the residue collected
OC = % combustibles in the original coal
RC = % combustibles in the residue collected

The determination of carbon conversion by TGA using the ash tracer method tends to be relatively inaccurate due to 1) the small quantities of sample used, 2) the assumption that no ash is lost from the sample before analysis, and 3) the insensitivity of the method during the early stage of combustion (0%-25% conversion).

Calculation of carbon conversion by the gas analysis method uses the gas flow rate and the ideal gas law, PV = nRT, to convert the concentrations of CO_2 and CO in the gas stream into molar quantities. The molar feed rate of carbon was calculated from the coal feed rate and the percentage of carbon in the ultimate analysis of the fuel. The equations for the calculation are as follows:

$$\text{moles } CO_2 = (\text{total gas flow rate}) \frac{\frac{\%CO_2}{100} \frac{P}{760 \text{ mm Hg}}}{R \cdot T_k} \qquad \text{[Eq. 2]}$$

$$\text{moles CO} = (\text{total gas flow rate}) \frac{\frac{\%CO}{100} \frac{P}{760 \text{ mm Hg}}}{R \cdot T_k} \qquad \text{[Eq. 3]}$$

where P is the barometric pressure (mm Hg), R is the universal gas constant (0.082 L atm/mole K), and T_K is the gas temperature in Kelvin. The carbon feed rate is calculated by:

$$\text{molar feed rate} = \frac{\% \text{ carbon}}{100} (\text{coal feed rate}) \frac{1 \text{ mole°C}}{12 \text{ g°C}} \qquad \text{[Eq. 4]}$$

and the percent carbon conversion is calculated by:

$$\% \text{ carbon conversion} = \frac{\text{moles } CO_2 + \text{moles CO}}{\text{molar feed rate}} 100\% \qquad \text{[Eq. 5]}$$

Factors that can influence the determination of carbon conversion by gas analysis are 1) decreased gas analyzer sensitivity and a very steep calibration curve for the CO_2 analyzer at low concentrations, 2) accuracy of the coal feed rates, and 3) fluctuations in the vacuum flowmeter which determines how much gas is being sampled (the molar concentrations of CO and CO_2 are based on the liters per minute of gas passing through this flowmeter). This occasionally results in carbon conversion percentages that exceed 100%.

The amount of coal burned was calculated from the weight loss of the coal fed in the DTF. The amount of ash fed is determined from the percent ash in the coal, derived from a proximate analysis, multiplied by the amount of coal fed. The char or residue that is left from the test is collected on a filter and weighed. The percentage of carbon conversion is then calculated by:

$$\% \text{ carbon conversion} = 100 \frac{\text{char collected (g)} - \text{ash (g) fed}}{\text{coal fed (g)} - \text{ash fed (g)} - \text{water fed (g)}} \qquad \text{[Eq. 6]}$$

The calculation of the percentage of coal burned using the weight loss method tends to be higher than that of the percentage of carbon loss determined by the gas analysis method due to the assumption that all of the ash and unburned coal is collected and weighed. In practice, some of the uncombusted material may not reach or be retained on the filter before weighing, resulting in higher conversion values than actually obtained.

4.3 Formulation of Synthetic Coals

4.3.1 Introduction

Synthetic coal model mixtures provide an excellent means of studying inorganic transformations in a physically and chemically controlled system because the complexity of inorganic reactions that occur in real coal systems is minimized. Accurate quantities and sizes of known minerals can be included in a synthetic organic matrix in order to isolate specific reactions and transformations of selected inorganic constituents. A controlled combustion environment, such as a DTF, is used to combust the model mixture. Key phenomena to be studied include fragmentation of the synthetic coal grains and coalescence of the inorganics within the synthetic coal particles.

The goal of the model mixture studies during this past year was to perform combustion testing on three model mixtures, including:

- Sodium-silica-sulfur system (simulation of organically bound Na).
- Calcium-silica-sulfur system (simulation of organically bound Ca).
- Calcium-silica-sulfur system (mineral-bound Ca as calcite).
- Iron-aluminosilicate system (using pyrite and kaolinite).

The purpose of using the Ca-Si-S systems was to demonstrate the differences in interactions between included quartz and 1) Ca that is mineral bound as included calcite, and 2) Ca that is organically bound or dispersed on an ionic level within the organic matrix. The reactions involving Ca, Si, and S during combustion are of particular interest when burning low-sulfur and calcium-rich western U.S. subbituminous coals, since calcium sulfate and calcium silicate phases play important roles in the formation of convective pass ash deposits. The effect of temperature on the particle size and composition distribution of ash produced from included calcite and quartz and organically associated calcium and quartz are of specific interest, as are the reactions of sulfur oxides with the available calcium oxide. Past work (3,16) on a Na(org.)-Si-S system has shown that higher temperatures result in the formation of smaller ash particles, probably due to the fragmentation of the chars. Additional work was conducted on the Na(org.)-Si-S system to add another dimension to the role of organically associated elements in the formation of ash, especially with regard to the formation of low melting point Na sulfates and Na silicates on the surface of quartz particles.

The purpose of studying the Fe-Al-Si system was to examine the interactions between pyrite and an alumina-silica clay. Such minerals have a significant effect on slag viscosity when firing eastern bituminous coals.

4.3.2 Methodology

Preparation of the synthetic coal is modified from Senior (17), as outlined by Erickson (18) and Ludlow and others (16). The procedure for preparing the synthetic coals has been described in detail previously for the organic Na-Si-S, organic Ca-Si-S, and calcite-Si-S synthetic coals (19). The preparation of the Fe-Si-Al synthetic coal is similar. Briefly, the synthetic coal is produced from the product of the polymerization of furfural alcohol in six steps: 1) polymerization of furfural alcohol using p-toluenesulfonic acid as a catalyst, 2) addition of carbon black and intrinsic mineral matter, 3) removal of acetone, 4) high-temperature curing of the polymer, 5) grinding and sizing of the cured polymer, and 6) addition of extrinsic matter.

Each of the synthetic mixtures was comprised of approximately 250 g of unsized coal which was then sonic-sieved to produce approximately 50-g samples of 38- to 106-μm synthetic coal. Since the mineral matter sizes are smaller than the selected coal size fraction, excluded minerals inadvertently produced by the grinding operation are removed by the sizing step.

Two calcium, silica, and sulfur synthetic coal systems were prepared: one system having calcium in the mineral form as 10-μm calcite (Ca[min.]-Si-S) and the other having calcium associated in a simulated organic association as ionically dispersed calcium acetate (Ca[org.]-Si-S). A third system consisted of sodium, silica, and sulfur, with the sodium being associated as sodium benzoate, simulating an organic association (Na[org.]-Si-S). Silica, in all three systems, consisted of 10-μm quartz that was associated within the synthetic coal particles. Sulfur was extraneously added to these model mixtures in an elemental form and was also included in the organic polymer in very small amounts. The calcite particles were added to the organic matrix during polymerization to allow for their incorporation into the synthetic coal particles.

The iron-aluminosilicate synthetic coal system was prepared with iron in the form of pyrite (FeS_2), of mean size 13.5 μm, and kaolinite ($Al_2[Si_2O_5][OH]_4$), of mean size approximately 5 μm, added as intrinsic mineral matter. Aside from the pyrite, a small amount of included sulfur results from the p-toluenesulfonic acid catalyst used. Carbon black equal to approximately 1/3 of the polymer weight was added intrinsically to the model mixtures.

The synthetic coals were combusted in the DTF using a one-furnace configuration. Runs were made for the model mixtures at four temperatures: 900°, 1100°, 1300°, and 1500°C. Varied particle residence time runs of 0.1, 0.2, and 0.8 seconds were performed at 900° and 1500°C on the Ca(org.)-Si-S, Ca(min.)-Si-S, and the Fe-Al-Si coal systems. The combustion ash and chars are being analyzed using CCSEM, Malvern, TGA, and XRD analyses. Carbon conversion rates were calculated for the chars.

Pure pyrite used in the production of the Fe-Al-Si model mixture was also injected into the DTF at 900° and 1500°C using air as the carrier gas and at 1500°C under a nitrogen atmosphere. The residues were collected on a bulk filter and submitted for analysis.

The fly ash collected on the bulk filters was analyzed to determine particle-size and composition distributions using CCSEM (20). Approximately

2000 ash particles were analyzed for each sample using CCSEM. The primary outputs of CCSEM are particle average diameters, particle aspect ratios or shape factors, and particle compositions expressed as normalized x-ray energy counts for twelve major elements. In addition, the x-ray counts are corrected and used to identify inorganic phases using stoichiometric constraints. This allows for comparisons of quantities of specific mineral phases between ash samples. In the case of fly ash, there are very few true minerals; however, particles may have compositions that are close to identifiable phases. The ash samples were prepared and analyzed in two different ways: 1) as whole grain mounts by dispersing them onto a filter which essentially gives a surface analysis of the particles (depth of electron beam penetration was between 1 and 2 μm), and 2) as cross-sectioned epoxy mounts which give an interior analysis of the particle. Malvern sizing, a laser-based particle-sizing technique, was also performed on each of the ash samples, and x-ray diffraction analysis was performed on selected ash samples to verify some of the CCSEM mineral determinations.

4.3.3 Results

4.3.3.1 Inorganic Composition of the Synthetic Coals

The projected quantity of inorganic components in the three synthetic coal model mixtures (on a synthetic coal basis) was compared to the actual levels obtained. The results are summarized as follows:

1. Ca(min.)-Si-S: CaO (5%), S (1%), and SiO_2 (10%), where the calcium was added as limestone during the polymerization along with the SiO_2 to inherently bind it. The sulfur was added extraneously after polymerization. Actual analysis on a synthetic coal basis was CaO (3.5%), S (1.1%), and SiO_2 (11.7%).

2. Ca(org.)-Si-S: CaO (5%), S (1%), and SiO_2 (10%), where the calcium is bound organically, the sulfur was added extraneously, and the SiO_2 was added to the coal during the polymerization to bind it inherently in the coal. The actual analysis on a synthetic coal basis was CaO (0.3%), S (0.6%), and SiO_2 (6.8%).

3. Na(org.)-Si-S: Na_2O (5%), S (1%), and SiO_2 (10%), where the sodium is bound organically by adding Na benzoate, the sulfur was added extraneously, and the SiO_2 was added to the coal during polymerization to inherently bind it in the coal. Actual analysis on a synthetic coal basis was Na_2O (1%), S (0.6%), and SiO_2 (8%).

Some of the sulfur was derived from the catalyst used in the polymerization of the synthetic coal. The sulfur was less than 1%, so additional sulfur was added extraneously to obtain a sulfur level of approximately 1% total. Some problems were encountered in formulating the desired inorganic constituent contents, especially for the mixtures containing organically associated sodium and calcium.

4.3.3.2 Results of the Combustion Tests of the Synthetic Coals

The Na(org.)-Si-S, Ca(org.)-Si-S, Ca(min.)-Si-S, and Fe(min.)-Al-Si synthetic coal systems were fired in the DTF at various temperatures and

residence times to calculate conversion rates. The combustion runs were made for each model mixture at four temperatures: 900°, 1100°, 1300°, and 1500°C. The initial oxygen concentration for testing was set at 21% for all tests. Ash samples were collected and gas analysis recorded during each test. Table 3 shows the run conditions for each test. For each system, at each temperature, ash was collected on a bulk filter at longer residence times of over two seconds. Carbon conversion was calculated from both gas and TGA analyses for these longer residence time runs. Carbon conversion was also determined from the loss of weight of the total amount of coal fed. Table 4 shows the proximate analyses results. Table 5 shows the comparison of carbon conversion calculated from the gas analysis, from TGA results, and from the weight loss method. Varied particle residence time runs of 0.1, 0.2, and 0.8 seconds were also performed at 900° and 1500°C on the Ca(org.)-Si-S, Ca(min.)-Si-S, and Fe(min.)-Al-S systems. Carbon conversion was determined for these tests (Table 5). Table 4 shows the TGA results. The combustion ash and chars were subsequently analyzed using CCSEM, Malvern, TGA, and XRD analyses.

Figure 22 shows the carbon conversion tests as determined by gas analysis at 900°C. Figure 23 shows the carbon conversion at 1500°C. The conversion of the Ca[org]-Si-S system with the organically bound calcium was significantly more rapid than that of the Ca(min.)-Si-S system with the mineral calcium at the lower temperature. About 50% carbon conversion of the Ca-Si-S system (mineral calcite) was not obtained until approximately 2.4 sec. At 1500°C, the organic Ca blend shows greater conversion at the 0.1-second residence time with the mineral Ca blend obtaining the same conversion as the organic Ca blend at approximately 0.5 seconds and thereafter. The Fe(min.)-Al-Si system exhibits essentially the same carbon conversion behavior as the Ca(min.)-Si-S system. The anomalously low conversion for the Fe(min.)-Al-Si material at 1500°C and 0.2-sec residence time is probably an experimental artifact.

The enhanced rate of conversion of the material with the organic calcium is in agreement with previous studies on the effect of organically bound calcium on demineralized lignite chars in which the organic calcium appeared to act as a catalyst to enhance the char-burning rate at lower temperatures (21).

An interesting result is the substantial negative conversions obtained for the Fe(min)-Al-Si chars at 0.1- and 0.2-sec residence time from the TGA analysis method, as seen in Table 4. The percentage of volatile matter and fixed carbon in the 0.1- and 0.2-sec residence time chars is determined to be more than in the starting coal. A possible explanation is the decomposition of pyrite during TGA.

4.3.4 Mineral Transformations in the Synthetic Coals

Table 6 gives a summary of the composition of the Ca(min.)-Si-S synthetic coal ash and combustion ash products, including cross-section and surface CCSEM analyses and XRD crystalline phase identifications. The XRD analysis indicates that the calcite grains have transformed and reacted to produce $Ca(OH)_2$, CaO, anhydrite ($CaSO_4$), and amorphous calcium silicate. The $Ca(OH)_2$ may be a product of CaO reacting with the moisture in air. The amorphous calcium silicate appears to be more prevalent at higher temperatures and is abundant both in the interior and at the surface of the ash particles, possibly an indicator as to the extent of the reaction that has taken place.

TABLE 3

Run Conditions for DTF Synthetic Coal Tests

Test ID	Syn. Coal Type	Res. Time (sec)	DTF Temp. (°C)	O_2 Init. (%)	Feed Rate (g/m)	CO_2 Calc. (%)	CO Calc. (%)	O_2 Calc. (%)	Pri. Flow (L/m)	Sec. Flow (L/m)	Quench Flow (L/m)	Vac. Flow (L/m)	CO_2 Moles (min)	CO Moles (min)	Pb Press (mm Hg)	(Amb.) Temp. (°C)	Carbon Orig (%)	Gas Carbon Conv. (%)
SYN-0391	Ca-Si-S (min.)	0.10	900	21.0	0.092	0.05	0.0368	21.16	0.8	3.2	3.0	7.0	0.0001	0.000059	748.77	24.5	80.34	2.36
SYN-0291	Ca-Si-S (min.)	0.20	900	21.0	0.102	0.10	0.0543	20.68	0.8	3.2	3.0	7.0	0.0002	0.000088	748.77	24.5	80.34	3.64
SYN-0191	Ca-Si-S (min.)	0.80	900	21.0	0.095	0.04	0.0221	20.84	0.8	3.2	3.0	7.0	0.0001	0.000036	748.77	24.5	80.34	1.54
SYN-2591	Ca-Si-S (min.)	0.80	900	21.0	0.107	0.19	0.0562	20.64	0.8	3.2	3.0	7.0	0.0003	0.000091	748.77	24.5	80.34	5.46
SYN-0491	Ca-Si-S (min.)	2.89	900	21.0	0.083	3.55	0.0037	17.88	0.8	3.2	3.0	7.0	0.0056	0.000006	732.17	25.5	80.34	100.66
SYN-0591	Ca-Si-S (min.)	2.68	1100	21.0	0.089	3.82	0.0000	17.39	0.8	3.2	3.0	7.0	0.0061	0.000000	734.48	23.5	80.34	101.86
SYN-0791	Ca-Si-S (min.)	2.47	1300	21.0	0.103	4.16	0.0001	17.23	0.8	3.2	3.0	7.0	0.0065	0.000000	730.34	26.0	80.34	94.55
SYN-1091	Ca-Si-S (min.)	0.10	1500	21.0	0.105	0.55	0.0735	20.19	0.8	3.2	3.0	7.0	0.0009	0.000114	728.73	28.0	80.34	13.87
SYN-0991	Ca-Si-S (min.)	0.20	1500	21.0	0.093	1.74	0.1663	19.37	0.8	3.2	3.0	7.0	0.0027	0.000258	728.73	28.0	80.34	47.68
SYN-0891	Ca-Si-S (min.)	0.80	1500	21.0	0.110	4.77	0.0070	16.60	0.8	3.2	3.0	7.0	0.0074	0.000011	728.73	28.0	80.34	100.70
SYN-0691	Ca-Si-S (min.)	2.28	1500	21.0	0.097	3.82	0.0000	17.58	0.8	3.2	3.0	7.0	0.0061	0.000000	736.06	25.0	80.34	93.19
SYN-2491	Ca-Si-S (org.)	0.10	900	21.0	0.100	0.37	0.1295	20.55	0.8	3.2	3.0	7.0	0.0006	0.000206	744.82	28.0	91.13	10.36
SYN-2391	Ca-Si-S (org.)	0.20	900	21.0	0.094	0.17	0.0744	20.70	0.8	3.2	3.0	7.0	0.0003	0.000118	744.82	28.0	91.13	5.52
SYN-2291	Ca-Si-S (org.)	0.80	900	21.0	0.096	3.49	0.1129	17.98	0.8	3.2	3.0	7.0	0.0055	0.000179	744.82	28.0	91.13	78.55
SYN-1391	Ca-Si-S (org.)	2.37	900	21.0	0.099	3.79	0.0018	21.00	0.8	3.2	3.0	7.0	0.0060	0.000003	738.49	26.0	91.13	79.93
SYN-1491	Ca-Si-S (org.)	2.27	1100	21.0	0.112	4.63	0.0000	17.01	0.8	3.2	3.0	7.0	0.0073	0.000000	738.28	27.0	91.13	86.06
SYN-1591	Ca-Si-S (org.)	2.15	1300	21.0	0.100	4.19	0.0000	17.53	0.8	3.2	3.0	7.0	0.0066	0.000000	737.97	28.0	91.13	87.11
SYN-2191	Ca-Si-S (org.)	0.10	1500	21.0	0.089	1.47	0.1085	19.64	0.8	3.2	3.0	7.0	0.0024	0.000174	745.74	25.0	91.13	37.58
SYN-2091	Ca-Si-S (org.)	0.20	1500	21.0	0.112	2.65	0.1418	18.72	0.8	3.2	3.0	7.0	0.0043	0.000228	745.74	25.0	91.13	52.78
SYN-1991	Ca-Si-S (org.)	0.80	1500	21.0	0.103	4.77	0.0026	16.59	0.8	3.2	3.0	7.0	0.0075	0.000004	744.74	29.0	91.13	96.48
SYN-1891	Ca-Si-S (org.)	2.03	1500	21.0	0.106	4.53	0.0000	16.93	0.8	3.2	3.0	7.0	0.0072	0.000000	741.56	26.0	91.13	89.88
SYN-1191	Na-Si-S	2.49	900	21.0	0.105	4.04	0.0018	17.30	0.8	3.2	3.0	7.0	0.0064	0.000003	731.60	26.0	85.04	85.40
SYN-1291	Na-Si-S	2.37	1100	21.0	0.105	4.10	0.0000	17.18	0.8	3.2	3.0	7.0	0.0064	0.000000	732.40	28.0	85.04	86.41
SYN-1691	Na-Si-S	2.23	1300	21.0	0.095	4.20	0.0000	17.50	0.8	3.2	3.0	7.0	0.0066	0.000000	737.97	28.0	85.04	98.21
SYN-1791	Na-Si-S	2.09	1500	21.0	0.108	4.60	0.0000	16.89	0.8	3.2	3.0	7.0	0.0072	0.000000	738.00	30.0	85.04	94.06
SYN-3191	Fe-Al-Si	0.10	900	21.0	0.102	0.01	0.0119	20.80	0.8	3.2	3.0	7.2	0.0000	0.000018	739.48	32.0	84.02	0.49
SYN-3091	Fe-Al-Si	0.20	900	21.0	0.100	0.01	0.0035	20.84	0.8	3.2	3.0	7.2	0.0000	0.000005	739.48	32.0	84.02	0.28
SYN-2991	Fe-Al-Si	0.80	900	21.0	0.100	0.01	0.0087	20.79	0.8	3.2	3.0	7.2	0.0000	0.000014	739.48	32.0	84.02	0.46
SYN-3291	Fe-Al-Si	3.55	900	21.0	0.101	4.39	0.0020	16.88	0.8	3.2	3.0	7.2	0.0068	0.000003	739.48	32.0	84.02	96.57
SYN-3391	Fe-Al-Si	3.15	1100	21.0	0.091	3.91	0.0009	17.42	0.8	3.2	3.0	7.2	0.0062	0.000002	741.88	26.0	84.02	97.69
SYN-3491	Fe-Al-Si	2.82	1300	21.0	0.098	4.18	0.0011	17.28	0.8	3.2	3.0	7.2	0.0067	0.000002	744.20	26.0	84.02	97.29
SYN-2891	Fe-Al-Si	0.10	1500	21.0	0.089	0.71	0.0511	20.06	0.8	3.2	3.0	7.2	0.0011	0.000081	739.90	27.0	84.02	19.28
SYN-2791	Fe-Al-Si	0.20	1500	21.0	0.095	0.45	0.0347	20.13	0.8	3.2	3.0	7.2	0.0007	0.000055	739.90	27.0	84.02	11.43
SYN-2691	Fe-Al-Si	0.80	1500	21.0	0.098	4.39	0.0040	16.70	0.8	3.2	3.0	7.2	0.0070	0.000006	739.90	27.0	84.02	101.42
SYN-3591	Fe-Al-Si	2.55	1500	21.0	0.101	4.38	0.0013	16.61	0.8	3.2	3.0	7.2	0.0070	0.000002	742.79	26.0	84.02	98.86

TABLE 4

TGA Results for Synthetic Coal Chars and Ashes

Run No.	Syn. Coal Sample	H_2O %	Vol%	Fixed Carbon %	Ash %
COAL	Ca-Si-S (min.)	0.59	5.04	76.04	18.34
COAL	Na-Si-S	2.60	13.74	74.30	9.35
COAL	Ca-Si-S (Org.)	1.00	8.37	82.93	7.68
COAL	Fe-Al-Si	1.00	7.52	80.69	10.77
CIT-SYN-0191	Ca-Si-S (min.)	0.74	4.70	77.92	16.64
CIT-SYN-0291	Ca-Si-S (min.)	0.78	5.66	72.98	20.58
CIT-SYN-0391	Ca-Si-S (min.)	0.72	3.90	73.58	21.82
CIT-SYN-0491	Ca-Si-S (min.)	0.04	0.90	-0.29	99.34
CIT-SYN-0591	Ca-Si-S (min.)	0.10	0.21	-0.33	100.00
CIT-SYN-0691	Ca-Si-S (min.)	0.08	0.01	-0.15	100.10
CIT-SYN-0791	Ca-Si-S (min.)	0.10	0.26	0.00	99.65
CIT-SYN-0891	Ca-Si-S (min.)	0.19	1.70	-0.31	98.41
CIT-SYN-0991	Ca-Si-S (min.)	0.70	4.53	64.92	29.83
CIT-SYN-1091	Ca-Si-S (min.)	0.92	6.69	66.88	25.53
CIT-SYN-1191	Na-Si-S	2.68	9.74	23.79	63.96
CIT-SYN-1291	Na-Si-S	2.53	4.58	0.17	92.70
CIT-SYN-1491	Ca-Si-S (org.)	0.00	0.27	1.29	98.50
CIT-SYN-2091	Ca-Si-S (org.)	3.54	1.48	83.46	11.55
CIT-SYN-2191	Ca-Si-S (org.)	4.01	2.01	83.52	10.47
CIT-SYN-2291	Ca-Si-S (org.)	1.49	1.70	78.30	18.49
CIT-SYN-2391	Ca-Si-S (org.)	6.08	3.52	81.52	8.90
CIT-SYN-2491	Ca-Si-S (org.)	6.21	2.79	82.08	8.90
CIT-SYN-2591	Ca-Si-S (min.)	4.42	7.01	68.25	20.33
CIT-SYN-2691	Fe-Al-Si	0.65	2.05	7.32	89.97
CIT-SYN-2791	Fe-Al-Si	2.12	4.57	84.23	9.07
CIT-SYN-2891	Fe-Al-Si	1.80	6.00	83.83	8.37
CIT-SYN-2991	Fe-Al-Si	0.85	6.41	82.17	10.66
CIT-SYN-3091	Fe-Al-Si	0.94	6.60	84.17	8.60
CIT-SYN-3191	Fe-Al-Si	0.68	6.48	82.79	10.06
CIT-SYN-3291	Fe-Al-Si	0.55	4.19	6.30	88.96
CIT-SYN-3391	Fe-Al-Si	0.32	0.77	0.09	98.85

TABLE 5

Carbon Conversion Results for Synthetic Coals

Test ID	Syn. Coal Type	Res. Time (sec)	Temp. (°C)	Ash-Fired (g)	Coal Fed (g)	Ash Fed (g)	Residue (g)	Coal Burned by wt%[a]	Gas Carbon Conv. (%)[b]	TGA Carbon Conv. (%)[c]
SYN-0391	Ca(min.)	0.10	900	5.42	2.72	0.49	2.63	4.13	2.36	19.70
SYN-0291	Ca(min.)	0.20	900	5.16	3.08	0.55	2.83	9.80	3.64	13.60
SYN-2591	Ca(min.)	0.80	900	5.01	1.60	0.29	1.43	13.08	5.46	16.30
SYN-0191[d]	Ca(min.)	0.80	900	5.13	2.92	0.52	2.67	10.48	1.54	-12.30
SYN-0491	Ca(min.)	2.89	900	0.84	2.51	0.45	0.38	103.44	100.66	99.90
SYN-0591	Ca(min.)	2.68	1100	0.83	2.74	0.49	0.41	103.65	101.86	100.00
SYN-0791	Ca(min.)	2.47	1300	0.84	2.07	0.37	0.31	103.43	94.55	99.90
SYN-1091	Ca(min.)	0.10	1500	4.48	1.05	0.19	0.84	24.41	13.87	34.80
SYN-0991	Ca(min.)	0.20	1500	3.05	0.95	0.17	0.52	55.51	47.68	47.30
SYN-0891	Ca(min.)	0.80	1500	0.84	2.21	0.39	0.33	103.47	100.70	99.70
SYN-0691	Ca(min.)	2.28	1500	0.83	1.98	0.35	0.29	103.61	93.19	100.00
SYN-2491	Ca(org.)	0.10	900	11.23	1.00	0.08	0.86	14.86	10.36	19.80
SYN-2391	Ca(org.)	0.20	900	11.80	0.94	0.07	0.85	10.11	5.52	19.60
SYN-2291	Ca(org.)	0.80	900	3.62	2.41	0.19	0.67	78.24	78.55	83.60
SYN-1391	Ca(org.)	2.37	900	1.22	2.96	0.23	0.28	98.14	79.93	NA
SYN-1491	Ca(org.)	2.27	1100	0.91	3.33	0.26	0.23	100.74	86.06	99.90
SYN-1591	Ca(org.)	2.15	1300	0.91	3.04	0.23	0.21	100.73	87.11	NA
SYN-2191	Ca(org.)	0.10	1500	8.97	0.88	0.07	0.61	33.71	37.58	31.30
SYN-2091	Ca(org.)	0.20	1500	7.43	1.12	0.09	0.64	46.50	52.78	38.10
SYN-1991	Ca(org.)	0.80	1500	0.80	3.09	0.24	0.19	101.66	96.48	NA
SYN-1891	Ca(org.)	2.03	1500	0.86	3.15	0.24	0.21	101.13	89.88	100.00
SYN-1191	Na(org.)	2.49	900	1.22	3.16	0.30	0.36	97.71	85.40	94.40
SYN-1291	Na(org.)	2.37	1100	0.82	3.13	0.29	0.24	101.88	86.41	99.50
SYN-1691	Na(org.)	2.23	1300	0.72	2.85	0.27	0.19	102.86	98.21	NA
SYN-1791	Na(org.)	2.09	1500	0.66	3.25	0.30	0.20	103.46	94.06	NA
SYN-3191	Fe-Al-Si	0.10	900	8.43	2	0.17	1.40	10.25	0.49	-8.34
SYN-3091	Fe-Al-Si	0.20	900	8.75	2	0.16	1.43	6.42	0.28	-28.84
SYN-2991	Fe-Al-Si	0.80	900	8.39	3	0.32	2.72	10.80	0.46	-1.46
SYN-3291	Fe-Al-Si	3.55	900	0.96	3	0.33	0.32	100.48	96.57	98.56
SYN-3391	Fe-Al-Si	3.15	1100	0.83	3	0.30	0.25	101.99	97.69	99.89
SYN-3491	Fe-Al-Si	2.82	1300	0.80	3	0.32	0.25	102.39	97.29	NA
SYN-2891	Fe-Al-Si	0.10	1500	6.62	2	0.19	1.27	32.19	19.28	-31.06
SYN-2791	Fe-Al-Si	0.20	1500	6.73	2	0.21	1.39	30.80	11.43	-19.52
SYN-2691	Fe-Al-Si	0.80	1500	1.00	2.93	0.32	0.32	100.02	101.42	98.73
SYN-3591	Fe-Al-Si	2.55	1500	0.77	3	0.33	0.25	102.81	98.86	NA

[a] Derived from original proximate analysis.
[b] Derived from ultimate analysis carbon %.
[c] Derived from residue TGA and original proximate analysis.
[d] Test repeated (SYN-2591).

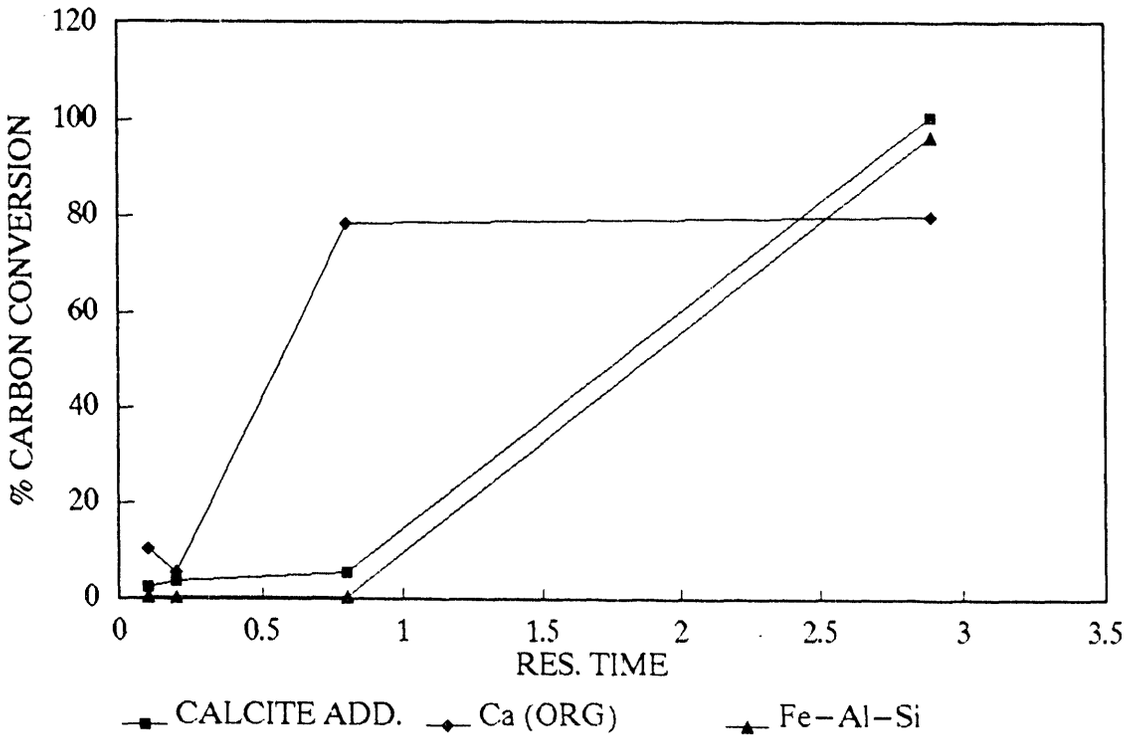

Figure 22. Synthetic coal carbon conversion test results at 900°C.

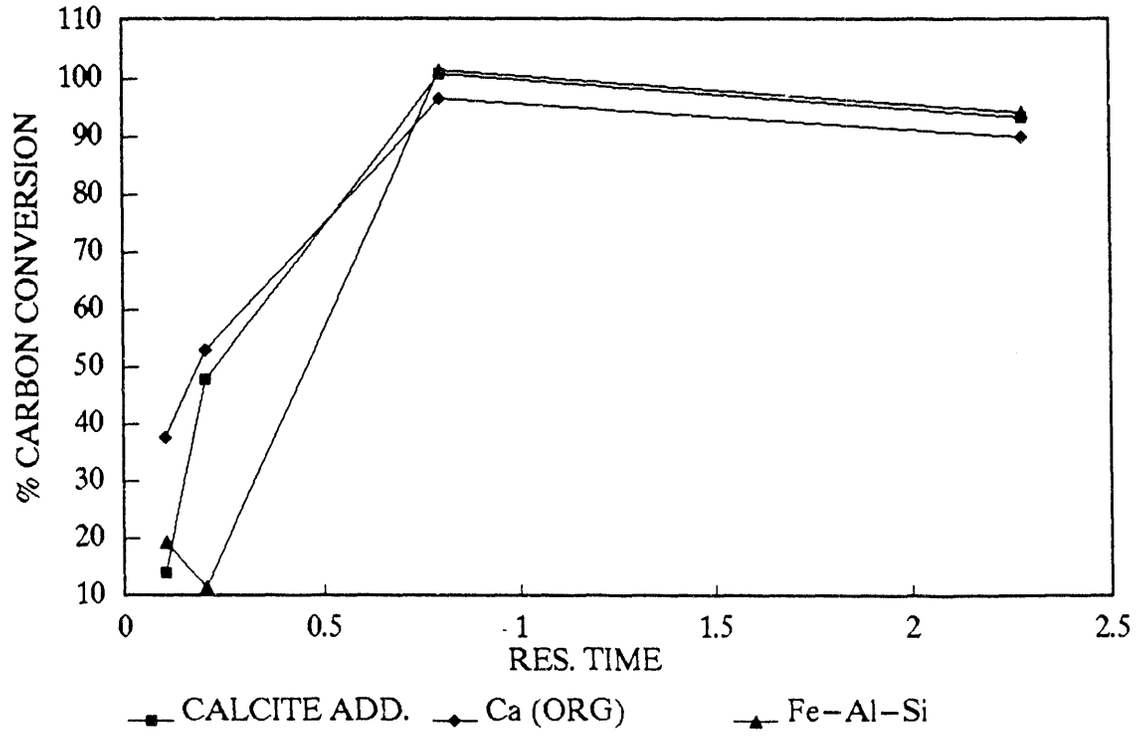

Figure 23. Synthetic coal carbon conversion test results at 1500°C.

TABLE 6

Mineral and Amorphous Phase Composition of Ca(min.)-Si-S Synthetic Coal and Fly Ash (wt%)

Mineral/Phase	Syn. Coal	Fly Ash 900°C	Fly Ash 1100°C	Fly Ash 1300°C	Fly Ash 1500°C
CCSEM Cross-Section Analysis					
Quartz	54.0	42.6	52.7	52.9	48.1
Calcite/CaO	39.9	8.5	4.0	18.4	14.0
Ca Silicate	0.8	18.5	39.4	21.5	28.2
Gypsum/Anhydrite	0.1	0.9	0.2	0.0	0.0
Ca-Si-S Mixture	4.7	27.6	3.5	6.9	9.4
CCSEM Surface Analysis					
Quartz	--	42.0	41.1	32.7	43.1
Calcite/CaO	--	2.8	3.3	6.4	9.8
Ca Silicate	--	10.5	15.3	17.7	26.1
Gypsum/Anhydrite	--	12.9	7.2	19.1	0.0
Ca-Si-S Mixture	--	31.5	31.5	22.4	20.6
XRD Bulk Analysis					
Major	Quartz Calcite	Quartz	Quartz	Quartz	Quartz
Minor		Anhydrite $Ca(OH)_2$ CaO	Anhydrite $Ca(OH)_2$ CaO	Anhydrite $Ca(OH)_2$ CaO Calcite	$Ca(OH)_2$ CaO Calcite

Evidence for the instability of anhydrite at 1500°C is given by the lack of detection of this mineral using either CCSEM or XRD. Most of the anhydrite resulted from the reaction of gas phase SO_2 with surface calcium oxide or calcium silicate. The PSD of the Ca(min.)-Si-S ash along with the synthetic coal minerals showed more mineral coalescence with increasing temperature (Figure 24). This indicates that the quartz and calcite particles locked within the synthetic coal matrix coalesced at higher temperatures, producing large ash particles that were derived from several mineral grains within a single coal particle.

Composition of the Ca(org.)-Si-S ash samples shows evidence of more calcium reacting on the surface of quartz particles rather than being captured on the interior (Table 7). The surface CCSEM analysis indicates more reaction to form amorphous calcium silicate at 1500°C. The PSDs for this system show the 900°C ash to be the largest (Figure 25). This indicates that the organically associated calcium reacts with the quartz within the synthetic coal particle in a manner that is different from the calcite, because instead of causing the least coalescence at the lower temperature, there is actually more (Figure 25). This effect may be due to higher reactivity of the char matrix at 900°C for the organic calcium mixture, as compared to the calcite mixture; therefore, more melting and interaction occurred between the quartz grains, causing a larger PSD to result. Measured reaction rates and corresponding particle temperatures were much greater for the Ca(org.)-Si-S system as compared to the Ca(min.)-Si-S at 900°C. The carbon conversion versus residence times for the Ca(org.)-Si-S and Ca(min.)-Si-S have been previously given in Figures 22 and 23.

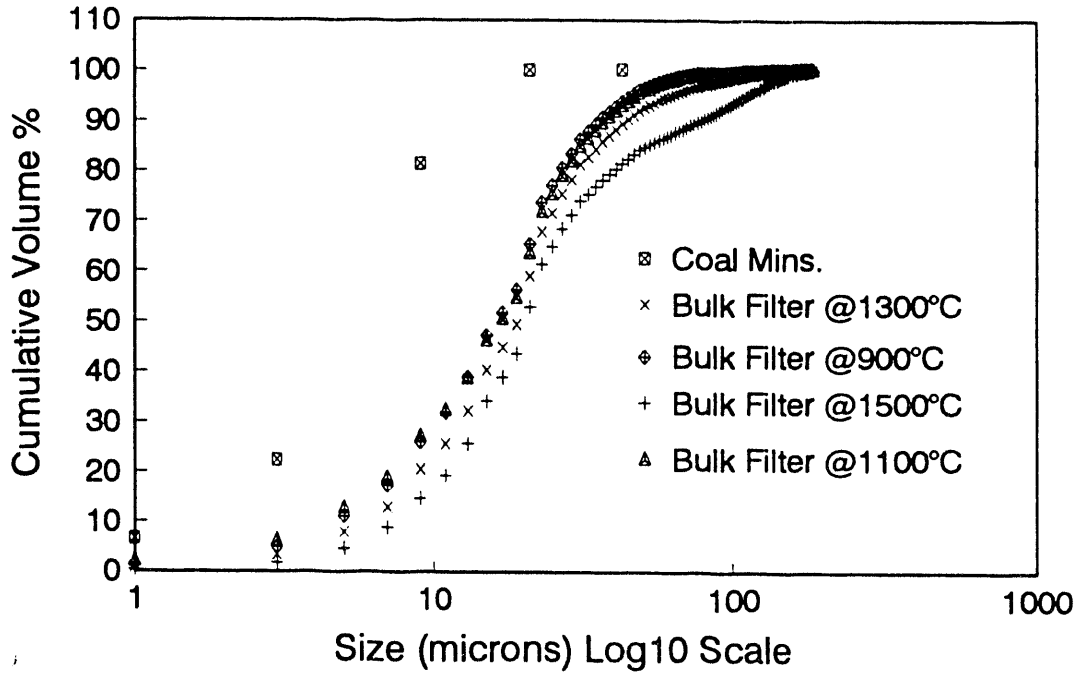

Figure 24. Particle-size distribution of minerals in Ca(min.)-Si-S coal (determined using CCSEM) and fly ash (determined using Malvern analysis).

TABLE 7

Mineral and Amorphous Phase Composition of Ca(org.)-Si-S Synthetic Coal and Fly Ash (wt%)

		Fly Ash			
Mineral/Phase	Syn. Coal	900°C	1100°C	1300°C	1500°C
CCSEM Cross-Section Analysis					
Quartz	92.9	82.6	89.2	92.8	90.4
Calcite/CaO	1.6	0.0	0.1	0.1	0.1
Ca-Silicate	0.1	4.2	4.6	4.6	4.2
Gypsum/Anhydrite	0.0	0.6	0.1	0.0	0.0
Ca-Si-S Mixture	2.1	4.1	1.6	1.3	1.5
CCSEM Surface Analysis					
Quartz	--	78.2	85.2	86.8	79.2
Calcite/CaO	--	0.0	0.1	0.3	0.1
Ca-Silicate	--	10.9	10.6	11.2	11.8
Gypsum/Anhydrite	--	1.9	0.3	0.0	4.6
Ca-Si-S Mixture	--	6.1	2.7	1.2	3.4
XRD Bulk Analysis					
Major	Quartz	Quartz			Quartz
Minor		Anhydrite			CaO

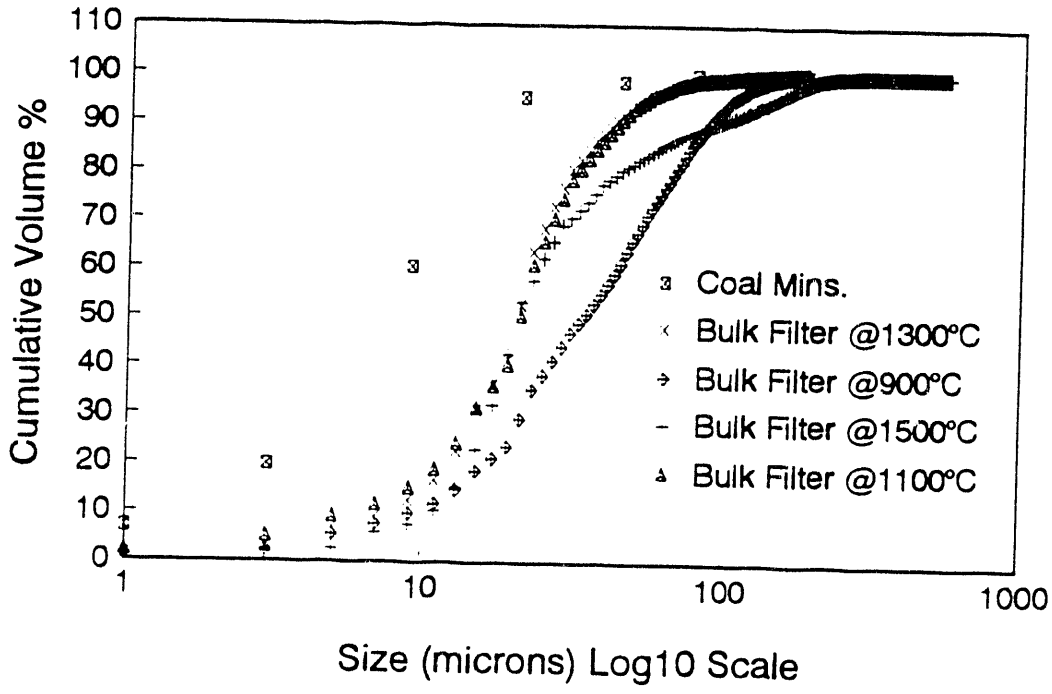

Figure 25. Particle-size distribution of minerals in Ca(org.)-Si-S coal (determined using CCSEM) and fly ash (determined using Malvern analysis).

The Na(org.)-Si-S system, summarized in Table 8, produced lower levels of quartz and increasing levels of sodium sulfate and amorphous sodium silicate at lower temperatures (900° and 1100°C). Bulk compositions based on CCSEM data for Na, Si, and S show decreases in the Na and S and increases in the Si with increased temperature. Phases in the Na-Si-S mixture, as identified by CCSEM, contained Si and S as either amorphous sodium silicate or sodium sulfate. XRD did confirm the presence of a sodium-carbonate-sulfate mineral in the 900°C ash. The presence of the sodium-containing phases at lower temperatures was due to their greater stability at the lower temperatures. With increased temperature, sodium and sulfur become unstable and enter the vapor phase. Therefore, at 1500°C, virtually no Na, S, or amorphous Na-Si-S mixture was left in the ash (Table 8). The particle-size distribution of the Na(org.)-Si-S fly ashes (Figure 26) indicates that the 1500°C ash is much smaller than ash produced at the lower temperatures. This agrees with previous results from another experiment by Ludlow and others (16). The finer ash size was not the result of the fragmentation of quartz grains or the formation of fine sodium sulfates, but may have been the result of the burning char itself fragmenting. Another viable explanation is that agglomeration of the quartz particles was prohibited because the low melting point sodium silicates and sulfates, which act as "glue" to cause particle coalescence, were not able to remain stable at 1500°C. Sodium silicates and sulfates are generally stable at temperatures ranging between 800°-1000°C.

TABLE 8

Mineral and Amorphous Phase Composition of
Na(org.)-Si-S Synthetic Coal and Fly Ash (wt%)

		Fly Ash			
Mineral/Phase	Syn. Coal	900°C	1100°C	1300°C	1500°C
CCSEM Cross-Section Analysis					
Quartz	81.3	62.3	87.4	98.2	95.9
Na-Si-S Mixture	9.6	30.1	7.5	1.0	0.9
CCSEM Surface Analysis					
Quartz	81.3	86.4	97.3	94.8	96.0
Na Si-S Mixture	9.6	10.5	1.8	2.3	1.6
XRD Bulk Analysis					
Major	Quartz	Quartz		Quartz Cristobalite	Amorphous
Minor		$Na_6CO_3(SO_4)_2$			
Bulk Composition (XRF)					
Na*	17.0	27.3	7.3	2.9	0.5
Si	60.8	46.7	62.0	89.5	91.7
S*	15.6	18.8	21.1	1.2	1.0

* Expressed as normalized x-ray energy counts.

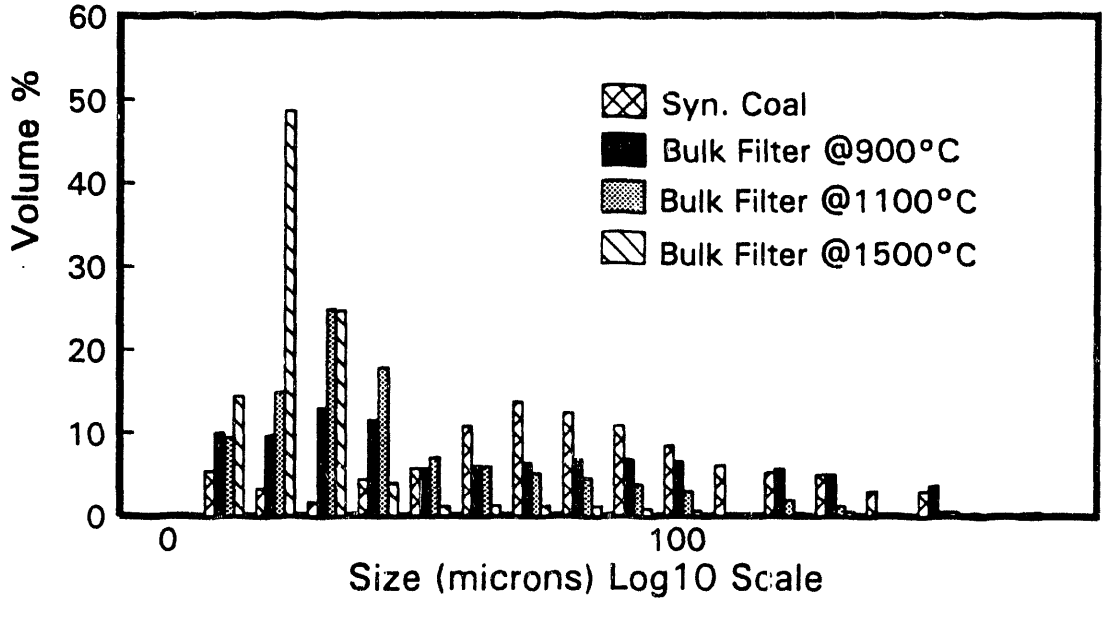

Figure 26. Particle-size distribution of minerals in Na(org.)-Si-S coal and ash.

The Fe(min)-Al-Si system compositions are given in Table 9. Decomposition of the pyrite is nearly complete at 900°C, with only small amounts of oxidized pyrrhotite remaining and the bulk of the iron converted to iron oxide. Some interaction of the iron oxide with the kaolinite to form an iron aluminosilicate phase is seen at 900°C. The degree of interaction remains relatively constant until 1500°C, whereupon the proportion of iron aluminosilicate approximately doubles. This behavior is consistent with the decomposition/oxidation behavior of pure pyrite in air at 900°C, which, as shown in Table 9, primarily forms iron oxide with a lesser amount of oxidized pyrrhotite. Although some interaction between the kaolinite and iron oxide occurs at lower temperature and long residence times, the lack of a fluxing agent discourages substantial interaction until, at 1500°C, the ash approaches the melting points of aluminosilicates (1500°C) and iron(III) oxide (1565°C).

The size distributions of the Fe(min.)-Al-Si coal and bulk filter ashes are shown in Figure 27. There is a small decrease in ash particle size of the 900°C bulk filter from that of the parent coal. This is attributed to some fragmentation of the pyrite as it oxidizes to form iron oxide. The remainder of the bulk filter ash samples at higher temperature have size distributions very similar to each other and intermediate between that of the 900°C ash and the parent coal.

4.4 Discussion

Interactions between the inorganic components of the synthetic coals were followed as a function of residence time and furnace temperature by analysis of individual mineral particles employing CCSEM. Samples analyzed were prepared by two techniques: cross-sectioning of particles embedded in an epoxy matrix, and dispersion on double-stick tape. The use of the two techniques provides complementary information as to the mineral composition of the particles. Cross-sectioning is more sensitive to bulk composition, while dispersion will more readily detect surface deposition on a particle.

TABLE 9

Mineral and Amorphous Phase Composition of Fe(min.)-Al-Si Synthetic Coal and Fly Ash (wt%)

Minerals (CCSEM)	Syn. Coal	Bulk Filter 900°C	Bulk Filter 1100°C	Bulk Filter 1300°C	Bulk Filter 1500°C
Iron Oxide	0.6	39.2	33.4	35.9	35.8
Kaolinite	21.4	37.0	40.3	39.1	25.2
Fe Aluminosilicate	0.0	13.7	13.3	12.3	25.2
Aluminosilicate	1.2	1.0	2.4	4.5	5.7
Pyrite	65.6	0.0	0.0	0.0	0.0
Pyrrhotite	3.6	0.0	0.0	0.0	0.0
Oxidized Pyrrhotite	0.6	2.1	1.5	0.0	0.7
Other	3.5	2.5	3.2	4.1	3.1
Unknown	3.5	4.5	5.9	4.1	4.3

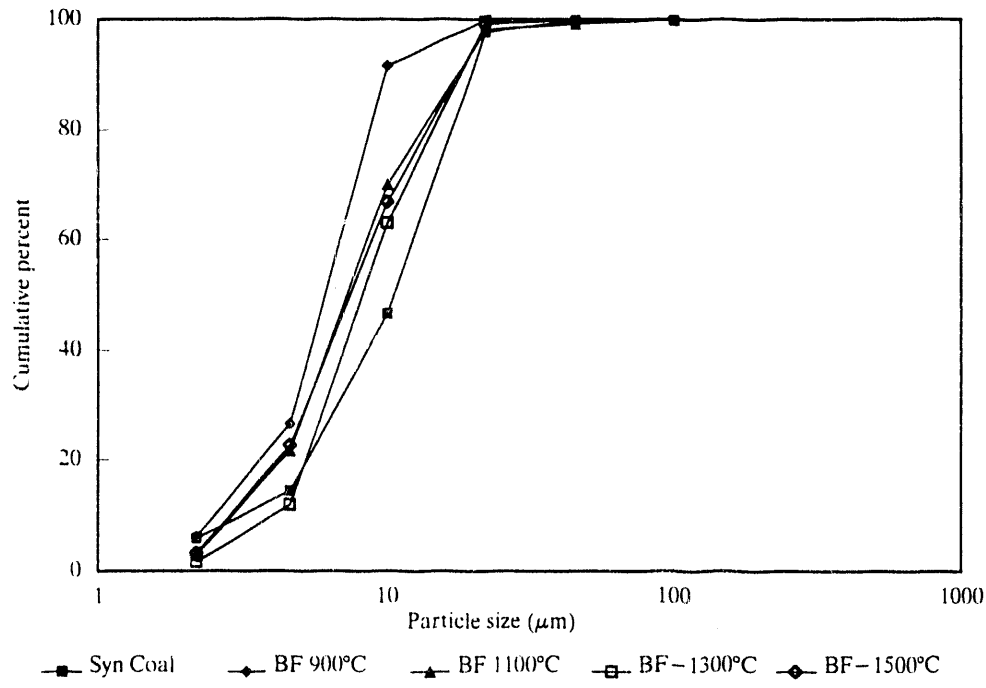

Figure 27. Particle-size distribution of minerals in Fe(min.)-Al-Si coal and ash.

Elemental analyses of about 1000 to 3000 mineral particles were obtained for each CCSEM analysis. Although CCSEM cannot identify specific mineral phases per se, the elemental percentages obtained can be used to infer interactions between the initial discrete inorganic components of the coals.

Since the synthetic coals under consideration contain simple three- and four-component inorganic systems, it is feasible to follow trends in particle composition even though individual compositions are not classifiable as particular mineral species, as has been done in previous studies of natural ash samples using CCSEM. Due to the large volume of composition data for individual ash particles, the data is presented as ternary scattergraphs of particle compositions versus percentage of three primary elemental components.

4.4.1 The Ca(min.)-Si-S System

Interaction of the inorganic components begins at 900°C, as shown in Figure 28. X-ray diffraction of the 900°C sample indicates the presence of calcium sulfate, as well as calcium oxide and $Ca(OH)_2$ as minor crystalline phases, although essentially all particles contain <25% sulfur. Figure 28 also shows the particles contain a wide continuous range of calcium and silicon compositions. At higher temperatures, sulfur phases are not stable, as the maximum sulfur composition generally decreases to <10% at 1500°C. The Ca(min.)-Si-S system shows the same broad range of calcium-silicon composition at the maximum temperature studied, as shown in Figure 29. Examination of the PSD data revealed a very slight increase in particle size with increasing temperature (Figure 24).

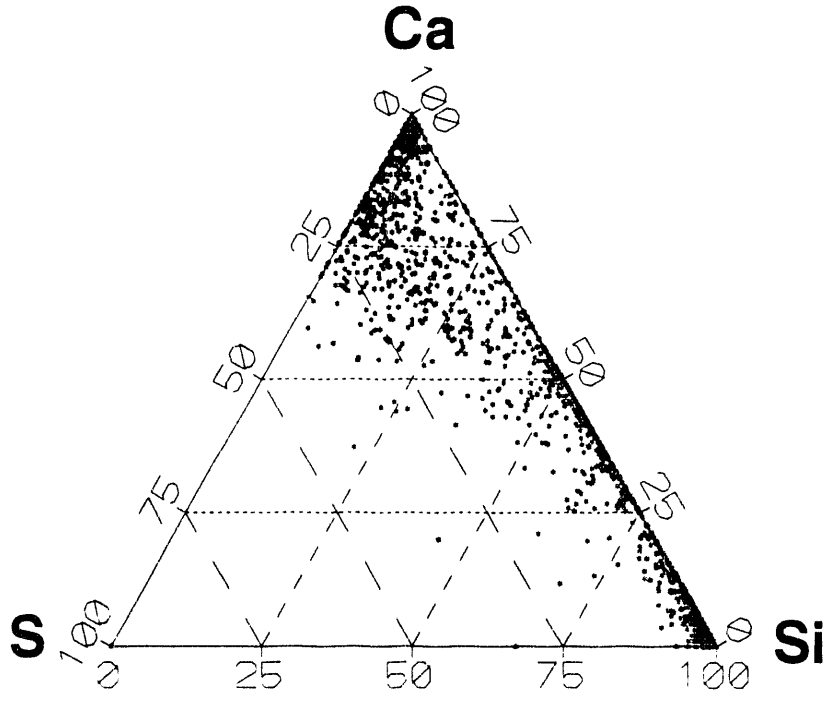

Figure 28. Composition of ash particles produced from Ca(min.)-Si-S at 900°C. Data from cross section of bulk filter ash.

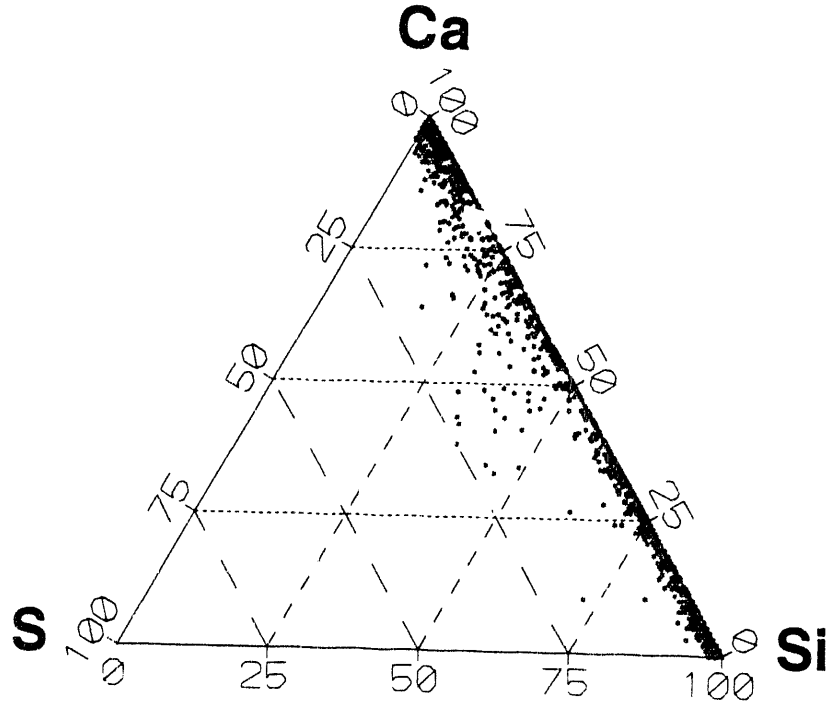

Figure 29. Composition of ash particles produced from Ca(min.)-Si-S at 1500°C. Data from cross section of bulk filter ash.

4.4.2 The Ca(org.)-Si-S System

Due to the highly dispersed nature of the organic calcium in the synthetic coal, the organic calcium appears to react with the silica particle surface, as the coal matrix burns away. Higher levels of calcium are detected by the CCSEM on the surfaces of the particles. Although initially highly dispersed, the distributions of the organic calcium-silica-sulfur with increasing temperature are generally similar to those for the Ca(min.)-Si-S system. The major difference is the scarcity of calcium oxide and calcium-sulfur species. Some indication of a calcium-sulfur species is seen in the 900°C distribution in Figure 30. The presence of sulfated species at 1500°C was negligible, as illustrated in Figure 31. Particle-size distribution analysis showed an initial decrease in mean particle size from 900° to 1100°C, with little change in mean diameter thereafter (Figure 25).

4.4.3 The Na(org.)-Si-S System

Interaction of the ash components of the Na(org.)-Si-S coal is seen to occur at 900°C, as shown in Figure 32. Clusters of data points close to 100% Si and Na indicate the expected presence of silica and a pure sodium phase, probably Na_2O. Another cluster at 50%-75% Na and 25%-50% S is indicative of the formation of a sodium sulfate species. X-ray diffraction analysis of the ash does, in fact, confirm the presence of burkeite ($Na_6[CO_3][SO_4]_2$) as a minor crystalline phase. A significant number of points indicate interaction of Na, Si, and S across a wide compositional range.

There is a dramatic compositional change in the ash collected at 1100°C and higher temperatures. The intermediate compositions disappear, and the great majority of the particles now are comprised of >90% silicon and <10% sodium and sulfur. At 1500°C, essentially all the sodium and sulfur species are in the vapor phase, and very little interaction with the silica is observed. This is illustrated in Figure 33 and is indicative of the loss of sodium and sulfur by devolatilization. PSDs show a gradual decrease in mean particle size with increasing temperature, indicating that little or no mineral particle agglomeration occurred or that some fragmentation of the char particles occurred during combustion (Figure 26). Examination of the fly ash produced at high temperatures indicated that melting of the quartz grains had occurred.

4.4.4 The Fe(min.)-Al-Si System

The S-Fe-Si and Al-Fe-Si compositional diagrams of the raw Fe(min.)-Al-Si synthetic coal obtained from CCSEM analysis are shown in Figures 34 and 35, respectively. Figure 34 shows the iron and sulfur to be associated primarily as pyrite, and Figure 35 shows the aluminum and silica associated as kaolinite. The diagrams for the bulk filter ash produced at 900°C are shown in Figures 36 and 37. As shown, the sulfur has almost entirely disappeared to a level of less than 10%, and the iron is isolated primarily as an iron compound, probably iron oxide. The Al and Si are still clustered together as kaolinite, but with a small scattering of values up the midline of Figure 35, indicating some interaction with the iron to form iron aluminosilicates. Figures 38 and 39 of the ash at 1500°C are virtually identical to the corresponding diagrams at 900°C, with the exception of a slight broadening of the kaolinite cluster, indicating increasing interaction with the iron oxide at the higher temperature.

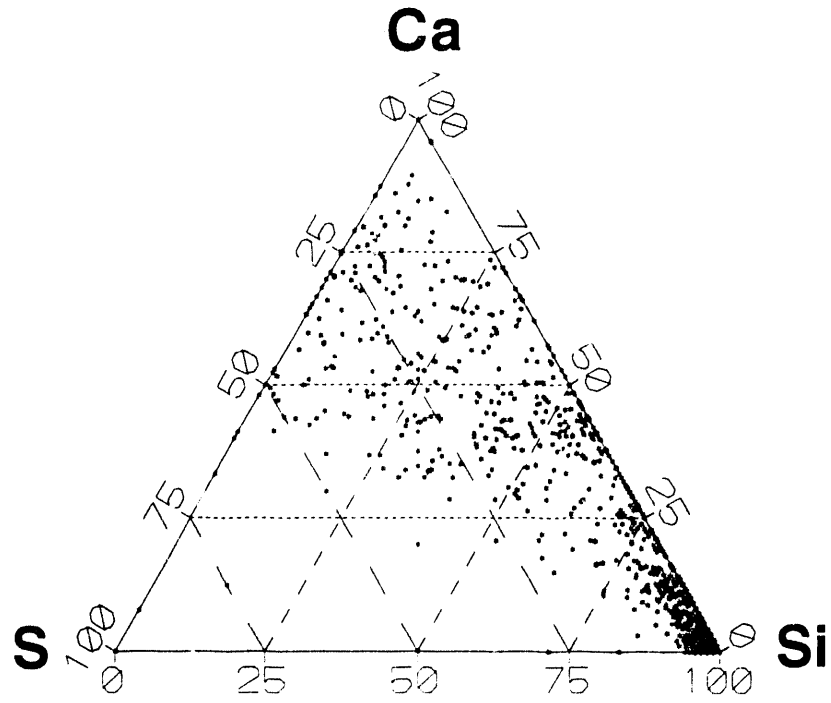

Figure 30. Composition of ash particles produced from Ca(org.)-Si-S at 900°C. Data from a cross section of the bulk filter ash.

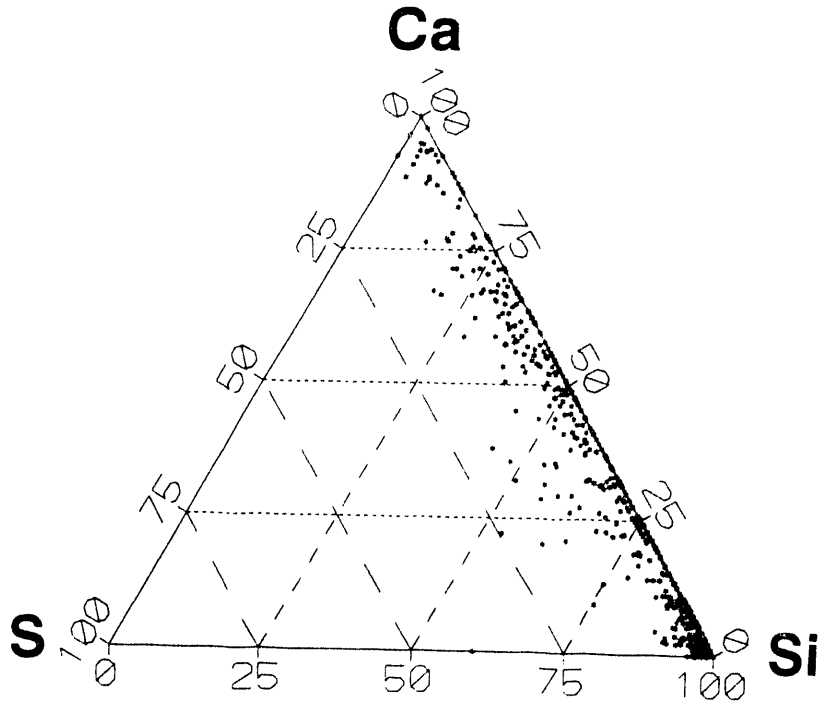

Figure 31. Composition of ash particles produced from Ca(org.)-Si-S at 1500°C. Data from a cross section of the bulk filter ash.

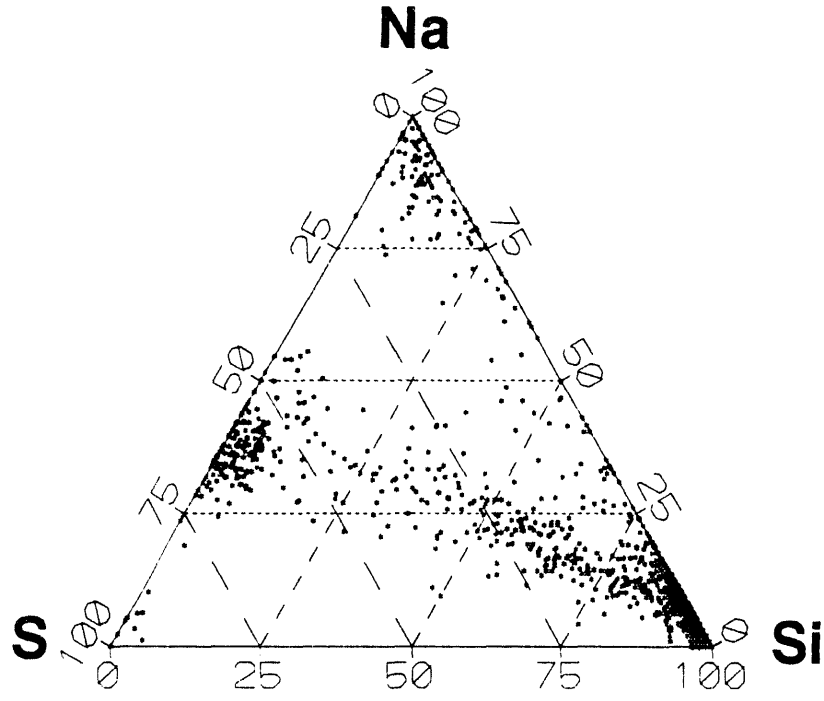

Figure 32. Composition of ash particles produced from Na(org.)-Si-S at 900°C. Data from a cross section of the bulk filter ash.

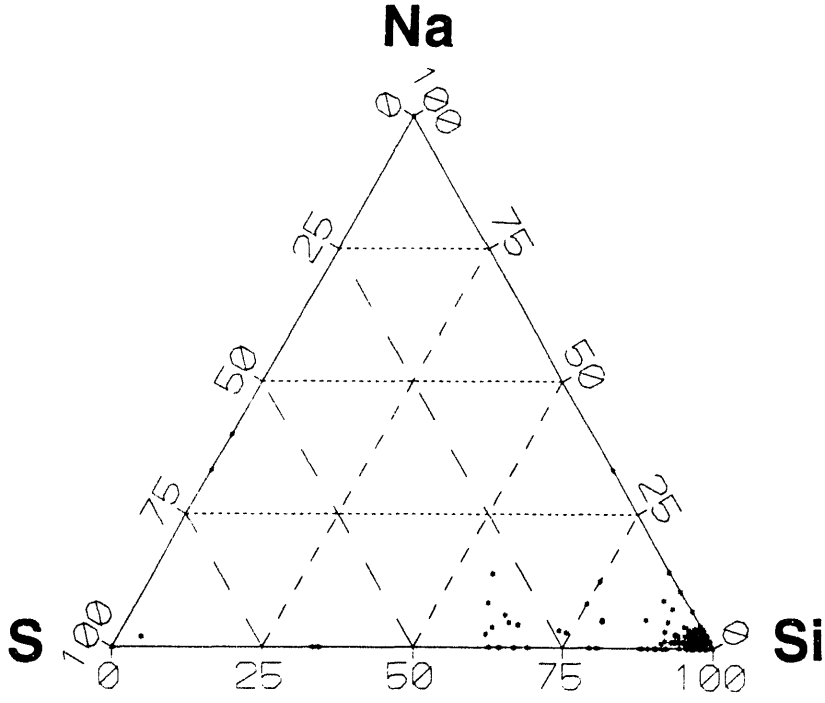

Figure 33. Composition of ash particles produced from Na(org.)-Si-S at 1500°C. Data from a cross section of the bulk filter ash.

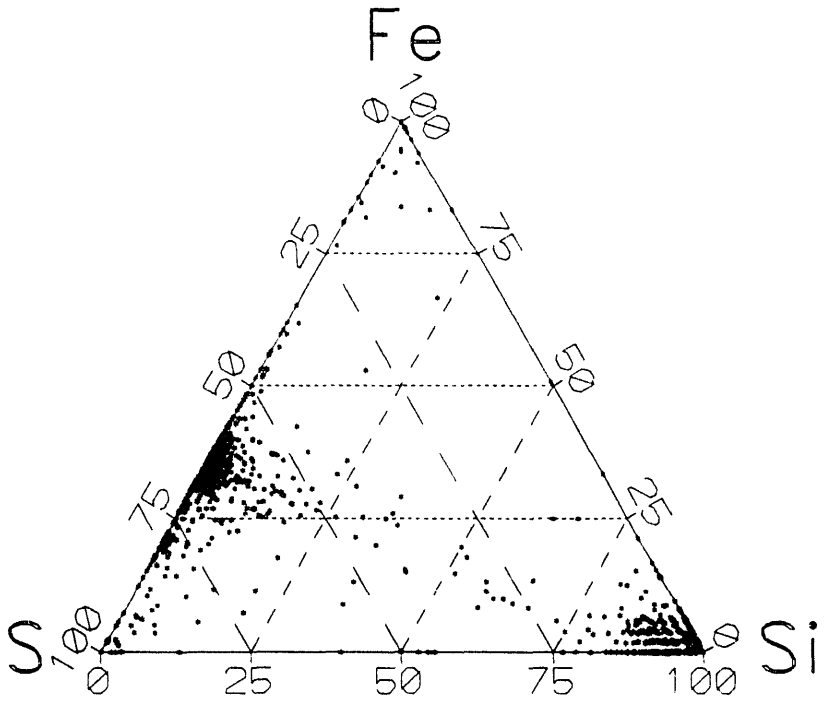

Figure 34. S-Fe-Si composition of Fe(min.)-Al-Si synthetic coal. Data from cross-section analysis.

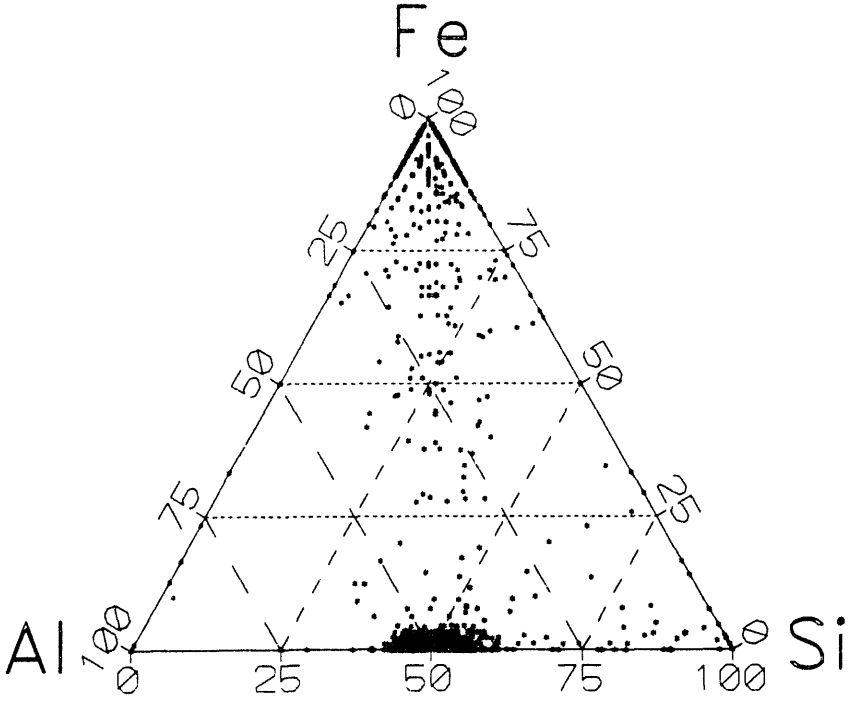

Figure 35. Al-Fe-Si composition of Fe(min.)-Al-Si synthetic coal. Data from cross-section analysis.

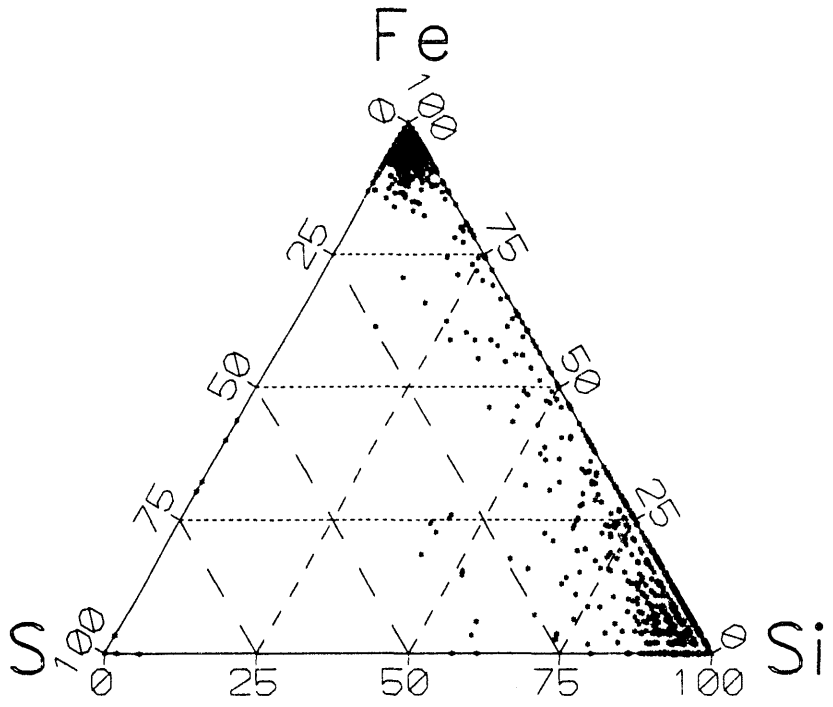

Figure 36. S-Fe-Si composition of ash particles produced from Fe(min.)-Al-Si at 900°C. Data from a cross section of the bulk filter ash.

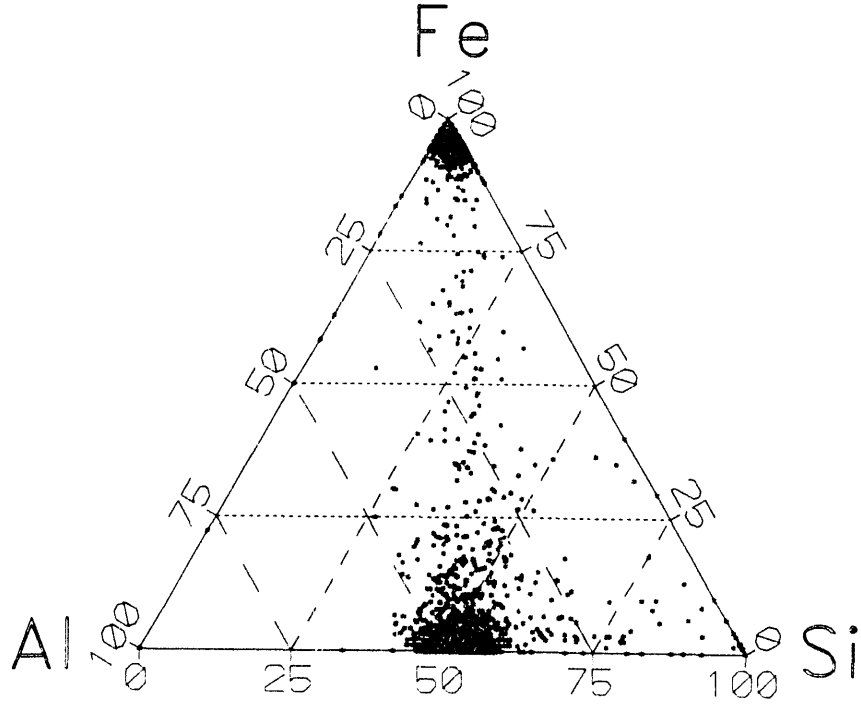

Figure 37. Al-Fe-Si composition of ash particles produced from Fe(min.)-Al-Si at 900°C. Data from a cross section of the bulk filter ash.

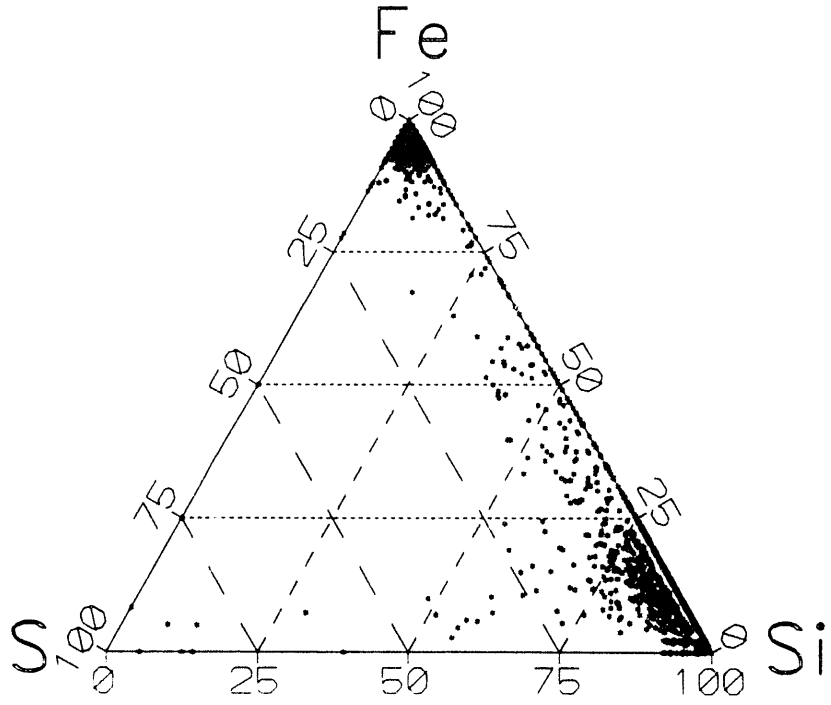

Figure 38. S-Fe-Si composition of ash particles produced from Fe(min.)-Al-Si at 1500°C. Data from a cross section of the bulk filter ash.

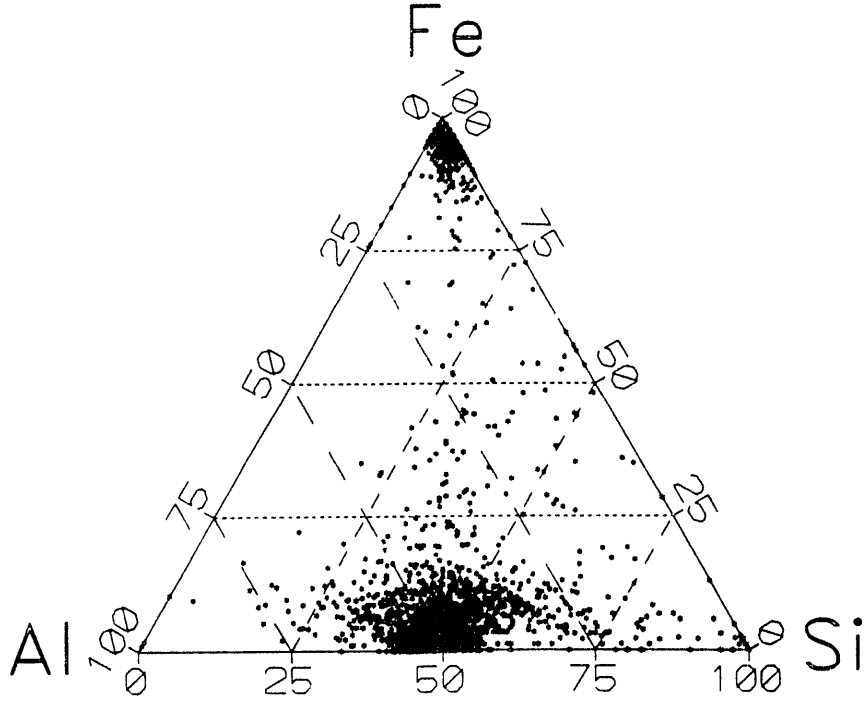

Figure 39. Al-Fe-Si composition of ash particles produced from Fe(min.)-Al-Si at 1500°C. Data from a cross section of the bulk filter ash.

4.5 Combustion Testing of the Eagle Butte/Kentucky #9 Blend

4.5.1 Introduction

Reductions in SO_2 emissions from coal-fired power plants are required to meet increasingly stringent emission standards. One of the methods used to achieve lower emissions is to blend coals. Blending can reduce the total sulfur content of an eastern high-sulfur coal boiler fuel by diluting with a lower-sulfur western coal, but not without complications. The distribution of inorganic components in the western subbituminous coals differs significantly from eastern bituminous coals. Subbituminous coals contain high levels of organically associated cations (Na, Ca, Mg). Upon combustion, these organically associated species form small particles that are very reactive fluxing agents and reduce the viscosity of liquid phases responsible for some slagging and fouling problems.

In addition, these alkali and alkaline earth components can become sulfated, causing SO_2 capture, but possibly also causing backpass fouling on superheater surfaces. One approach to predict the ash behavior of blended coals is to generate experimental fly ash from the coals and the blend in a laboratory-scale DTF to simulate temperatures and particle residence conditions in a full-scale boiler. The initial coals, blend, and fly ashes are analyzed using CCSEM and SEMPC. The closely controlled combustion experiments and detailed analyses provide insights into ash behavior and the effects of coal blending on combustion systems.

4.5.2 Methods

The two coals selected for the experiment were 1) Kentucky #9, a high-sulfur eastern bituminous coal; and 2) Eagle Butte, a low-sulfur western subbituminous coal high in calcium. A blend ratio of 70% Eagle Butte and 30% Kentucky #9 was chosen on the basis of sulfur dioxide compliance levels. This ratio considers both dilution of the high-sulfur coal and sulfur capture by calcium contained in the western coal.

4.5.2.1 Eagle Butte/Kentucky #9 Coal Blend Preparation

Approximately 1000 pounds of Eagle Butte and Kentucky #9 coal was obtained to prepare an Eagle Butte/Kentucky #9 blend. Each coal was crushed and pulverized separately to obtain an approximate 70% -200-mesh grind. Proximate/ultimate and ash analyses were performed on each of these parent coals to determine a blend ratio for testing. Based on the results of these analyses, a blend of 70% Eagle Butte/30% Kentucky #9 by weight was prepared.

The 70/30 Eagle Butte/Kentucky #9 blend was prepared by weighing out appropriate amounts of the two coals in a hopper. The 70/30 ratio was then placed in a revolving mixer to blend the two coals. The blend was split into five approximately 150- to 200-lb samples by using a five-way rotating splitter. One of the five splits was further riffled to obtain a 100-, 30-, and 1-lb sample, as well as samples for analysis and testing in the EERC DTF. All samples were stored in sealed containers purged with nitrogen. Malvern, proximate/ultimate, chemical fractionation, and ash analyses were performed on the coal blend.

4.5.2.2 Char and Fly Ash Production for Eagle Butte Kentucky #9 Blend

The 70/30 Eagle Butte/Kentucky #9 blend was injected into the DTF at a furnace temperature of 1500°C and collected at residence times of 0.05, 0.1, 0.2, 0.5, and 0.8 seconds to produce chars at various degrees of burnout and ultimately a carbon-free fly ash. Carbon dioxide and carbon monoxide levels were recorded during these runs to determine carbon conversion. TGA was performed on the ash collected for each of the tests.

Carbon conversion percentages were calculated for the Eagle Butte/ Kentucky #9 blend tests performed in the DTF by the three methods described earlier. Carbon conversion comparisons at 1500°C furnace temperature are shown in Figure 40.

Fly ash production in the DTF of Eagle Butte/Kentucky #9 under air was performed at a furnace temperature of 1500°C and residence time of 2.6 seconds. The ash was collected on a bulk filter and submitted for analysis. The DTF run conditions used for the short residence time and fly ash production tests are shown in Table 10.

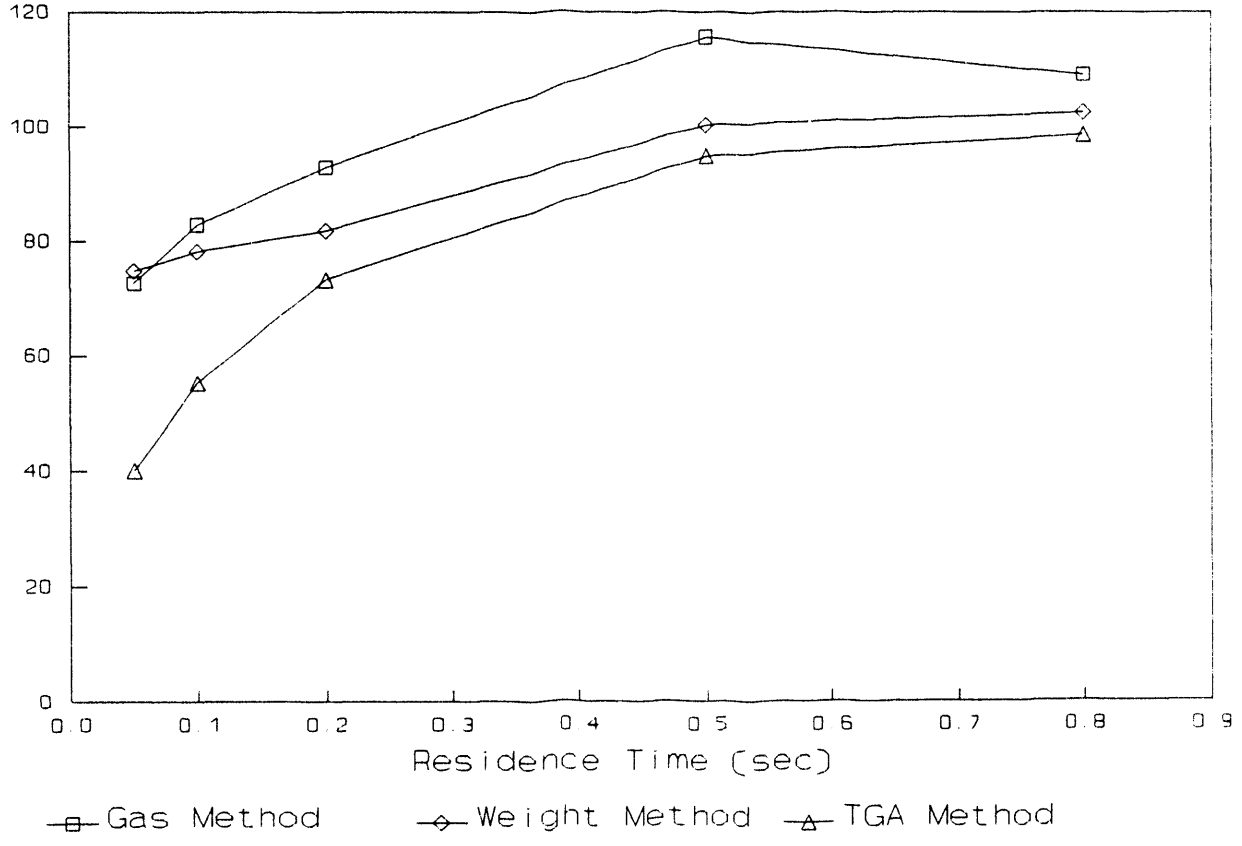

Figure 40. Carbon conversion determinations during the DTF combustion of Eagle Butte/Kentucky #9 blend. Three methods were used to make the determinations including a method which used on-line gas analyzers, a weight loss method, and a TGA method.

TABLE 10

DTF Run Conditions for Eagle Butte/Kentucky #9 Blend

		Drop-Tube Furnace Carbon-Loss Tests																	
Test ID	Coal Type	Res Time (Sec)	DTF Temp (°C)	O_2 (%) Init	Coal Feed Rate (g/m)	CO_2 Act (%)	CO Act (%)	O_2 Act (%)	Pri Flow (L/m)	Sec Flow (L/m)	Quench Flow (L/m)	Vac Flow (L/m)	CO_2 Moles (min)	CO Moles (min)	Pb Press (mm Hg)	Amb. Temp. (°C)	Carbon Orig (%)	Carbon Conv. (%)	Coal Burned (%)	Comb. Conv. (%)
EB/KY-0191	70/30 BL	0.80	1500	21.0	0.098	2.92	0.0052	18.53	0.8	3.2	3.0	7.2	0.0046	0.000008	736.89	27.0	51.8	109.0	102.5	98.5
EB/KY-0291	70/30 BL	0.50	1500	21.0	0.094	2.95	0.0221	17.94	0.8	3.2	3.0	7.2	0.0047	0.000035	736.89	27.0	51.8	115.6	100.2	94.9
EB/KY-0391	70/30 BL	0.20	1500	21.0	0.090	2.17	0.1157	18.74	0.8	3.2	3.0	7.2	0.0034	0.000182	736.89	27.0	51.8	92.9	81.8	73.3
EB/KY-0491	70/30 BL	0.10	1500	21.0	0.092	1.92	0.1688	18.85	0.8	3.2	3.0	7.2	0.0030	0.000266	736.89	27.0	51.8	82.9	78.2	55.3
EB/KY-0591	70/30 BL	0.05	1500	21.0	0.100	1.74	0.2447	18.77	0.8	3.2	3.0	7.2	0.0028	0.000386	736.89	27.0	51.8	72.6	74.8	40.1
EB/KY-0691	70/30 BL	2.63	1500	21.0	0.084	2.37	0.0005	18.84	0.8	3.2	3.0	7.2	0.0038	0.000001	742.79	26.0	51.8	104.3	103.1	0.0
EB/KY-0791	70/30 BL	2.63	1500	21.0	0.084	2.72	0.0000	17.23	0.8	3.2	3.0	7.2	0.0043	0.000000	738.69	25.0	51.8	119.4	106.6	0.0

TABLE 11

Five-Stage Multicyclone Data and Exit Gas Composition Results for Eagle Butte/Kentucky #9 Blend Fly Ash Production

Run # CIT-EBKY9-0791 1

Furnace Configuration: Slagging

Coal Type	EB/KY#9 70/30 Blend
Coal Ash %	7.34
Coal Size (μm)	31.4
Density (g/c³)	1.18
Coal Fed (g)	6.3
Furnace Wall Temp (°C)	1530
Cyclone Box Temp (°C)	101
Ambient Temp (°C)	25
Pb (mm Hg)	738.69
Vacuum (L/m)	7.2
Viscosity (micropoise)	211.79

Gas Composition	
Nitrogen	78.44
Oxygen	17.23
Carbon Monoxide	0.00
Carbon Dioxide	2.72
Moisture	1.61
Run Time (min)	75
Max. Particle Size (μm)	31.4

	Stage 1	Stage 2	Stage 3	Stage 4	Stage 5	Filter	Totals
MASS(g)	0.0626	0.0076	0.0206	0.0190	0.0304	0.0271	0.1673
PCT	37.42	4.54	12.31	11.36	18.17	16.20	100.00
D50 (μm)	17.11	14.79	8.90	5.55	2.19	16.20	

The six-stage cascade multicyclone collection device was used to aerodynamically size segregate ash produced from the blend in the DTF. The run conditions used for this test were a 1500°C furnace temperature and a residence time of 2.6 seconds. Table 11 shows the multicyclone and exit gas composition results from this test. Most of the fly ash mass (37%) was collected in Stage 1 of the multicyclone. This stage collected ash that had an aerodynamic diameter size average of 17 μm. The multicyclone filter had significant quantities of fly ash that were less than 2 μm, primarily due to the production of fine ash from the Eagle Butte coal.

Ash deposits were also grown under fouling conditions for the Eagle Butte, Kentucky #9, and Eagle Butte/Kentucky #9 blend in the optical DTF. The optical DTF deposition probe is designed to simulate a boiler tube typical of those found in full-scale utility boilers. The probe maintains a sacrificial sample coupon attached to the probe at a specific temperature by aspirating water and nitrogen into an inner shell housing the coupon. The coupon temperature can be varied over a broad temperature range by adjusting the mixture of nitrogen and water in the deposition probe. The deposition probe consists of inner and outer shells surrounding a sample coupon, all attached to a stainless steel tube. In the inner shell, a series of annular tubes carry nitrogen and water to and from the probe to cool it and also to help keep the outer shell cool. The inner shell is removable from the probe and extends the full length of the probe. The annular tubes are surrounded by an outer shell which is attached to the end of the probe. The outer shell is insulated to minimize temperature loss in the optical zone and to help prevent oxidation. The deposits are grown on a sample coupon attached to the end of the deposition probe. These sacrificial coupons can be machined from any desired metal. A constrictor is used to accelerate the gas flow to approximately 15 m/sec before it impinges on the coupon. The upper surface of the coupon is curved to match the radius of the probe. The probe accepts a thermocouple to provide temperature measurements.

Table 12 gives the furnace conditions for the deposits. The deposit morphology was determined by optical and SEM examinations. The chemical content of the bases and main portions of the deposits was determined using SEMPC analysis.

4.5.2.3 Coal, Char, and Ash Analysis Techniques

The CCSEM technique was used to analyze the original coal particles and the DTF-generated fly ash. This technique determines the size, shape, quantity, and composition of the mineral grains in coal (20). The chemical composition data obtained are used to classify particles into mineral or chemical categories. By inspection of simultaneously collected digital backscatter images, the mineral grains can be further classified as locked into or liberated from the coal particle. Chemical fractionation analysis (2) was used to determine the amount of organically bound elements in the Eagle Butte, Kentucky #9, and the Eagle Butte/Kentucky #9 blend.

The SEMPC technique was used to analyze the DTF-generated fly ash and deposits to determine detailed chemistry of the liquid phase and to derive the viscosity. This technique quantitatively determines the relative amounts of phases present in entrained ashes and deposits (3). The method involves microprobe analysis of a large number of random points in a polished cross

TABLE 12

Drop-Tube Furnace Parameters for Ash Deposits, Using Slagging Conditions

Parameter	Eagle Butte	Kent. #9	Blend
Gas Flow per Minute:			
Primary Air	0.8	0.8	0.8
Secondary Air	3.2	3.2	3.2
Vacuum	7.2	7.2	7.2
Temperatures (°C):			
Preheater	1000	1000	1000
Furnace 1	1530	1530	1530
Furnace 2	1530	1530	1530
Optical Zone	1100	1100	1100
Substrate	525	535	530
Other Parameters:			
Coal Burned (g)	2.07	0.18	0.69
Feed Rate (g/min)	0.094	0.090	0.099
Run Duration (min)	22	2	7
Ash Fed (g)	0.0865	0.0256	0.053
Ash Collected (g)	0.0614	0.0155	0.0266
Ash Collected/fed (%)	70.98	60.56	50.19

section of a sample. The sample matrix-corrected compositions are classified into mineral or chemical categories based on various weight and molar ratios developed from stoichiometry of the phases. Points not classifiable into the phase categories are assumed to be amorphous and represent the liquid phase during deposition. Since the chemistry of the liquid phase is known, the viscosity can be calculated (22).

4.5.3 Coal Characterization

Table 13 gives the coal characteristics for the Eagle Butte and Kentucky #9 coals and the 70% Eagle Butte/30% Kentucky #9 blend. The ash content is greatest for the high-volatile bituminous Kentucky #9 coal as compared to the subbituminous Eagle Butte coal. The blend has an ash content intermediate between the two parent coals.

The proximate and ultimate analyses of the blend correspond extremely well to what would be predicted from a 70/30 mixture based on the analyses of the parent coals. It thus appears that the blending operation was quite successfully performed. The elemental content of the blend reported as oxide percents and the mineral composition of the blend also correspond closely to that calculated for a blend of 70% Eagle Butte and 30% Kentucky #9. The slightly higher iron and sulphur concentrations may be caused by the density and computational properties of the pyrite during the pulverizing and blending process.

TABLE 13

Analyses of As-Fired Fuels: Eagle Butte and Kentucky #9
X-Ray Fluorescence and Proximate/Ultimate Results (in weight percentages)

	EB	KY	Meas. EB/KY	Calc. EB/KY
Proximate				
Moisture	27.3	6.5	21.8	21.1
Volatile Matter	35.0	37.3	34.5	35.7
Fixed Carbon	33.5	42.3	36.3	36.1
Ash	4.2	13.8	7.3	7.1
Caloric Value	9,254	11,618	9,815	9,963
Ultimate				
Hydrogen	6.7	5.2	6.3	6.3
Carbon	51.8	63.7	53.8	55.4
Nitrogen	0.6	1.3	0.8	0.8
Sulfur	0.4	4.1	1.5	1.5
Oxygen	36.3	11.9	30.2	29.0
Ash	4.2	13.8	7.3	7.1
Elemental Oxides				
SiO_2	29.1	44.2	36.5	37.9
Al_2O_3	17.1	19.2	18.3	18.3
Fe_2O_3	7.2	23.8	17.3	16.9
TiO_2	1.5	0.6	1.0	1.0
P_2O_5	0.9	0.5	0.7	0.7
CaO	31.4	7.5	19.2	17.4
MgO	11.0	1.5	4.0	5.4
Na_2O	1.4	0.8	1.4	1.0
K_2O	0.4	2.0	1.4	1.3
SO_3	18.1	6.1	17.1	11.1
Mineral Basis (from CCSEM)				
Quartz	31.20	9.10	11.00	18.3
Iron Oxide	2.00	0.10	0.20	0.9
Periclase	0.00	0.00	0.00	0.0
Rutile	0.90	0.10	0.40	0.4
Alumina	0.00	0.00	0.00	0.0
Calcite	0.40	7.50	7.60	4.6
Dolomite	0.10	0.20	0.30	0.2
Ankerite	0.00	0.00	0.00	0.0
Kaolinite	30.50	11.40	12.80	19.3
Montmorillonite	1.90	3.20	2.60	2.7
K Al-Silicate	0.50	19.20	14.80	11.4
Fe Al-Silicate	0.10	0.80	0.90	0.5
Ca Al-Silicate	1.00	0.10	0.20	0.5
Na Al-Silicate	0.30	0.20	0.20	0.2
Aluminosilicate	2.60	1.20	0.80	1.8
Mixed Al-Silica	0.00	0.20	0.40	0.1
Fe Al-Silicate	0.00	0.00	0.00	0.0
Ca-Silicate	0.00	0.20	0.00	0.1
Ca Aluminate	0.00	0.00	0.00	0.0

(continued)

TABLE 13 (continued)

	EB	KY	Meas. EB/KY	Calc. EB/KY
Mineral Basis (from CCSEM) (continued)				
Pyrite	11.30	36.80	38.90	26.2
Pyrrhotite	0.00	0.10	0.10	0.1
Oxidized Pyrrhotite	0.80	0.00	0.00	0.3
Gypsum	0.00	0.10	0.70	0.1
Barite	0.40	0.00	0.30	0.2
Apatite	0.00	0.40	0.00	0.2
Ca-Al-P	7.00	0.00	0.40	2.9
KCl	0.00	0.00	0.00	0.0
Gypsum/Barite	0.20	0.00	0.10	0.1
Gypsum/Al-Silicate	0.30	0.20	0.10	0.2
Si-Rich	1.40	3.00	1.70	2.3
Ca-Rich	0.00	0.20	0.10	0.1
Ca Si-Rich	0.00	0.00	0.00	0.0
Unknown	6.90	5.90	5.40	6.3

Major differences in mineral content are apparent between the parent coals in Table 13, as determined using CCSEM analysis. Major minerals in the Eagle Butte coal are quartz, kaolinite, and pyrite, while the Kentucky #9 coal has major amounts of pyrite, kaolinite, and K-aluminosilicates with little quartz. The blend mineral composition, primarily with the exception of pyrite, is approximately that expected.

PSDs of the mineral particles in the fuels (Figure 41) show the Eagle Butte coal to have the smallest mean particle size and Kentucky #9 coal to have the largest. The blend is closest in PSD to that of the Eagle Butte coal. Figure 42 shows an SEM image of the blend. The lighter-colored particles are Eagle Butte coal, while the darker particles are Kentucky #9 coal. The difference in brightness is due to the higher calcium content of the Eagle Butte coal, in which the calcium is highly dispersed as organically bound calcium ions (Table 14). Again, the blend compares well with the composition calculated for a 70% Eagle Butte/30% Kentucky #9 mixture. Detailed results of the chemical fractionation analyses for the coals are given in Appendix A.

4.5.4 Char and Fly Ash Characterization

The 70/30 Eagle Butte/Kentucky #9 blend was combusted in the DTF at a furnace temperature of 1500°C and residence times of 0.05, 0.10, 0.20, 0.50, and 0.80 seconds. The extracted chars were characterized by Malvern and CCSEM analysis. Table 15 gives the CCSEM-determined mineral composition as a function of residence time. The most significant change in mineral composition is the rapid decrease in pyrite concentration after 0.10 second, accompanied by a concurrent increase in the iron oxide concentration, arising from the decomposition of the pyrite. Little change in the intermediate pyrrhotite and oxidized pyrrhotite concentrations is seen. A similar rapid decomposition of pyrite was seen with the pyrite-silica-aluminum

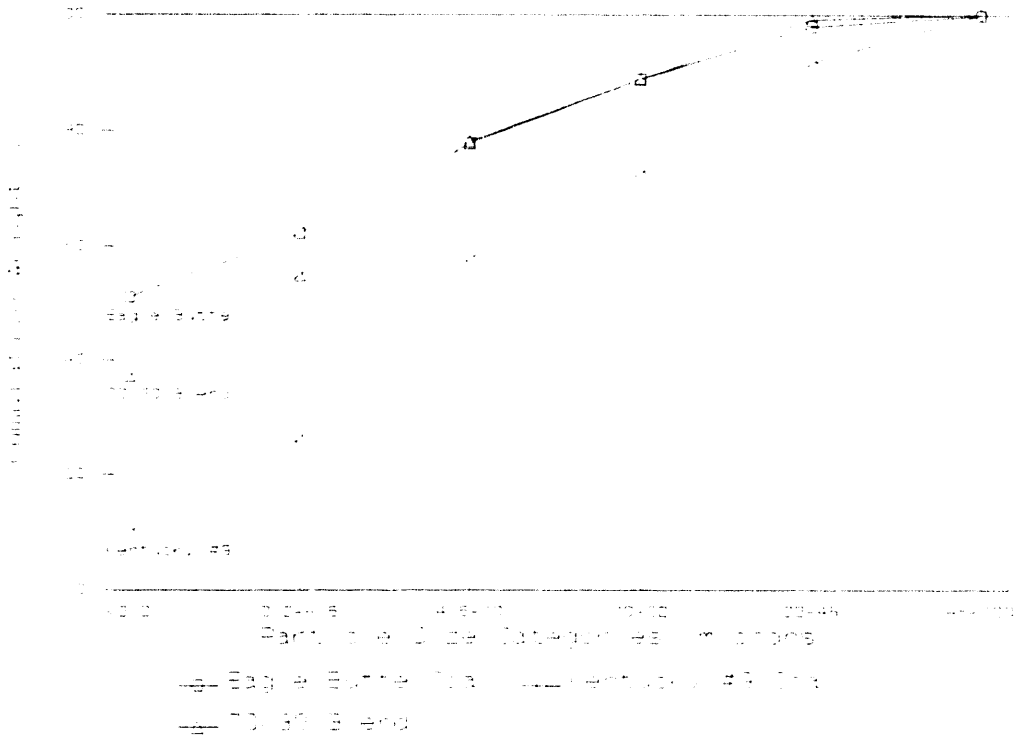

Figure 41. CCSEM particle-size distribution of parent coals and 70/30 blend.

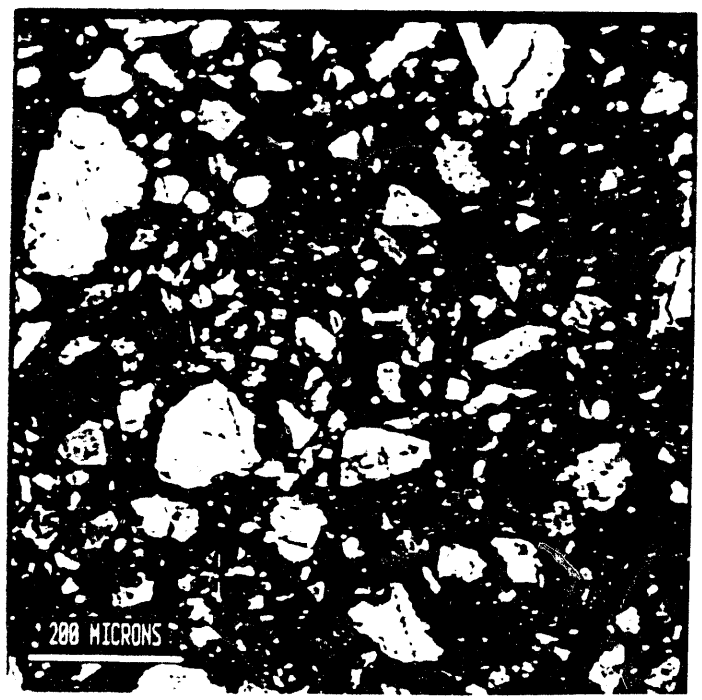

Figure 42. SEM photograph of 70/30 Eagle Butte/Kentucky #9 blend.

TABLE 14

Summary of Organically Bound Constituents in Eagle Butte and Kentucky #9 Coals CIT Test Fuels (wt% coal basis)

	EB	KY #9	EB/KY	Calc. EB/KY
Silicon	0.00	0.00	0.00	0.00
Aluminum	0.27	0.08	0.24	0.21
Iron	0.13	0.60	0.41	0.27
Titanium	0.00	0.00	0.00	0.00
Phosphorus	0.00	0.07	0.03	0.02
Calcium	1.03	0.00	0.69	0.77
Magnesium	0.36	0.02	0.21	0.26
Sodium	0.04	0.06	0.07	0.05
Potassium	0.01	0.03	0.00	0.02
Total Org. Bound	1.84	0.86	1.65	1.56
Total % Ash	4.20	13.80	7.30	7.08

synthetic coal in an earlier section of this report. After 0.50 seconds, an increase of a few percent is seen in the concentration of Fe Al-silicate, indicating some interaction of the iron with the clay minerals present in the char.

As shown in Table 14, the majority of the calcium in the blend is present as organically bound calcium species. There is a substantial increase in Ca-Al-silicate and Ca-aluminate species with residence time, indicating that the organically bound calcium has coalesced onto the ash and is interacting with the silica and clay minerals as the organic portion of the char burns away.

The Malvern size analysis for the 70/30 Eagle Butte/Kentucky #9 blend and the chars is shown in Figure 43. The mean particle size increases at the shorter residence times from 0.01 to 0.50 seconds. This increase is probably due to the swelling of the Kentucky #9 portion of the blend. Subsequent combustion of the char at 0.50- and 0.8-second residence times causes the char mean size to decrease again. In contrast, the CCSEM sizing of mineral particles for the chars is shown in Figure 44. In this case, the size of the ash particles actually increases somewhat with increasing residence time, indicative of some agglomeration of the mineral matter.

A comparison can be made from the iron-alumina-silica ternary diagrams for the blend coal and blend fly ash shown in Figures 45 and 46. As is seen, the majority of interaction between mineral phases during the fly ash formation is a broadening of the composition of the original alumina-silica clays. Very little interaction of the iron with aluminum and silica is seen. This suggests that iron-rich particles arising primarily from the Kentucky #9 portion of the blend experience only limited interaction with the alumina-silica clays of the Eagle Butte portion of the blend.

Viscosity distributions of silicate liquid phases were constructed for the 70/30 Eagle Butte/Kentucky #9 fly ash, the fly ashes from the two parent coals, and a weighted 70-30 mixture derived from the viscosity distributions

TABLE 15

Drop-Tube Furnace Test Results of Blend Char and Fly Ash at 1500°C
Weight Percentages on a Mineral Basis

	3108 EB/KY #9 coal	3370 EB/KY #9 Char	3371 EB/KY # 9 Char	3372 EB/KY #9 Char	3373 EB/KY #9 Char	3374 EB/KY #9 Char	3375 EB/KY #9 Ash	Calc. EB/KY #9 Ash
		0.05 sec	0.1 sec	0.2 sec	0.5 sec	0.8 sec	bf-cx[a]	
Quartz	11.0	19.6	16.3	19.0	10.6	13.2	13.7	5.6
Iron Oxide	0.2	4.4	5.7	6.0	8.0	6.3	12.6	13.2
Periclase	0.0	0.0	0.0	0.0	0.0	0.0	0.0	0.0
Rutile	0.4	0.5	0.1	0.2	0.1	0.1	0.3	0.3
Alumina	0.0	0.0	0.0	0.0	0.6	0.0	0.0	0.0
Calcite	7.6	6.9	8.4	4.4	10.7	8.3	5.6	3.4
Dolomite	0.3	0.4	1.0	0.8	1.0	0.3	0.4	1.9
Ankerite	0.0	0.1	0.0	0.1	0.0	0.1	0.1	0.1
Kaolinite	12.8	17.2	13.0	14.7	16.6	12.0	11.1	4.2
Montmorillonite	2.6	4.5	2.0	5.9	3.2	4.0	6.7	6.3
K Al-Silicate	14.8	12.9	8.7	14.3	7.0	6.0	3.1	2.5
Fe Al-Silicate	0.9	0.3	0.4	0.6	2.0	2.8	2.3	8.8
Ca Al-Silicate	0.2	0.8	1.0	1.0	5.4	5.3	5.6	5.4
Na Al-Silicate	0.2	0.2	0.3	0.3	0.0	0.6	0.0	0.0
Aluminosilicate	0.8	2.2	0.8	2.6	2.4	2.5	2.9	2.2
Mixed Al-Silica	0.4	0.4	0.3	1.2	1.1	1.4	0.9	1.1
Fe-Silicate	0.0	0.1	0.1	0.0	1.2	0.1	1.6	0.6
Ca-Silicate	0.0	0.2	0.2	0.5	1.0	1.8	1.4	3.4
Ca-Aluminate	0.0	1.3	2.3	3.3	7.3	9.6	5.8	11.4
Pyrite	38.9	13.0	22.1	5.7	0.3	0.1	0.0	0.0
Pyrrhotite	0.1	0.8	1.5	0.6	0.0	0.0	0.0	0.0
Oxidized Pyrrhotite	0.0	1.7	1.4	0.5	0.3	0.2	0.1	0.0
Gypsum	0.7	0.4	0.1	0.4	0.2	0.0	0.0	0.0
Barite	0.3	0.2	0.1	0.0	0.0	0.0	0.0	0.0
Apatite	0.0	0.2	0.0	0.3	0.6	0.0	0.2	0.0
Ca-Al-P	0.4	0.0	0.1	0.1	0.0	0.0	0.0	0.0
KCl	0.0	0.0	0.0	0.0	0.0	0.0	0.0	0.0
Gypsum/Barite	0.1	0.1	0.0	0.1	0.0	0.0	0.0	0.0
Gypsum/Al-Silicate	0.1	0.1	0.0	0.1	0.1	0.2	0.4	0.1
Si-Rich	1.7	1.8	1.0	3.7	2.1	2.8	4.8	4.3
Ca-Rich	0.1	0.3	0.9	0.7	1.9	1.9	1.3	5.0
Ca Si-Rich	0.0	0.0	0.3	0.1	0.4	0.6	1.2	1.6
Unknown	5.4	9.7	11.8	12.9	15.9	19.6	17.9	18.9

[a] Bulk filter cross section.

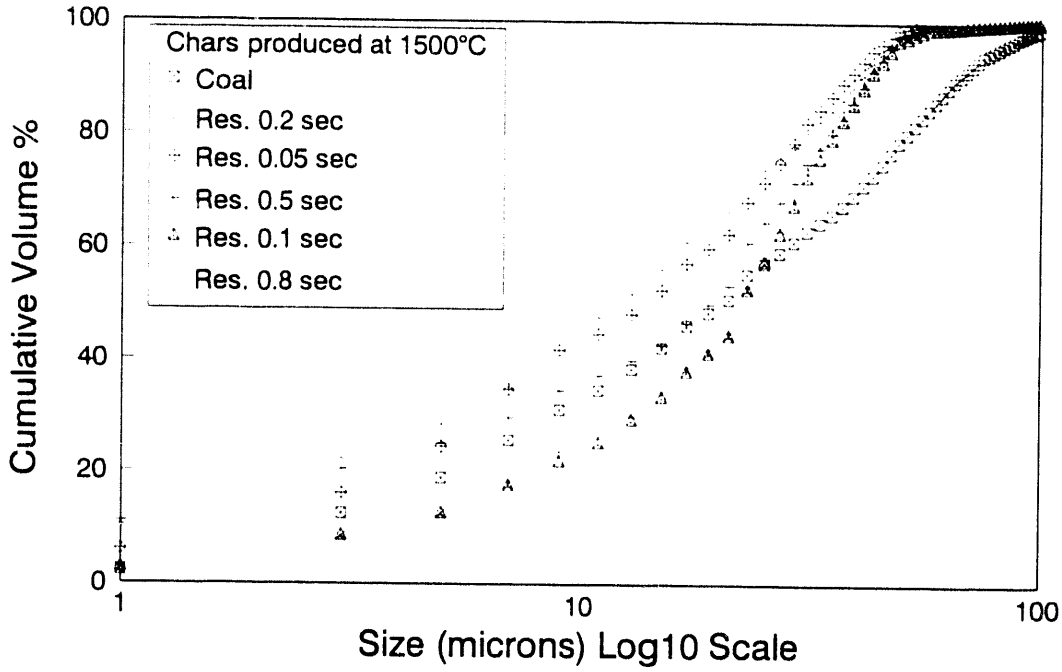

Figure 43. Malvern particle-size distribution of 70/30 Eagle Butte/ Kentucky #9 chars.

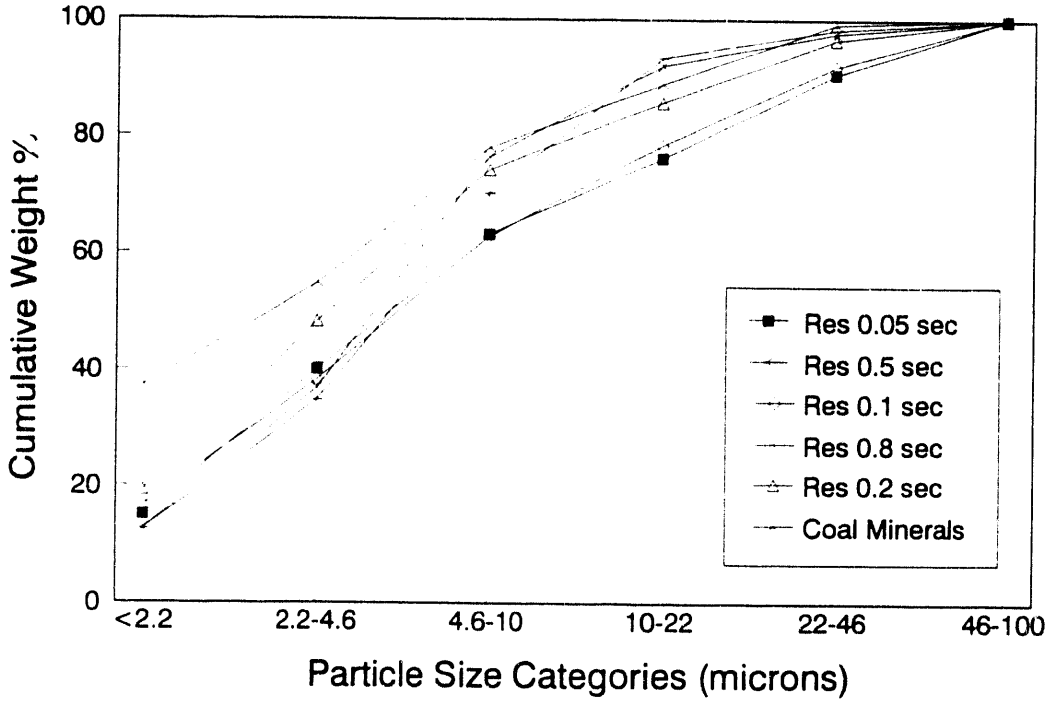

Figure 44. CCSEM particle-size distribution of 70/30 Eagle Butte/Kentucky #9 chars.

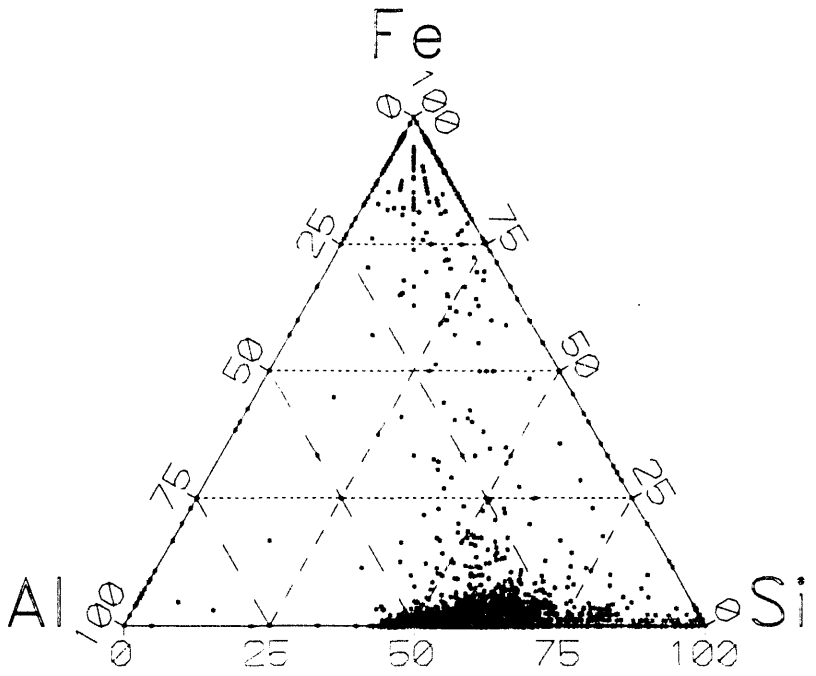

Figure 45. Fe-Al-Si ternary diagram of the 70/30 Eagle Butte/Kentucky #9 blend coal.

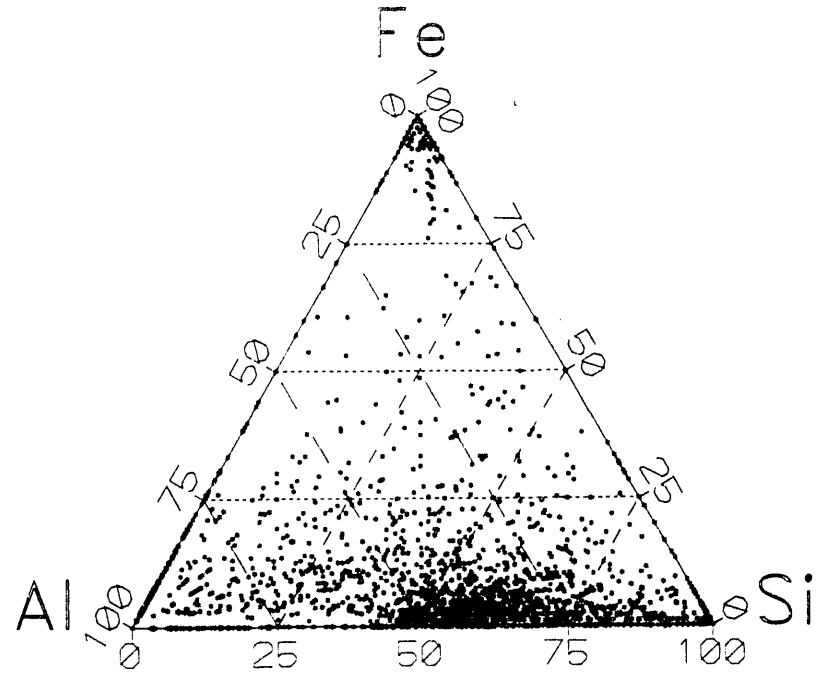

Figure 46. Fe-Al-Si ternary diagram of the 70/30 Eagle Butte/Kentucky #9 blend fly ash.

of the two parent coals. A cumulative frequency plot of these four viscosity distributions is shown in Figure 47. It is seen that the fly ash from the parent Eagle Butte coal has the lowest viscosity distribution, and the fly ash from the parent Kentucky #9 coal has the highest. Viscosity distributions for the weighted mixture of the parent coals and the 70/30 Eagle Butte/Kentucky #9 blend fly ash are intermediate between the parent ash distributions. From this information, it can be deduced that the Eagle Butte fly ash tends to be the stickiest ash and the Kentucky #9 ash is the least sticky. When the parent coals were blended and fired in the DTF, their product ash was intermediate in viscosity distribution between that of the parent ash viscosity distributions. The blend distribution is actually intermediate between the weighted average of the parent fly ashes and the Kentucky #9 viscosity distribution. This may indicate that some limited interaction occurred between the inorganic constituents of the 70/30 Eagle Butte/Kentucky #9 blend during combustion in the DTF.

Viscosity distributions were also constructed for the bases and main portions of the deposits grown under fouling conditions for the two parent coals and the blend. Cumulative frequency plots of these viscosity distributions, along with calculated viscosity distributions based on a weighted average of the parent deposits, are shown in Figures 48 and 49. The viscosity distribution of the blend base deposit is significantly less than that calculated from the weighted average of the parent base deposits and is approximately the same as that of the Kentucky #9 parent base deposit viscosity distribution. Thus, the Kentucky #9 ash appears to dominate the portion of the deposit that forms first. In contrast, the viscosity distributions of the main deposits of the parent coals and the blend appear to be nearly the same.

The results of the viscosity calculations indicate that the blend is closer in viscosity distribution to that of the parent Kentucky #9, even though the blend coal is comprised of 70% Eagle Butte coal and only 30% Kentucky #9 coal. This indicates that a substantial reduction in sulfur emissions could be achieved by blending, with only moderate deviation of the ash viscosity from that of the parent Kentucky #9 ash.

Analysis of ashes generated in the DTF using fouling, fuel-rich conditions showed interesting variations with different fuel-air stoichiometric ratios. Ashes for each of the three coals, the Eagle Butte, the Kentucky #9, and the Eagle Butte/Kentucky #9 blend, were produced using a stoichiometric ratio of unity. The Fe-Al-Si synthetic coal was also combusted under similar conditions with a stoichiometric ratio of unity. For comparison, the stoichiometric ratio was varied for the blend; blend ash samples with stoichiometric ratios of 0.75 and 1.4 were also analyzed. Mineral compositions of each ash sample were determined using CCSEM, and are shown in Table 16. As would be expected, the synthetic coal ash has the simplest composition, containing primarily iron oxide, kaolinite, iron aluminosilicate, and aluminosilicate. For the Eagle Butte, Kentucky #9, and blend ash samples with stoichiometric ratios of unity, the composition of the blend is intermediate between that of the two parent coal ashes, with the exception of calcium aluminosilicate, which is higher in the blend than in either of the parent ashes. This discrepancy may be the result of the inclusion of one or more large calcium aluminosilicate particles in the blend ash analysis. In general, the intermediate composition of the blend ash corroborates the conclusions regarding coal blending discussed above.

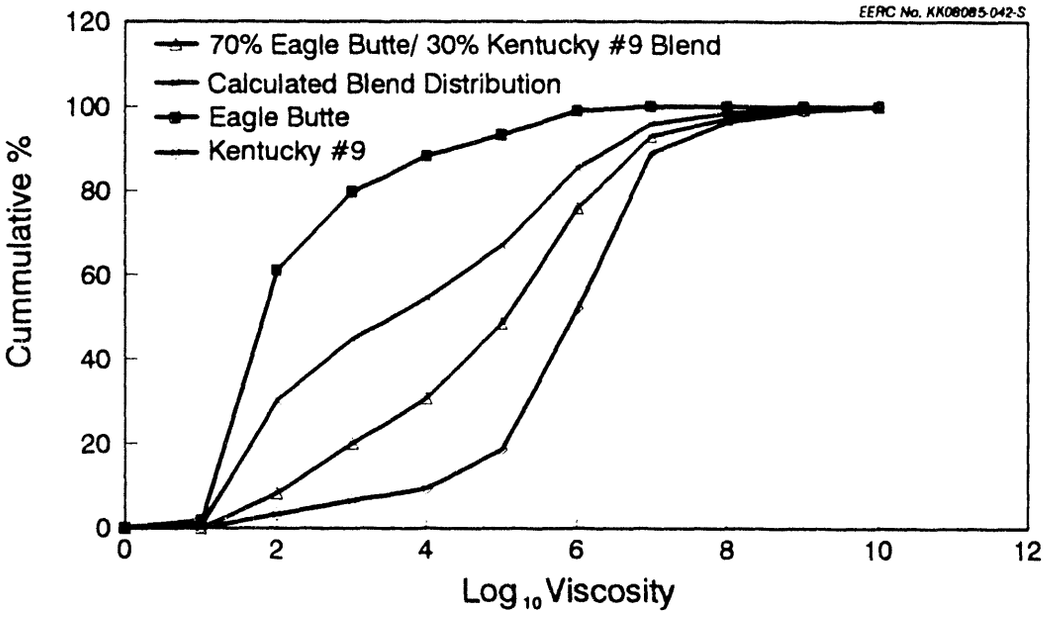

Figure 47. Viscosity distributions of Eagle Butte, Kentucky #9, and blend ashes.

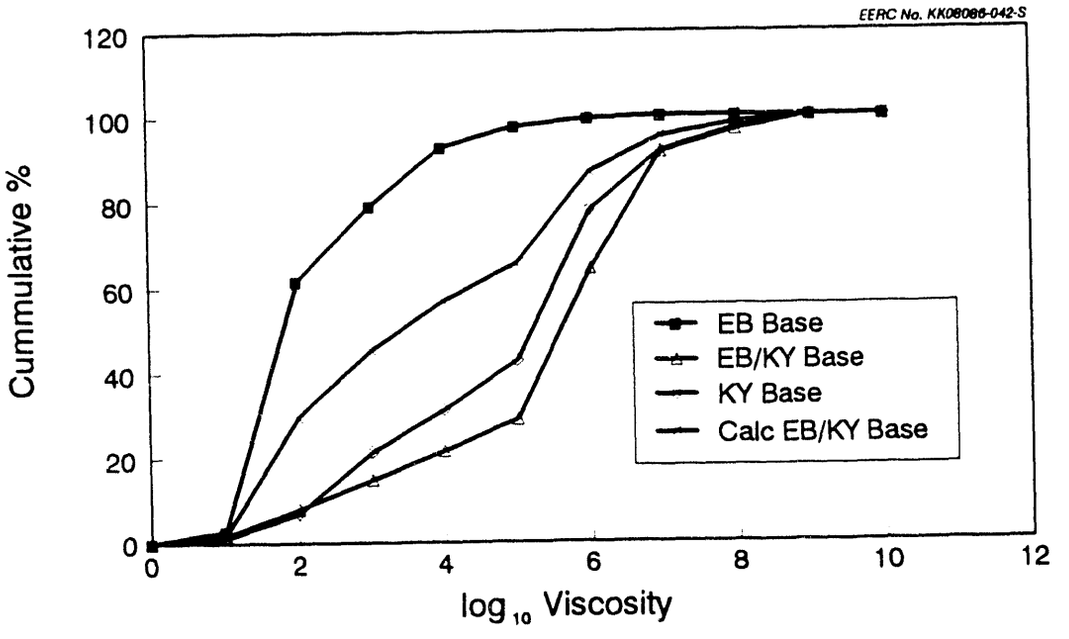

Figure 48. Eagle Butte and Kentucky #9 viscosity distributions for base deposits.

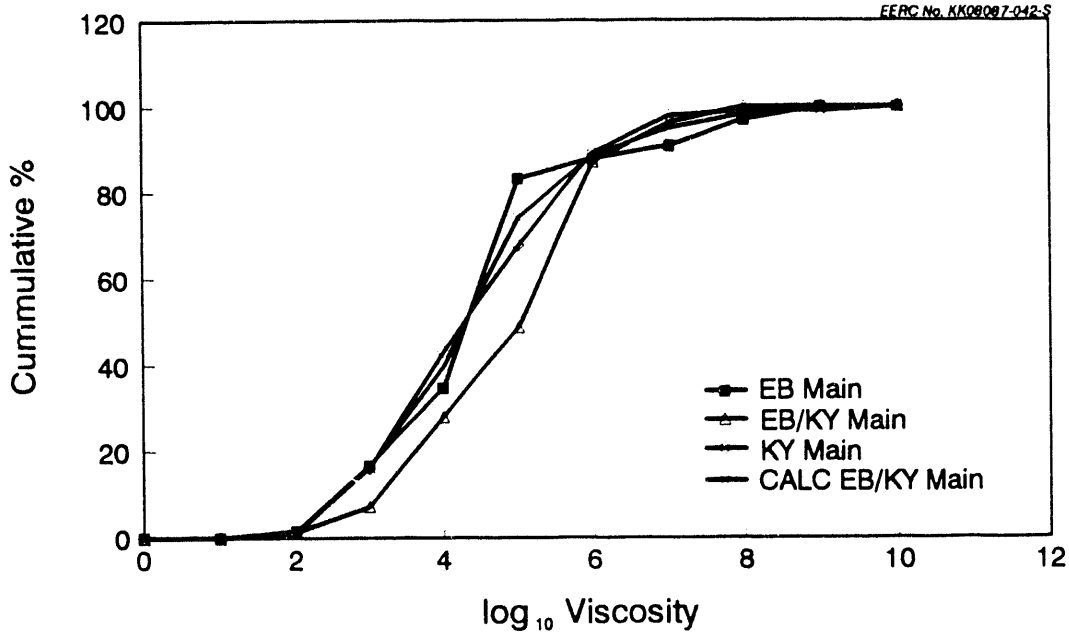

Figure 49. Eagle Butte and Kentucky #9 viscosity distributions for main deposits.

Comparison of blend ashes produced at varied fuel/air stoichiometric ratios indicates several different trends among the mineral categories. Weight percentages of Ca-Al-silicate and ankerite are directly proportional to the stoichiometric ratio. The minerals calcite, K Al-silicate, Fe Al-silicate, and Ca silicate show the opposite trend, with concentrations that are inversely proportional to the changes in stoichiometric ratio. Several other minerals, including iron oxide, dolomite, aluminosilicate, and Ca aluminate, are present in greatest concentrations for a stoichiometric ratio of unity, and decrease when the ratio is increased or decreased. The kaolinite, gypsum/Al-silicate, and Si-rich categories are present in the smallest weight percentages for a stoichiometric ratio of unity, and increase in concentration as the ratio is varied. The fact that minerals of similar chemical composition (i.e., Ca-bearing, silica-bearing, etc.) exhibit different trends as the stoichiometric ratio is varied suggests that these ratios have a complex effect on mineral transformation processess. The fuel-rich conditions used during the experiments suggest that the coal may not have been completely combusted, thus preventing the inorganic transformations from proceeding to completion. The varied compositional trends observed in the CCSEM data may thus be understood as representative of a range of partially complete transformations.

TABLE 16

CCSEM Results for Ashes Produced Under Fuel-Rich, Fouling Conditions
Area Percent Mineral Basis (SR = stoichiometric ratio)

Mineral	Fe-Al-Si SR = 1	Eagle Butte SR = 1	KY #9 SR = 1	Blend SR = 1	Blend SR = 0.75	Blend SR = 1.4	Eagle Butte O-rich	KY #9 O-rich	Blend O-rich
Quartz	0.3	4.5	13.8	9.7	9.9	6.1	4.6	7.3	9.3
Iron oxide	14.8	0.1	5.8	1.9	0.1	0.4	0.5	4.8	1.0
Rutile	0.0	0.0	0.0	0.1	0.1	0.1	0.1	0.0	0.0
Alumina	0.0	0.0	0.0	0.4	0.0	0.0	0.0	0.1	0.0
Calcite	0.0	0.9	3.6	1.5	1.7	1.1	0.6	1.0	0.9
Dolomite	0.0	12.1	0.0	3.7	2.6	1.0	2.9	0.0	0.0
Ankerite	0.0	0.4	0.0	0.6	0.1	1.1	0.4	0.2	0.3
Kaolinite	36.3	0.5	16.6	6.8	12.0	9.1	0.3	10.8	5.1
Montmorillonite	1.9	0.0	12.4	4.9	5.8	4.8	0.1	6.3	2.5
K Al-Silicate	0.0	0.1	9.1	2.0	5.3	1.6	0.0	4.2	1.3
Fe Al-Silicate	22.0	0.0	6.2	1.4	2.0	1.3	0.0	7.3	1.5
Ca Al-Silicate	0.5	7.0	3.0	11.4	8.4	14.2	6.4	2.8	8.1
Na Al-Silicate	0.3	5.0	1.4	1.5	2.0	4.7	3.7	0.0	0.0
Aluminosilicate	12.6	0.1	3.5	2.1	1.7	1.8	0.5	4.3	1.0
Mixed Al-Silicate	0.2	2.1	3.1	2.5	2.5	2.2	1.1	5.9	3.0
Fe-Silicate	0.2	0.0	0.8	0.1	0.0	0.1	0.0	0.5	0.0
Ca-Silicate	0.0	2.3	0.9	1.1	1.9	0.9	4.7	0.1	1.8
Ca Aluminate	0.0	13.5	0.2	6.3	3.7	4.2	17.1	0.0	1.5
Pyrite	0.0	--	0.1	0.0	3.3	0.0	0.0	0.0	0.0
Pyrrhotite	0.0	--	0.1	0.0	1.9	0.0	0.0	0.0	0.0
Oxidized Pyrrhotite	0.8	0.0	0.3	0.0	0.5	0.0	0.0	0.4	0.3
Gypsum	0.0	0.0	0.4	0.0	0.3	0.5	0.0	2.1	3.5
Apatite	0.2	0.0	0.0	0.1	0.0	0.1	0.0	0.1	0.0
Ca-Al-P	0.0	0.0	0.0	0.0	0.4	0.1	0.0	0.0	0.0
Gypsum/Al-Silicate	0.0	0.3	0.1	0.9	1.6	2.6	5.5	0.4	3.5
Si-Rich	1.0	0.4	5.6	2.7	3.8	3.1	0.9	6.3	3.3
Ca-Rich	0.0	1.7	1.7	1.0	1.1	1.2	3.8	0.7	0.4
Ca Si-Rich	0.0	0.3	0.1	0.5	0.6	0.3	1.6	0.2	0.7
Unknown	8.9	48.4	11.1	36.7	27.0	37.5	45.1	34.3	50.9
Totals	100.0	100.0	100.0	100.0	100.0	100.0	100.0	100.0	100.0

XRD analysis of the blend ash samples produced at three different stoichiometric ratios shows that two ferrite spinel, $(Mg,Fe)(Fe,Al)_2O_4$, a reduced phase, is a major component of the two ashes produced at stoichiometric ratios of 1.4 and 1.0. In contrast, ferrite spinel is present only as a minor phase in the ash produced using a stoichiometric ratio of 0.75. This variation suggests a reducing environment was present at the lowest stoichiometric ratio, preventing the oxidation of pyrite and pyrrhotite that would otherwise occur.

PSDs for the ashes generated under fuel-rich, fouling conditions are shown in Figures 50 and 51. Figure 50 displays size distributions for four different ashes, all produced using a fuel/air stoichiometric ratio of unity. Distributions for the synthetic Fe-Al-Si ash and for the Eagle Butte ash both peak in the 2.2- to 4.6-μm size range. The distribution of the Kentucky #9 ash peaks in the 10- to 22-μm size range, and the blend ash peaks in the 4.6- to 10-μm range. Each size distribution is unimodal. The positioning of the peak for the blend size distribution in between that of the two parent coal ashes is expected based on the behavior of the blend as a weighted mixture. If the two components of the blend behaved independently, a bimodal size distribution would result.

Size distributions for Eagle Butte/Kentucky #9 blend ash produced under three different fuel/air stoichiometric ratios are presented in Figure 51. All three size distributions are unimodal. The distribution for a ratio of unity peaks in the 4.6- to 10-μm size range. The distributions for ratios of 0.75 and 1.4 both peak in the range 2.2- to 4.6 μm. The ash produced using a ratio of 1.4 has the narrowest size distribution (i.e., the greatest percentage of mass in the peak range), whereas the ash produced using a stoichiometric ratio of 0.75 has the broadest size distribution. These data suggest that a greater stoichiometric ratio leads to a more uniform ash formation process, yielding a greater concentration of particles in a single size range.

4.5.5 Conclusions

The analyses of the parent coals and the 70/30 Eagle Butte/Kentucky #9 blend indicates that the blending operation was quite successful, since most of the blend physical properties are very close to a weighted average of those of the parent coals. Pyrite was seen to decompose to iron oxide early in the combustion process, with some subsequent interaction of the iron with clay minerals to form Fe-Al-silicate species. The calculated viscosity distribution of the blend ash is intermediate between those calculated for the ashes of the parent coals, and similar to a simple weighted average of the viscosity distributions of the parent coal ashes.

Carbon conversion results from the gas analysis and weight methods indicate that the Eagle Butte/Kentucky #9 blend was 100% combusted by 0.5 seconds with a furnace temperature of 1500°C. TGA results indicate that combustion of the coal blend was almost complete by 0.8 seconds. The gas analysis and weight methods of carbon conversion show conversions higher than 100% for the longer residence times. In general, the different methods of conversion follow the same trends of conversion, with the TGA method showing lower conversion percentages than the other two methods at all residence times.

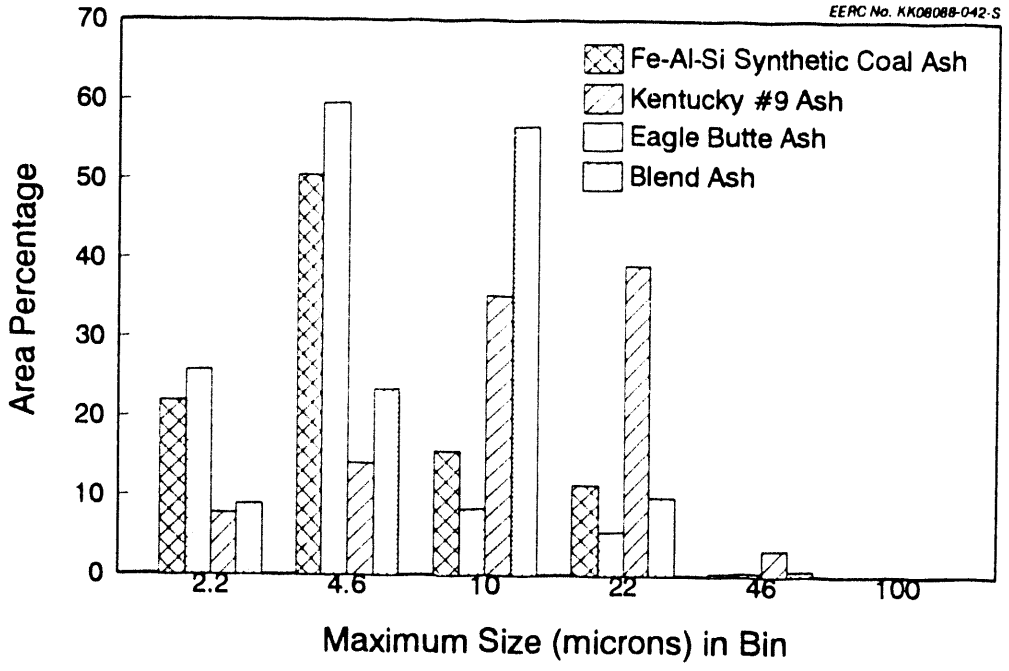

Figure 50. Size distributions for ash samples produced in the DTF, using fuel-rich, fouling conditions with stoichiometric ratios of unity.

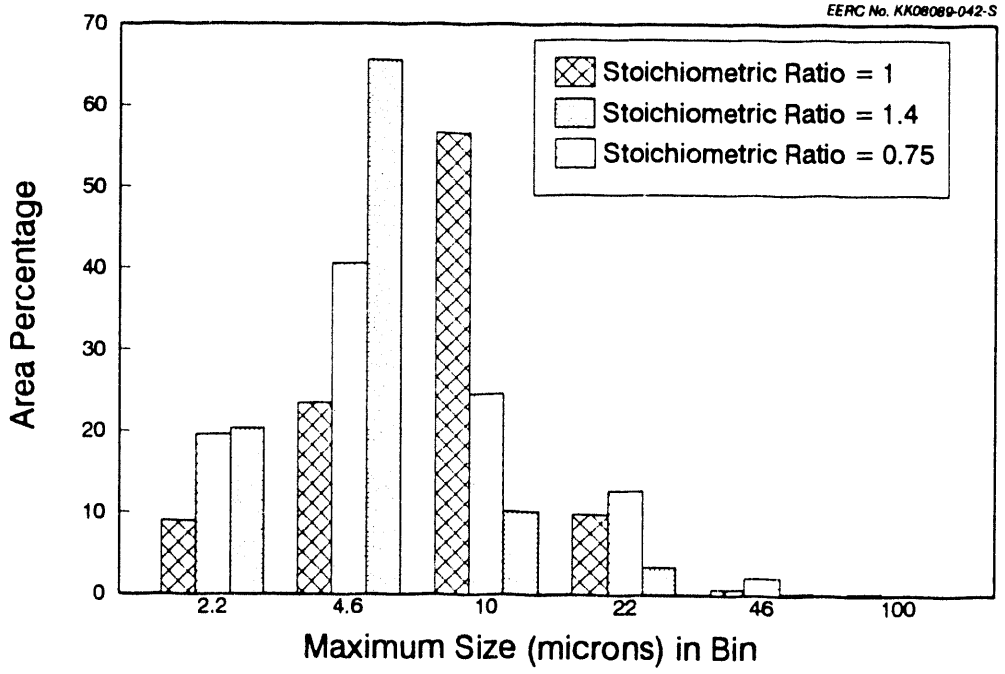

Figure 51. Size distributions for Eagle Butte/Kentucky #9 ash samples produced in the DTF, using fuel-rich, fouling conditions with varied stoichiometric ratios.

A blend of 70% Wyoming Eagle Butte low-sulfur (<1% mf) subbituminous coal and 30% Kentucky #9 high-sulfur (4% mf) bituminous coal was analyzed using CCSEM. Experimental fly ash was generated in the DTF using a gas temperature of 1500°C and residence time of about 2.5 seconds (slagging conditions). The fly ash was analyzed using SEMPC and CCSEM. Coal analyses revealed that the blending operation was quite successful since the physical and chemical components are nearly weighted averages of the components in the parent coals. The fly ash revealed little interaction between the mineral components of the two different coals. The viscosity distributions of liquid phases in the blend fly ash under slagging conditions were intermediate between those of the weighted average of the parent fly ashes and the Kentucky #9 ash.

The bases and main portions of ash deposits grown under fouling conditions were produced and then analyzed using SEMPC. The viscosity distribution of the base deposit of the blend was less than that calculated for the weighted average of the parent base deposits, and approximately identical to that of the Kentucky #9 base deposit. The viscosity distributions of the main portion of the deposits were similar for both parent coals and for the blend. Although only 30% of the coal blend is Kentucky #9, it appears to dominate the ash viscosity distributions more than expected based on a calculated weighted average of the parent ash viscosity distributions.

Iron-rich particles derived from the pyrite in the Kentucky #9 coal experienced only limited interaction with aluminosilicates, most of which had sources in the Kentucky #9.

5.0 TASK 3: DEVELOPMENT OF ANALYTICAL METHODS

The objective of Task 3 was to enable a precise characterization of the minerals present in pulverized coals and to coordinate an effort between laboratories performing CCSEM analysis on coal in order to develop a consistent methodology. Standard methods of coal mineral characterization do not provide the level of detail needed to predict the interactions that take place during combustion. The characteristics of minerals which affect their behavior during combustion include 1) chemical composition, 2) size, 3) association of the minerals with the coal matrix, 4) associations among minerals, and 5) mineral shape. Presently, coal minerals are characterized using a CCSEM, which yields mineral compositions and sizes. The goals of Task 3 were to enhance the present methodology to include other significant mineral characteristics, such as mineral associations, mineral shapes or morphology, the relationship of the minerals to the coal matrix, and the analysis of individual submicron particles. CCSEM was used together with an automated image acquisition and characterization program to provide the needed data. One resultant methodology is a PBPSEM technique. A final objective of this task focused on standardizing CCSEM as a viable interlaboratory technique. A round-robin analysis of coal was initiated for the purpose of providing a sound basis for different laboratories to compare CCSEM results. A possible result of the round-robin CCSEM work is certification of the CCSEM method through an appropriate professional society.